Power Management and Distribution (PMAD) Model Development

Final Report

Kenneth J. Metcalf
Boeing Corporation, Canoga Park, California

NASA STI Program . . . in Profile

Since its founding, NASA has been dedicated to the advancement of aeronautics and space science. The NASA Scientific and Technical Information (STI) program plays a key part in helping NASA maintain this important role.

The NASA STI Program operates under the auspices of the Agency Chief Information Officer. It collects, organizes, provides for archiving, and disseminates NASA's STI. The NASA STI program provides access to the NASA Aeronautics and Space Database and its public interface, the NASA Technical Reports Server, thus providing one of the largest collections of aeronautical and space science STI in the world. Results are published in both non-NASA channels and by NASA in the NASA STI Report Series, which includes the following report types:

- TECHNICAL PUBLICATION. Reports of completed research or a major significant phase of research that present the results of NASA programs and include extensive data or theoretical analysis. Includes compilations of significant scientific and technical data and information deemed to be of continuing reference value. NASA counterpart of peer-reviewed formal professional papers but has less stringent limitations on manuscript length and extent of graphic presentations.

- TECHNICAL MEMORANDUM. Scientific and technical findings that are preliminary or of specialized interest, e.g., quick release reports, working papers, and bibliographies that contain minimal annotation. Does not contain extensive analysis.

- CONTRACTOR REPORT. Scientific and technical findings by NASA-sponsored contractors and grantees.

- CONFERENCE PUBLICATION. Collected papers from scientific and technical conferences, symposia, seminars, or other meetings sponsored or cosponsored by NASA.

- SPECIAL PUBLICATION. Scientific, technical, or historical information from NASA programs, projects, and missions, often concerned with subjects having substantial public interest.

- TECHNICAL TRANSLATION. English-language translations of foreign scientific and technical material pertinent to NASA's mission.

Specialized services also include creating custom thesauri, building customized databases, organizing and publishing research results.

For more information about the NASA STI program, see the following:

- Access the NASA STI program home page at *http://www.sti.nasa.gov*

- E-mail your question via the Internet to *help@sti.nasa.gov*

- Fax your question to the NASA STI Help Desk at 443–757–5803

- Telephone the NASA STI Help Desk at 443–757–5802

- Write to:
  NASA Center for AeroSpace Information (CASI)
  7115 Standard Drive
  Hanover, MD 21076–1320

Power Management and Distribution (PMAD) Model Development

Final Report

Kenneth J. Metcalf
Boeing Corporation, Canoga Park, California

National Aeronautics and
Space Administration

Glenn Research Center
Cleveland, Ohio 44135

November 2011

Level of Review: This material has been technically reviewed by NASA expert reviewer(s).

TABLE OF CONTENTS

LIST OF TABLES

LIST OF FIGURES

1.0 SUMMARY

Power management and distribution (PMAD) models were developed in the early 1990's to model candidate architectures for various Space Exploration Initiative (SEI) missions. They were used to generate "ballpark" component mass estimates to support conceptual PMAD system design studies. The initial set of models was provided to NASA Lewis Research Center (since renamed Glenn Research Center) in 1992 [Ref. 1]. They were developed to estimate the characteristics of power conditioning components predicted to be available in the 2005 timeframe. Early 90's component and device designs and material technologies were projected forward to the 2005 timeframe, and algorithms reflecting those design and material improvements were incorporated into the models to generate mass, volume, and efficiency estimates for circa 2005 components.

The models are about ten years old now and NASA GRC requested a review of them to determine if they should be updated to bring them into agreement with current performance projections or to incorporate unforeseen design or technology advances. This report documents the results of this review and the updated power conditioning models and new transmission line models generated to estimate post 2005 PMAD system masses and sizes. This effort continues the expansion and enhancement of a library of PMAD models developed to allow system designers to assess future power system architectures and distribution techniques quickly and consistently.

These models are designed primarily for space missions that require continuous power for long periods and are capable of supporting manned operations. Model development is based on the premise that a power conditioning unit can be broken down into its major stages and elements, and that by developing mass trends as a function of power, voltage, and frequency for the basic devices and components within them, trends can be derived for the larger assemblies. The mass of a complete component is determined by summing the masses of the power conditioning stages and adding on the mass of the control and monitoring, enclosure, and thermal management subsystems. The thermal management algorithms are based on passive thermal control (heat pipe radiator) and calculate the associated coldplate and radiator mass. The model documentation explains the component equations, including their coefficients and exponents; identifies model limitations; specifies valid input ranges; and discusses methods for applying the component models.

The review indicated some of the technology and design advancement projections built into the models were too aggressive and significant modifications were made to the box (enclosure and baseplate) and thermal management (coldplate and radiator) equations. The as-built space station component boxes were substantially larger and heavier than originally estimated. Unanticipated structural panels, smaller boxes, were also installed in them. The original box algorithms were largely based on those designs and they were revised to agree with the as-built masses. The packaging density, which determines the box size, was also reduced, resulting in larger calculated box sizes. The original radiator equations were generated from a lunar base thermal management analysis. The DC to DC Converter Unit (DDCU) coldplate and heat pipe radiator design is more relevant to most space missions, so the coldplate and radiator size and mass equations were modified to agree with it. And finally, to support mass versus cost trades in the design of these elements, aluminum and carbon-carbon material options were incorporated into the box and radiator algorithms.

The model calculated too low of a mass for the converter electronics, even after its efficiency inputs were increased to agree with on-orbit DDCU efficiencies. Electronics mass can be traded against efficiency, and the algorithms contain equations to model this trade. The efficiency calculations were revised to reflect these improvements, and a Weinberg converter algorithm was added to better model this part of the DDCU. This algorithm and the previously developed resonant converter algorithm were modified to incorporate higher switch and diode masses, because previous estimates were judged too optimistic after a review of these devices. The transformer and dc filter mass estimation equations were changed to reflect improved performance at higher operating frequencies. A measure of the combined changes can be obtained by looking at the range of mass outputs the DDCU model can predict for the International Space Station (ISS) DDCU. The revised model predicts the mass of the ISS DDCU would be about 6% less if minimal advances were to occur, essentially today's technology, but if all the advances projected to be available in the 2005 to 2010 timeframe were incorporated, it predicts its mass could be reduced as much as 53%.

2.0 INTRODUCTION

This effort was initiated to update several PMAD models previously provided to NASA GRC in 1992 and to provide two new component and two new transmission line models. The predecessors of these models were originally developed to evaluate centralized versus decentralized lunar base power system architectures and to conduct voltage and frequency trade studies [Ref. 2]. When NASA GRC received the results of these early studies they had questions about the development, applications, and capabilities of the models that were used. It was decided these models needed to be documented to define their capabilities and limitations, and to allow critical review by experts in the field. Additional models were also required to allow a wider variety of power systems to be evaluated. This lead to the creation of the original Task Order 15 report, which documented the development and capabilities of ten of the most essential models [Ref. 1]. It was understood this was only the beginning and that subsequent reports would be required to add to this set of models and to periodically update previously provided models to incorporate technology advances. Later reports provided power processing unit models for electric propulsion system assessments and new power conditioning and transmission line models. Gradually a library of PMAD models was formed. This report continues that development.

The models contained in this report are intended to be simple to use and yield useful results. While these objectives are desirable, the simplicity of the models themselves may lead individuals not familiar with PMAD systems to assume the components are easy to design and the technology is mature. This is not the case. The size and complexity of the models is kept down by identifying the basic stages within components and developing generalized mass relationships for these stages from component designs presented in papers and employed on similar programs. Designers are constantly developing new design approaches and incorporating new technologies to achieve better performance and reduce mass. Consequently, to develop representative PMAD models of future components it was necessary to review emerging technologies and evaluate these against proposed space applications. The objective was to formulate a set of component characteristics and operating conditions that would be consistent with future PMAD designs.

This power conditioning model update was begun by reviewing many of the component designs and device technologies used as the starting point for the original models. The previous performance and technology advances incorporated into the models were then assessed against present designs, device capabilities, and material properties to evaluate the level of actual advancement against the original projections. Then using this power element technology assessment, the amount of advancement expected over the next five years was gauged to obtain device characteristics and material properties consistent with post 2005 technologies. The resulting values were compared against the original values used to generate the stage mass algorithms that are combined to form the various component models. The mass values generated by the updated models were compared against other component mass projections to validate their accuracy. The overall model estimates were then validated against other design projections to served as benchmarks, and they were the basis for mass breakdowns generated at other operating points. Equations representing the various component stages were developed from these data points using curve fitting techniques. The final step was to assimilate selected equations into a spreadsheet to form a complete component model.

Anticipated improvements in PMAD components are reflected in the models and discussed in the sections dedicated to those devices. Although a concentrated development effort is necessary to achieve many of these performance levels, this report does not propose methods for realizing them or identify critical technology areas. This is not its intent. Technology projections are addressed on a case by case basis, but in general they are based on information obtained from related power system studies and designs, and discussions with experts in the PMAD field. The purpose of this report is not to supply component design information, but to present models representative of future PMAD components and explain the rationale behind their development. Future studies are planned by NASA to generate technology road maps that will identify the critical technologies that must be developed to fabricate and deploy advanced power systems.

Every space application will have different operating requirements, many of which are not even envisioned at the present time. Although the models in this report are designed to accept a wide range of operating parameters, they are not capable of addressing all aspects of a particular application. It was necessary to

assume typical values for some parameters. This naturally introduces a certain amount of error and it is one reason model outputs should be compared with other sources of information.

These models also address a specific type of power system operation. They are designed to support assessments of long life, high reliability power systems supplying continuous power. Continuous power systems are designed for steady state operation and they typically operate for years. A PMAD system designed for long term operation requires radiators and passive and/or active thermal management techniques. Components in a passive system contain internal heat sinks and thermal paths that conduct generated heat to a coldplate. The hardware necessary to passively cool a device may account for 80 to 90% of its total mass. Heat pipes routed through the coldplate then transport this heat out to a radiator for dissipation. An active cooling system employing a coldplate would use a pumped loop containing a liquid to carry heat from the coldplate to a radiator surface.

These models should not be used for burst power applications because the thermal management approach employed with this type of system is very different. Burst power systems are designed for short term operation, generally less than fifteen minutes. This short operating life allows the use of adiabatic or cryogenic cooling techniques. Adiabatic cooling relies on the heat capacity of the component and adjacent structure to absorb generated heat. Mass constraints essentially limit adiabatic cooling times to under 120 seconds. Cryogenic cooling normally uses liquid hydrogen or nitrogen to cool the power conditioning components to near cryogenic temperatures. The cryogenic liquid and its tankage can be quite heavy; hence, the operating life of these systems is limited. Cryogenic cooling is typically used only when the cryogenic liquid has other uses, such as for a propellant. A person who incorrectly uses these models to estimate masses in burst power applications will obtain power conditioning mass estimates that are much too heavy. In some cases, the estimates may be ten times the actual values.

Another factor affecting PMAD mass is whether the platform is manned or unmanned. Man critical systems have higher reliability, availability, and maintainability requirements. Consequently, a more conservative design approach is usually employed. Components are operated at lower power densities and temperatures. This increases PMAD mass because added thermal management hardware is required and larger power devices are used throughout the system. The components in a manned system may also need to be designed for easy removal and maintenance. This also drives up PMAD mass because components will need to be equipped with electrical connectors, mechanical disconnects, and heat exchangers or fluid couplings to provide detachable heat transfer paths.

Since many proposed space missions are manned or support manned expeditions, reliability considerations influenced the model development. A detailed reliability analysis was not conducted during this study, therefore it was necessary to make some basic assumptions. It is anticipated that most missions will require the power conditioning components to achieve at least a ten year operating life. Because many of the present Space Station components are designed to meet a fifteen-year mean time between failure (MTBF), this data was relied on heavily during the model development. Reliability is normally improved in two ways: (1) key elements within a component can be made redundant, and (2) multiple smaller units, each sized to handle a percentage of the power, can replace a single large unit. Unfortunately, reliability considerations typically increase power system mass and place added demands on the instrumentation and control subsystem. Incorporating internal redundancy into a component increases its mass since additional elements are required. Replacing a single power conditioning unit with multiple smaller units increases mass because some economies of scale are sacrificed and ancillary hardware such as the enclosure, and control and monitoring now occupy a larger percentage of the total component mass. The size and complexity of the instrumentation and control (I&C) subsystem that oversees the entire power system is also expanded since it must monitor a larger number of units and coordinate their operation. The mass impacts associated with an enlarged I&C subsystem are not addressed by these models since they only pertain to individual power conditioning components.

3.0 POWER CONDITIONING MODEL DEVELOPMENT

Before the original power conditioning model development was begun in 1992, a power element technology assessment was conducted to determine the amount of advancement one could reasonably expect by the year 2000. This study was conducted in 1991 [Ref. 3] and examined the key power element technologies, switching devices, magnetic materials, and capacitors expected to be used in high power systems. The current and potential capabilities of existing elements were determined as well as the projected capabilities of advanced alternatives. After considering anticipated technology advances in the context of proposed SEI missions, general conclusions were reached. Numerous improvements were projected for converter elements, thermal management subsystems and packaging techniques. It was anticipated that carbon-carbon would be used extensively for enclosures and heat pipes, replacing aluminum in many applications. Component radiators would also utilize carbon-carbon extensively. Improvements in the magnetic materials area were expected to be fairly minor and occur mainly in the high frequency region. High frequency transformer and inductor core masses and losses were expected to decline modestly as a result. Incremental improvements in capacitors were also expected to yield modest gains in energy density and efficiency. At the time, most semiconductor switches were limited to operating voltages below 500 V [Ref. 4]. The exception was silicon controlled rectifiers (SCRs), one of the switch types within the thyristor family, were available at voltages up to 5000 V, but their turn off requirements limited their applications[1] [Ref. 5]. Anticipated advances in metal-oxide-semiconductor field-effect-transistors (MOSFETs) and MOS controlled thyristors (MCTs) indicated much higher voltage devices could be developed by the year 2000, possibly as high as 5000 V [Ref. 6, 7, 8]. The development of high voltage, high current density semiconductor switches was expected to make higher voltage, higher power converters more practical. Improvements in MOSFET construction, particularly changes that that lowered their losses, were expected to reduce the mass of converters and improve their efficiency.   However, these predicted technology advances were highly speculative because a key driver would be development funding and it could vary considerably.

Since these projections were for post 2000 semiconductor switches and its 2002, the capabilities of current switches can be reviewed to see if the original projections panned out. The on-resistance of MOSFETs has declined substantially, but not at much as was projected, necessitating an increase in the reference switch module mass (this is addressed in detail in section 3.1.1). Their voltage rating has also been increased, but they have only reached 1200 V [Ref. 9], well below the original 5000 V projection. This is may be partially due to the progress that has occurred in insulated gate bipolar transistors (IGBTs). IGBTs are available at voltages up to 4500 V [Ref. 10], with on-resistance and turn-on, turn-off times close to those of MOSFETs [Ref. 11]. The development of MCTs has also been slower than projected, which may again be partially due to the progress in high voltage IGBTs. Presently, 1400 V rated MCTs are available [Ref. 12]. Higher voltage MCTs can be manufactured, but the allowable conduction current density falls off rapidly at voltages above 2000 V. Thyristors with ratings up to 12,000 V are available [Ref. 13], but as noted previously their turn-off characteristics limit their use to rectifiers and ac switches, and their relatively slow turn-on time further limits them to low frequency applications. So in summary, the development of high voltage MOSFETs and MCTs has been slower than projected, but IGBTs have largely filled this gap. MOSFET losses have declined, but not as much as projected. The conclusion is the originally generated equations for the chopper and rectifier stages, which were partially based on the properties of these switches and diodes, must be changed to reflect less semiconductor switch development and reduced performance capabilities.

Based on the original technology assessment and this review, device characteristics were defined that were deemed to be consistent with future PMAD designs. This data served as a foundation for the actual component model development. Models were generated using a six step process: (1) the specific stages in a component were identified; (2) mass breakdowns for these stages were obtained by studying component designs or hardware; (3) projected technology advances were considered and used to adjust these mass

---

[1]   An SCR cannot be turned off by simply removing the gate signal, the current flow must either be interrupted or forced to flow in the opposite direction. For ac switching or rectification, these turn-off
requirements may be acceptable because the current naturally crosses through zero each half cycle.
However in a DC application, such as an inverter switch, they aren't usually acceptable.

breakdowns to yield mass values consistent with the 2005 to 2010 time period; (4) these adjusted mass breakdowns were used as benchmarks and they were extrapolated from to generate mass tabulations at other operating points; (5) equations were generated to fit these points using curve fitting techniques; and (6) selected equations were assimilated to form a complete model. This entire process is based on the theory that the mass of a power conditioning component can be estimated by summing the masses of its power processing stages and associated hardware (this approach is treated in detail in the next section).

The original stage equations contained in the models were developed and validated by comparing the mass breakdowns used for equation development and the resulting model generated mass estimates with existing designs [Ref. 1, Appendix A]. The original mass breakdowns were derived from Rocketdyne and Ford Aerospace SSF and TRW 20 kHz component mass breakdowns [Ref. 14, 15, 16], after they were modified to incorporate projected technology advances. To assess the accuracy of these original breakdowns against present designs, the masses of several of the ISS flight components were obtained [Ref. 17]. Unfortunately, it wasn't possible to obtain mass breakdowns of these components, but by obtaining the shipping masses of their enclosures and baseplates, and factoring known component design modifications into the original breakdowns, it was possible to develop reasonably accurate mass breakdowns of the current components. These derived mass breakdowns served as the new benchmarks for subsequent extrapolations. Because it was easier to project the improvements for a single item, each element in a stage was evaluated individually. To generate mass breakdowns at other operating points, the impact on mass as power, voltage, efficiency, and frequency are changed were considered separately. The individual element mass impacts were then summed to obtain an estimate of the total mass impact of a change in an operating parameter. This approach simplified the extrapolation process and resulted in greater confidence in the values.

3.1 POWER CONDITIONING STAGES APPROACH

Power conditioning components tend to have common stages. For example, the dc/dc converter, the dc/ac inverter and the ac/ac frequency converter, each have a chopper stage. The interconnection and control of these stages determine the function and operation of the total converter.   Hence, one can define the stages contained in a specified converter, calculate their individual masses, and then add these values to the control and monitoring hardware mass, the enclosure mass and the thermal management and radiator subsystem mass to determine the total mass of a complete converter.

The masses of power conditioning components were estimated by defining the stages in a component and generating mass equations for them using the previously described six step process. Much of the information used to develop these equations was obtained from SSF and ISS documentation. These designs were considered to best typify future space based components because the space station power levels and component life times are approaching those planned for future space missions. Because the intent is to model future systems, these mass figures were adjusted to incorporate projected technology advances. Equations were then developed to estimate the mass of ancillary hardware such as controllers, data interface modules and monitoring sensors. The masses of the individual stages and ancillary hardware are summed to obtain the total electronics mass. Based on this mass and a factor computed for the density of electronics, the enclosure and baseplate masses were estimated. These values are then summed to obtain the component mass. Finally, a mass is computed for the radiator and added to this component mass to obtain the total mass of a power conditioning component subsystem, including its thermal management hardware.

Because the PMAD component models contain interconnected stages, the best way to explain their development is to individually address the development of the component stage equations. To better present the supporting rationale, these equations will be further broken down and their parts discussed separately. Because many effects can't be easily explained mathematically, graphs will be used liberally to display the mass effects projected to occur as an operating point is varied over the range of interest. The equations incorporate information obtained from technical reports, program documentation, textbooks, design manuals, and vendor catalogues. These sources will be identified during the model discussions.

3.2 CHOPPER STAGE MODEL

The chopper stage converts dc into ac, and its included in the inverter, dc/dc converter and frequency converter models. The design of a chopper can follow one of several different topologies, depending on the design requirements. The chopper stage equations provided in this report are based on Weinberg converter and parallel resonant converter circuit topologies. They were developed from simplified representations of these topologies, though, and are only intended to provide rough mass estimates for comparing components. To obtain more accurate mass estimates, specific designs should be generated by a circuit designer.

The chopper section has switch modules, diodes, inductors and capacitors. Each switch module contains a semiconductor switch and is supported by a snubber circuit to dampen voltage spikes occurring during switching, a heat sink for thermal management, gate drive circuitry to turn it on and off, switch control logic to implement the selected switching scheme (e.g., pulse-width-modulation) and packing and mounting hardware. Estimated mass breakdowns for circa 1992, present 2002, and projected post 2005 1 kWe switch modules, including support hardware, are shown in Table 1. A 1 kWe power level was selected to provide a per unit basis for later mass extrapolations. The 1992 mass values were originally estimated from briefing packages prepared by TRW, Ford Aerospace, and Rocketdyne in support of SSF, and a power MOSFET catalogue [Ref. 14, 15, 16, 4]. The 2002 mass breakdown was developed from a comparison of present power MOSFET characteristics (obtained from ST Microelectronics data sheets dated 1998 through 2001) with 1992 power MOSFET characteristics (obtained from a 1992 Harris Semiconductor power MOSFET catalogue) [Ref. 18, 19]. These results are discussed later. The projected 2005 mass breakdown originates from articles discussing future power conditioning component developments, discussions with experts in the field of power conditioning [Ref. 20, 21, 22, 23], and an extrapolation from the 1992 and 2002 data. The projected 2005 mass breakdown was used as a basis for the subsequent equation development.

Table 1: 1 kWe Switch Module Mass Breakdown

Hardware Element	Circa 1992 Mass (grams)	Present 2002 Mass (grams)	Projected Post 2005 Mass (grams)
Active Switch Element	7	6	5
Snubber Circuitry	20	18	17
Heat Sink, Thermal Management	48	40	37
Gate Drive Circuitry	25	20	18
Switch Control Logic	20	15	13
Packaging and Mounting	40	33	30
Total Switch Module	160	132	120

When this model development effort was initiated in 1992, advances in switch fabrication techniques, better switch geometries, and continuing size reductions in integrated circuits were expected to reduce the mass of switch elements. Much of the power semiconductor development was expected to be aimed at improving their efficiency because the main limiting factor in electronics mass reduction was and still is the inability to remove waste heat [Ref. 23]. For this reason, the best method of evaluating semiconductor development was considered to be an assessment of the reduction in switch losses. In general switch losses are of two types, conduction losses and switching (or edge) losses occurring during switch turn-on and turn-off. Conduction losses can best be evaluated by comparing the on-resistance of the switch, while switching losses are best assessed by comparing the rise time when the switch is turned-on (t_r) and the fall time when the switch is turned-off (t_f). A better performing switch will have a lower on-resistance and shorter rise and fall times. MOSFETs were selected for this evaluation because they tend to be the most widely used type of power switch because of their good conduction and excellent gate turn-on, turn-off characteristics. The performance characteristics of power MOSFETs circa 1992 are presented in Table 2, while comparable power MOSFET characteristics are provided in Table 3. The worst case losses for the two sets of switches are also provided for 20 and 40 kHz switching frequencies, typical of what might be obtained under worst

case switching conditions with pulse-width-modulation (PWM). Table 4 compares the two sets of loss values, and shows how much these losses have been reduced from about 1992 to 2002.

Table 2: Key Power MOSFET Switch Characteristics – 1992

1992 MOSFET Harris P/N	V_{DSS} (volts)	I_{DS} (amps)	R_{DS} (ohms)	t_r (nsec)	t_f (nsec)	20 kHz Losses (watts)	40 kHz Losses (watts)
RFP40N10	100	40	0.04	30	20	68.0	72.0
IRF251R	150	30	0.085	120	80	94.5	112.5
IRF640R	200	18	0.14	50	35	51.5	57.6
IRF740R	400	10	0.47	25	25	51.0	55.0
IRFP460	500	20	0.27	81	65	137.2	166.4
IRFPC40R	600	8	1	18	20	67.6	71.3
IRFPG40R	1000	4.3	3.5	50	50	73.3	81.9

Harris - Harris Semiconductor

Table 3: Key Power MOSFET Switch Characteristics – 2002

2002 MOSFET STM P/N	V_{DSS} (volts)	I_{DS} (amps)	R_{DS} (ohms)	t_r (nsec)	t_f (nsec)	20 kHz Losses (watts)	40 kHz Losses (watts)
STP40NF10L	100	40	0.028	82	24		61.8
STB40NS15	150	30	0.065	45	35	65.7	72.9
IRF640MFP	200	18	0.15	27	25	52.3	56.1
IRF740	400	10	0.48	10	10	49.6	51.2
STW20NM50FD	500	20	0.22	20	15	95.0	102.0
STP8NM60FP	600	8	0.9	10	10	59.5	61.4
STW5NB100	1000	4.3	2.9	11	22	56.5	59.3

STM - STMicroelectronics

Table 4: Comparison of 1992 and 2002 MOSFET Power Losses

		2002 MOSFETs		1992 MOSFETs		2002 / 1992 Losses	
V_{DSS} (volts)	I_{DS} (amps)	20 kHz Losses (watts)	40 kHz Losses (watts)	20 kHz Losses (watts)	40 kHz Losses (watts)	20 kHz Losses (watts)	40 kHz Losses (watts)
100	40	53.3	61.8	68.0	72.0	78.4%	85.8%
150	30	65.7	72.9	94.5	112.5	69.5%	64.8%
200	18	52.3	56.1	51.5	57.6	101.7%	97.4%
400	10	49.6	51.2	51.0	55.0	97.3%	93.1%
500	20	95.0	102.0	137.2	166.4	69.2%	61.3%
600	8	59.5	61.4	67.6	71.3	88.0%	86.2%
1000	4.3	56.5	59.3	73.3	81.9	77.0%	72.4%
					Average	83.0%	80.1%

Table 4 indicates power MOSFET losses have declined about 20% since 1992, which should allow the mass of their associated heat sinks to be reduced a similar amount. The estimated heat sink mass in 1992 for a 1 kWe switch was 48 grams. Based on this reduction in losses, this value is now estimated to be 40 grams, and assuming similar efficiency improvements in the future its projected to be 37 grams post 2005. The expected introduction of graphite based fibers in heat sinks to facilitate heat removal should also allow heat sink mass reductions because graphite has superior heat transfer characteristics and its specific weight is about two-thirds that of aluminum. During the course of this investigation it was noted that the semiconductor manufacturers also claim the switch die size has been reduced 10%, while achieving these performance gains. These statements support the currently estimated and projected reduction in active switch element size shown in Table 1. The snubber and gate drive circuit masses are also assumed to decline, but at a slower rate. Continuing size reductions in integrated circuits, particularly in electrically erasable programmable read only memory (EEPROMs) and programmable logic arrays (PLAs), support the size reductions shown for switch control logic circuits. The packaging and mounting mass should decline in proportion to the mass reductions obtained in the other elements. The total projected mass of a 1 kWe switch assembly post 2005 is now projected to be 120 grams. When the original post 2005 estimate was made in 1992 the total mass of a 1 kWe switch module was estimated to be 100 grams. This now appears to have been slightly too optimistic, and the mass algorithms for the stages containing switch modules have been adjusted to reflect the new post 2005 projected 1 kWe switch module mass of 120 grams.

In addition to switch module mass, ancillary hardware is required in the chopper circuit to manage internal energy flows and to supply current during switch off periods. A parallel resonant topology has a tank circuit consisting of an inductor and capacitor that stores energy to facilitate current circulation and switching; a Weinberg converter topology requires an input inductor to maintain a constant current supply. In 1992 when these models were developed, inductor and capacitor masses were projected to decline about 10% by 2005, and most of this mass gain was expected to occur at higher frequencies. Research continues to develop alternate magnetic materials, but there haven't been any new materials introduced in the past ten years. The most recently developed materials, metglas and ferrites, were available in 1992. Long term, proven materials such as supermalloy and orthonal are still widely used, and are expected to continue to be widely used. The main change in magnetic materials has been a reduction in losses at higher frequencies, accomplished through thinner laminations or improved manufacturing capabilities. This has resulted in mass reductions in high frequency applications and enabled higher switching speeds in resonant and switch mode converters. Capacitor development has enabled improvements in energy storage density, particularly with aerocapacitors, but their application is limited by their voltage capabilities. Because aerocapacitor cells can only withstand a few volts, several must be stacked to reach the voltage levels required for high power circuits. This has sharply limited their use. Overall the mass of the tank hardware in a chopper circuit was expected to decline about 10% from 1995 to 2005, and this still seems to be reasonably valid. Consequently the inductor and capacitor mass equations weren't changed. Table 5 shows mass breakdowns for 1 kWe, 40 kHz, post 2005 resonant and Weinberg converters. These breakdowns were generated from information obtained from Rocketdyne, NASA LeRC, General Dynamics, and TRW [Ref. 14, 15, 23, 24, 25]. They don't include the transformer and rectifier diode masses, which are addressed in subsequent sections.

Table 5: Comparison of Resonant and Weinberg Converter Masses

Element or Device	Post 2005 1 kWe Resonant Converter	Post 2005 1 kWe Weinberg Converter
Switch Modules	285 grams	240
Diode Modules	130 grams	164
Inductor	182 grams	265
Capacitor	118 grams	-----
Total	**715 grams**	**669 grams**

Using these mass breakdowns, algorithms were developed for Weinberg and resonant converter topologies. The Weinberg converter equations are incorporated into the DC to DC Converter model, while the resonant converter equations are contained in the DC to AC Inverter and Frequency Converter models. The subsequent paragraphs explain the development of the single-phase and 3-phase chopper stage equations in detail. The variables that will be used during this discussion are shown in Table 6. When a factor is being discussed it will be underlined. Graphs accompany each section to illustrate the parameters that have been incorporated into the equations. Only the Weinberg converter graphs are shown, the ones for the resonant converter would look very similar.

Table 6: Chopper Model Variable Definitions

1CSM	Single-Phase Chopper Stage Mass
3CSM	3-Phase Chopper Stage Mass
CSE	Chopper Stage Efficiency (97.6%)
CSAM	Chopper Stage Available Modules
CSRM	Chopper Stage Required Modules
CSP_O	Chopper Stage Power Output (kWe)
CSV_I	Chopper Stage Voltage Input (Vdc)
CSF	Chopper Stage Frequency (kHz)

Mass Coefficient

$$1CSM = \underline{0.645}*((EXP0.01/(1-CSE)))/1.5169)*(CSAM/CSRM)*CSP_O*((CSP_O/CSRM)^{-0.065}$$
$$*(CSV_I/(CSV_I-2))^7*EXP(CSV_I/40000)*(20/CSF)^{0.45}*EXP(CSP_O^{0.1}*CSF/200))$$

$$3CSM = \underline{0.685}*((EXP0.01/(1-CSE)))/1.5169)*(CSAM/CSRM)*CSP_O*((CSP_O/CSRM)^{-0.07}$$
$$*(CSV_I/(CSV_I-2))^7*EXP(CSV_I/40000)*(20/CSF)^{0.45}*EXP(CSP_O^{0.1}*CSF/200))$$

The chopper stage mass coefficients in these equations were calibrated to yield values consistent with the post 2005 1 kWe switch mass breakdown and actual component designs [Ref. 14, 15, 16, 17, 26].

Efficiency Factor

$$1CSM = 0.645*\underline{((EXP0.01/(1-CSE)))/1.5169)}*(CSAM/CSRM)*CSP_O*((CSP_O/CSRM)^{-0.065}$$
$$*(CSV_I/(CSV_I-2))^7*EXP(CSV_I/40000)*(20/CSF)^{0.45}*EXP(CSP_O^{0.1}*CSF/200))$$

$$3CSM = 0.685*\underline{((EXP0.01/(1-CSE)))/1.5169)}*(CSAM/CSRM)*CSP_O*((CSP_O/CSRM)^{-0.07}$$
$$*(CSV_I/(CSV_I-2))^7*EXP(CSV_I/40000)*(20/CSF)^{0.45}*EXP(CSP_O^{0.1}*CSF/200))$$

The factors underlined above estimate the changes in specific weight that occur over a range of chopper efficiencies. Within reason, the interconnecting wiring and ancillary hardware resistive losses, and the switch conduction losses can be reduced by increasing the size of the wiring and ancillary hardware, and the active switch element area and snubber component ratings. If the switch losses are always less over the full operating range, it should be possible to reduce the heat sink mass. It was previously noted that power MOSFET improvements have enabled their losses to be reduced 20% and continuing research is expected to reduce their losses another 10 to 15%. Furthermore, the space station dc/dc converter, on which much of this model development is based, is exhibiting an on-orbit efficiency of about 94% at full load, a substantial improvement over the specified 92% efficiency on which these models were originally based. These factors

enabled the nominal chopper efficiency to be increased from 96% to 97.6%. By gauging the effect of power losses on individual elements within a switching module, chopper mass estimates were developed for efficiencies ranging from 96.8 to 98.4%. An efficiency factor was then calculated and incorporated into the chopper mass equation. Figure 1 shows a graph of the resulting specific weight versus efficiency values that were developed with this approach. Note that the depicted chopper efficiency range is relatively narrow.

Chopper efficiencies higher than about 98.5% aren't considered practical due to limitations in circuit topology designs and switch fabrication techniques. Lower efficiencies are undesirable because of the increased thermal management and radiator mass. However, low operating voltages cause addition losses and result in efficiencies poorer than those shown. This will be explained further in the discussion of voltage factors.
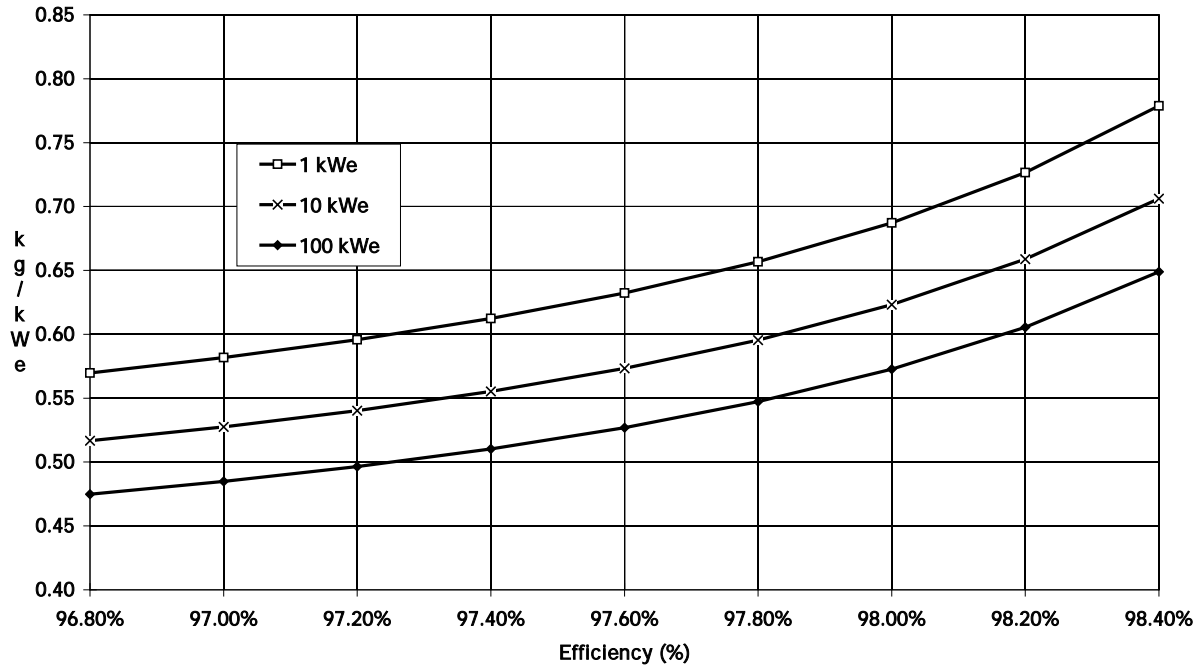
Figure 1: Chopper SPWT vs Efficiency

Redundancy Factor

$$1CSM = 0.645*((EXP0.01/(1-CSE)))/1.5169*\underline{(CSAM/CSRM)}*CSP_O*((CSP_O/CSRM)^{-0.065}$$

$$*(CSV_I/(CSV_I-2))^7*EXP(CSV_I/40000)*(20/CSF)^{0.45}*EXP(CSP_O^{0.1}*CSF/200))$$

$$3CSM = 0.685*((EXP0.01/(1-CSE)))/1.5169*\underline{(CSAM/CSRM)}*CSP_O*((CSP_O/CSRM)^{-0.07}$$

$$*(CSV_I/(CSV_I-2))^7*EXP(CSV_I/40000)*(20/CSF)^{0.45}*EXP(CSP_O^{0.1}*CSF/200))$$

The redundancy mass impacts that will occur for this stage when modules are added to enhance reliability are reflected in the above factor. This redundancy factor does not include the increased system control and monitoring requirements and their associated mass. The "available modules" value is the actual number of modules present in the component; the "required modules" number is the actual number of modules required to achieve full output power. If a design requires 4/3 redundancy to meet the reliability requirements, each channel will be rated to carry 33% of the power. 4 channels are available, but only 3 channels are needed to supply full power. The fourth channel represents the mass penalty incurred in this particular stage to achieve a higher reliability.

Power Level Multiplier

$1CSM = 0.645*((EXP0.01/(1-CSE)))/1.5169)*(CSAM/CSRM)*\underline{CSP_O}*((CSP_O/CSRM)^{-0.065}$

$*(CSV_I/(CSV_I-2))^7*EXP(CSV_I/40000)*(20/CSF)^{0.45}*EXP(CSP_O^{0.1}*CSF/200))$

$3CSM = 0.685*((EXP0.01/(1-CSE)))/1.5169)*(CSAM/CSRM)*\underline{CSP_O}*((CSP_O/CSRM)^{-0.07}$

$*(CSV_I/(CSV_I-2))^7*EXP(CSV_I/40000)*(20/CSF)^{0.45}*EXP(CSP_O^{0.1}*CSF/200))$

The equations can be used to calculate the mass or specific weight of the chopper. When the above multiplier is included, the value that results is a chopper mass estimate. To obtain the specific weight of the chopper, remove this multiplier.

Power Level Factor

$1CSM = 0.645*((EXP0.01/(1-CSE)))/1.5169)*(CSAM/CSRM)*CSP_O*(\underline{(CSP_O/CSRM)}^{-0.065}$

$*(CSV_I/(CSV_I-2))^7*EXP(CSV_I/40000)*(20/CSF)^{0.45}*EXP(CSP_O^{0.1}*CSF/200))$

$3CSM = 0.685*((EXP0.01/(1-CSE)))/1.5169)*(CSAM/CSRM)*CSP_O*(\underline{(CSP_O/CSRM)}^{-0.07}$

$*(CSV_I/(CSV_I-2))^7*EXP(CSV_I/40000)*(20/CSF)^{0.45}*EXP(CSP_O^{0.1}*CSF/200))$

As the power level of the chopper increases, certain economies of scale present themselves and allow a reduction in specific weight. Although, the active switch element, snubber circuitry, and thermal management hardware sizes will increase nearly linearly with power level, the mass of the gate drive circuitry and switch control logic will rise at a much slower rate. This causes switch module specific weights to decline as power levels rise. The specific weight of the tank hardware also declines slowly as the power level rises because the inductors, capacitors, diodes, resistors and interconnecting wiring forming this subsystem can be fabricated and configured more efficiently. Components can also be packaged more effectively at higher power levels, further reducing the packaging volume and mounting mass.

The masses of individual elements of a single-phase chopper were extrapolated to generate mass estimates for a complete unit at power levels ranging from 0.5 to 100 kWe. Based on these mass estimates, it was concluded that the specific weight of a single-phase chopper would decline at the 0.065 power as power level rose. The results of this evaluation are illustrated in Figure 2.

A 3-phase chopper has three single-phase choppers operating in unison. Regardless of whether a resonant or Weinberg converter is employed, each phase will require its own ancilliary hardware. This is necessary to generate three separate waveforms, each offset 120 degrees from the other. Power handling devices can not be shared between phases, only the control hardware is common. 3-phase chopper mass estimates were calculated by summing the masses of three single-phase choppers, each assumed to be processing exactly one-third of the power. Separate gate drive circuitry was assumed for each switch, but the switch control logic was integrated into a single unit to ensure synchronized operation and facilitate voltage regulation and frequency control. 3-phase chopper mass estimates were generated for power levels ranging from 10 to 250 kWe. These estimates indicated the specific weights of 3-phase choppers also decline at the 0.07 power as power levels increase. The specific weights of 10 to 250 kWe single- and 3-phase choppers are compared in Figure 3 at two resonant frequencies.
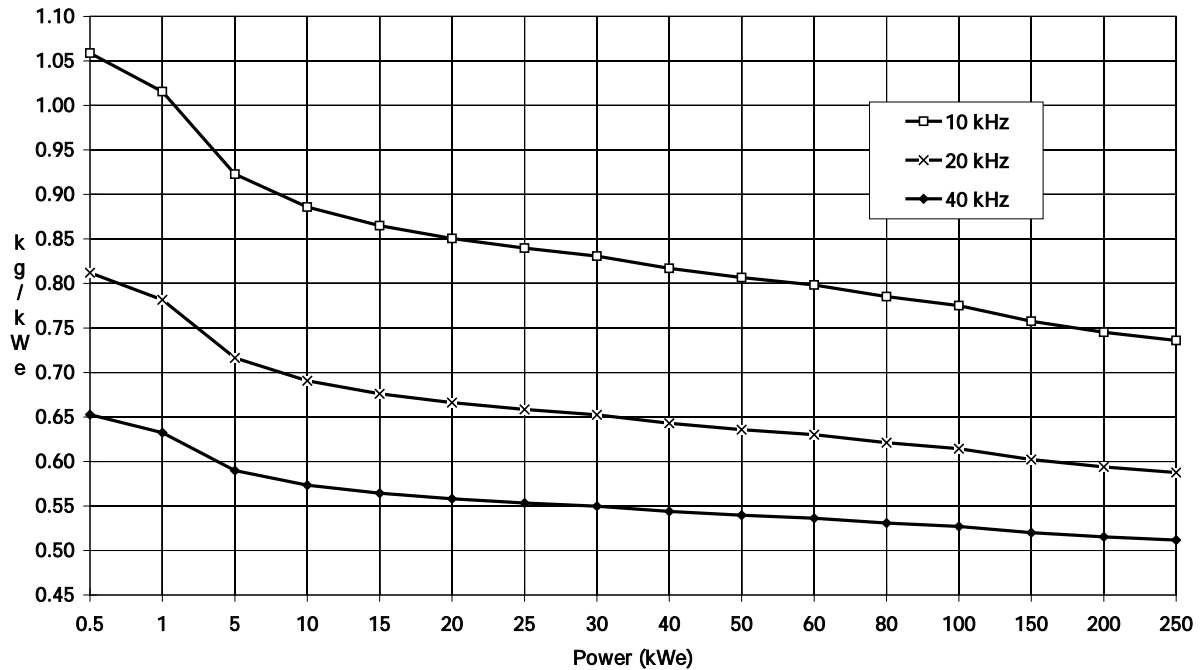
Figure 2: Chopper SPWT vs Power Level
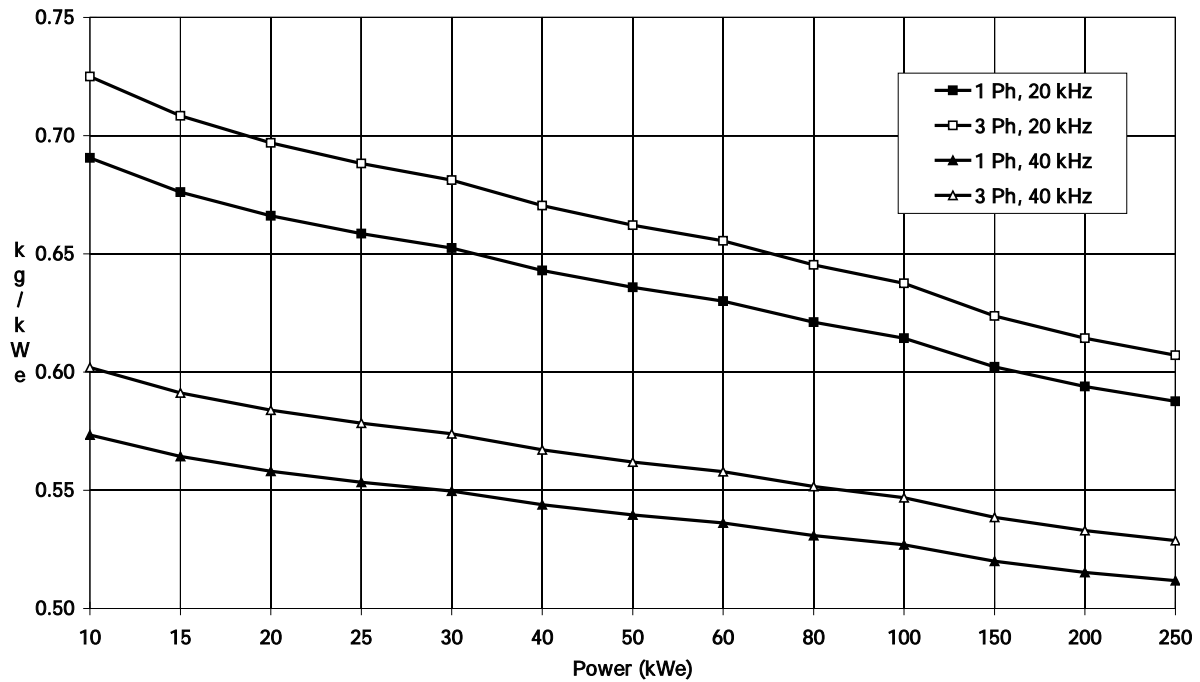
Figure 3: Chopper SPWT vs Power Level - 1 Phase and 3 Phase

The required number of modules is also included in this equation segment. A modular design approach with multiple power modules could be used to enhance reliability. If this approach is used each module would process a percentage of the total assembly output power, and the specific weight of each chopper must be calculated at this power level to obtain an accurate electrical system mass estimate. The masses of the separate choppers are then added together to obtain the mass of the complete assembly.

Voltage Level Factors

$1CSM = 0.645*((EXP0.01/(1-CSE)))/1.5169)*(CSAM/CSRM)*CSP_O*((CSP_O/CSRM)^{-0.065}$

$\quad *(CSV_I/(CSV_I-2))^7*EXP(CSV_I/40000)*(20/CSF)^{0.45}*EXP(CSP_O^{0.1}*CSF/200))$

$3CSM = 0.685*((EXP0.01/(1-CSE)))/1.5169)*(CSAM/CSRM)*CSP_O*((CSP_O/CSRM)^{-0.07}$

$\quad *(CSV_I/(CSV_I-2))^7*EXP(CSV_I/40000)*(20/CSF)^{0.45}*EXP(CSP_O^{0.1}*CSF/200))$

It was necessary to include two factors to cover the full voltage range that will be encountered by a chopper. The first, "$(CSV_I/(CSV_I-2))^7$", addresses the influences on power conductor and switch mass as the voltage level declines. The second, "$EXP(CSV_I/40000)$", covers the mass increases occurring as voltages increase.

Since conduction losses are calculated with the equation I^2R, and current levels rise as voltage declines, the chopper efficiency will be poorer at lower voltage levels[2]. In most designs, these higher losses are partially offset by lowering the resistances of circuit elements. To accomplish this the cross sectional areas of the conductors and switches must be increased, which causes their mass to increase. To obtain proper mass estimates for low voltage choppers, the efficiency parameter that is input into the chopper module should be decreased in accordance with Table 7. Using the values shown here, smooth specific weight versus input voltage curves will be generated for the Weinberg and resonant converter chopper designs. These values reflect the increase in mass and reduction in efficiency that occurs at lower voltages. The specific weight curves generated with these values are shown in Figure 4 for 0.5 and 1 kWe power levels.

Table 7: Efficiency Corrections for Low Voltage Chopper Mass Estimates

Input Voltage (Vdc)	Resonant Chopper Input Efficiency (percent)
120	97.60
110	97.60
100	97.57
90	97.53
80	97.47
70	97.36
60	97.23
50	97.00
40	96.67
30	96.00
20	93.60

High voltage chopper designs will require alternate design approaches. Currently MOSFETs are used most often for chopper switches, although MCTs may become more prominent in the future if their potentially lower forward voltage drop and higher voltage and power capabilities are realized [Ref. 21, 22, 27]. To switch very high voltages, it may be necessary to connect the switch modules in series. Theoretically, since the voltage across a single module is not increased, the insulating requirements and mass of the individual modules are unchanged. In practice, this probably will not be true. Added hardware will be needed to force the switch modules to voltage share and limit parasitic capacitance. Even with this added hardware, the insulation and

---

[2] The equation I^2R also applies in high frequency applications, but the skin effect drives the effective resistance of the conductors up. This increased resistance can be partially offset by employing alternate conductor constructions such as Litz wire, but mass and thermal conduction penalties are incurred. For 20 kHz designs a guideline is a conductor's ac resistance is 1.3 times its dc resistance.

switch ratings may need to be increased to tolerate uneven or improperly applied voltages. It is expected that the switch synchronization problems that are a concern in any chopper design will be exacerbated in a high voltage design. Unfortunately, little information is available on actual design techniques since there is not much demand for a high voltage chopper at the present time and very little space suitable hardware is rated for high voltage applications.
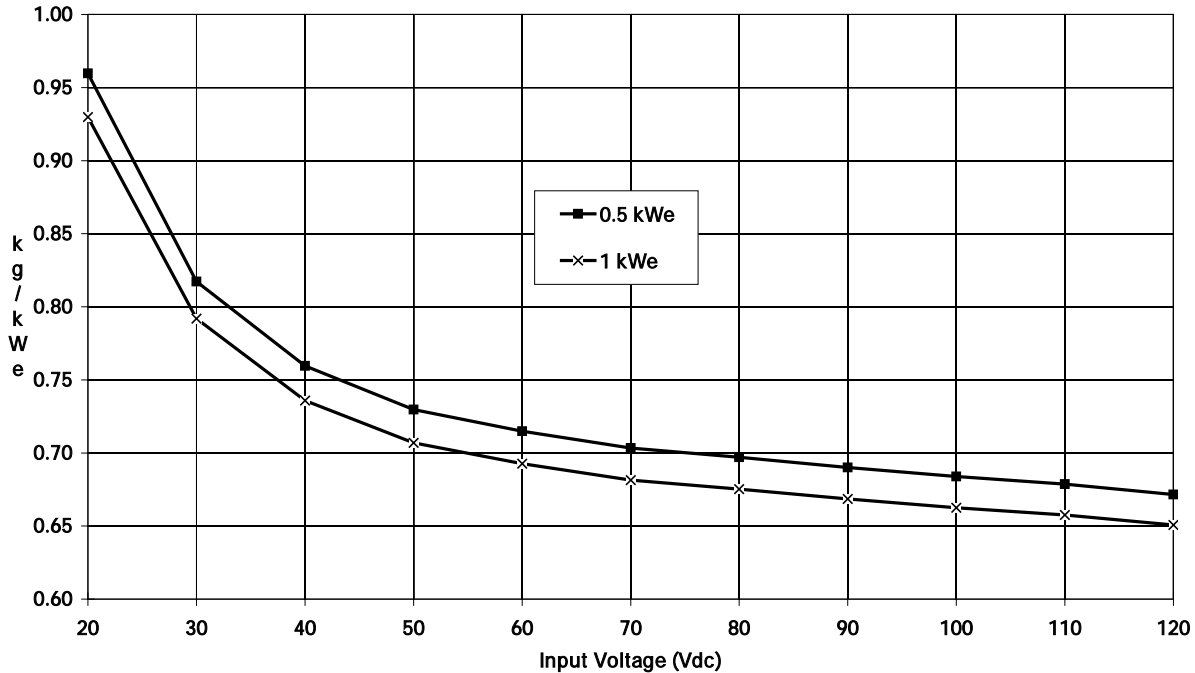
Figure 4: Chopper SPWT vs Voltage – Low Voltage Region

General Electric evaluated a 1 MWe inverter design for NASA [Ref. 28]. It used a module containing four parallel strings, each containing 100 amp MCTs. This module is rated for 200 amps total. Each string was composed of ten 1000 volt MCTs stacked in series to provide a 5000 volt switching potential. Based on the design results, the operating limits of the composite assembly were lower than the sum of the individual parts. Topology and component design modifications are necessary to insure proper voltage and current sharing between MCTs. These constraints result in size, mass, and loss penalties. It will also be challenging to achieve synchronized switching with these 40 MCTs at high frequencies. Poor synchronization will lead to excessive losses in the snubber circuits and result in a low switching efficiency.

Based on the items previously discussed, the following observations were made about high voltage chopper designs and masses. The data obtained to date from the high power inverter study indicates high voltage designs will incur mass penalties to insure voltage sharing and limit parasitic capacitance. The switch ratings and insulation levels will probably need to be increased to guard against potential voltage imbalances. Even power conditioning devices as rugged as transformers rise in mass as voltage levels increase. It is expected that the mass of a chopper will rise at a faster rate with voltage than a transformer since its components tend to be much more sensitive to over voltage conditions and voltage spikes. Based on this reasoning, the factor underlined in the above equation was developed. Specific weight curves for high voltage chopper designs obtained from this equation are shown in Figure 5 at 10, 100, and 250 kWe power levels.
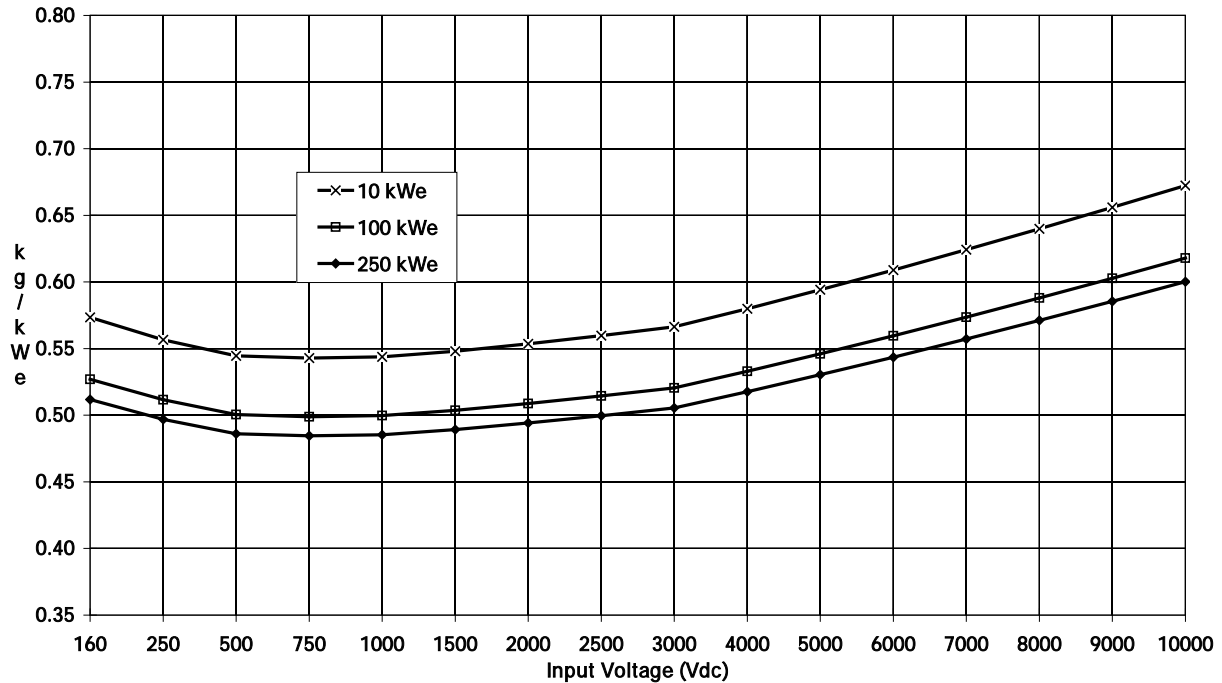
Figure 5: Chopper SPWT vs Voltage – High Voltage Region

Frequency Factors

1CSM=0.645*((EXP0.01/(1-CSE)))/1.5169)*(CSAM/CSRM)*CSP_O*((CSP_O/CSRM)$^{-0.065}$

*(CSV$_I$/(CSV$_I$-2))^7*EXP(CSV$_I$/40000)*$\underline{(20/CSF)^{0.45}}$*$\underline{EXP(CSP_O{}^{0.1}*CSF/200))}$

3CSM=0.685*((EXP0.01/(1-CSE)))/1.5169)*(CSAM/CSRM)*CSP_O*((CSP_O/CSRM)$^{-0.07}$

*(CSV$_I$/(CSV$_I$-2))^7*EXP(CSV$_I$/40000)*$\underline{(20/CSF)^{0.45}}$*$\underline{EXP(CSP_O{}^{0.1}*CSF/200))}$

The masses of the chopper switches are largely unaffected by changes in frequency. But, the masses of the current feed inductor in the Weinberg converter and the resonant converter tank inductor and capacitor are impacted by frequency. The critical inductance in the Weinberg converter is directly proportional to the switching frequency. The resonant frequency of a resonant circuit is calculated by the equation:

$$2\pi f=1/(L*C)^{0.5}$$

Where: f = the resonant frequency in hertz
L = the circuit inductance in henries
C = the circuit capacitance in farads

From this equation one can see that the inductor and capacitor values, and their associated masses, are a function of frequency. While this equation is correct, it does not convey all the factors that must be considered in a converter design. It indicates the mass of the tank hardware will change linearly in a direction opposite to the frequency change. This is not entirely true. Other factors such as parasitic reactances in the circuit and hysteresis and eddy current losses must be considered. Depending on the switching or resonant frequency, they may have a strong influence on the converter design.

At low frequencies, parasitic reactances are small and hysteresis and eddy current effects are minor. This allows more common, often lighter weight component types and materials to be employed. Other converter topologies may also be used because the mass increases occurring in the Weinberg converter inductor or

the tank hardware of a resonant converter may be unacceptable at low frequencies. A PWM converter topology may be better. Assuming a designer selects the topology that minimizes mass and considering the effects of frequency and circuit parasitics, chopper mass estimates were generated at several frequencies. These estimates were extrapolated from detailed design estimates and existing designs [Ref. 14, 15, 17, 23, 24, 26]. They were utilized to develop the frequency factors contained in the chopper mass equations. Figure 6 compares the specific weights obtained with these equations for single- and 3-phase designs at 10 and 100 kWe power levels for frequencies ranging from 1 to 50 kHz. Note that the 3-phase design is slightly heavier over the full frequency range due to its higher parts count.

As the switching or resonant frequency rises, the effects of parasitic reactances and hysteresis and eddy current losses become more pronounced and strongly influence the converter design. Its anticipated they will largely offset supposed improvements and cause the design to reach a point where its difficult to obtain further mass reductions by increasing the switching frequency. The product of power and frequency approaches a constant value. This is the reason the mass of the chopper circuit levels out above 60 kHz and may actually begin to rise at frequencies beyond this point. Since most of the available design information was based on 20 kHz and 40 kHz inversion frequencies, the equations were calibrated to yield good results at these frequencies. The single-phase Weinberg converter topology specific weight curves shown in Figure 7 depict the strong influence frequency has on chopper mass and show the specific weight of a chopper approaches a constant value of about 0.55 kg/kWe as the frequency and power level rises.
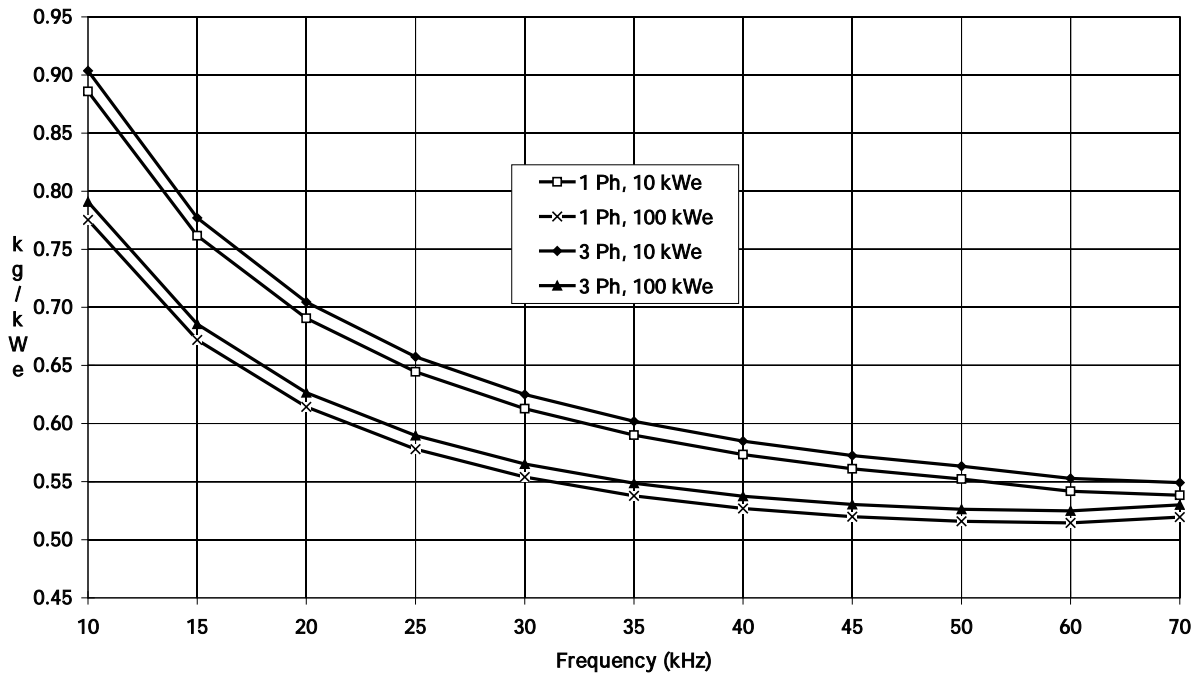
Figure 6: Chopper SPWT vs Frequency – Single & 3 Phase Designs

Before leaving this subject, it should be noted that at high power and frequency levels fewer switching devices are available. Therefore, even if there isn't a circuit limitation that precludes using a high resonant frequency, the availability of suitable parts may force the designer to settle for a lower frequency design. To make higher operating frequencies practical, high power switching devices with faster switching speeds are under development. For example, the 0.1-0.2 μsec switching times being projected for MCTs represent a significant improvement in high power switching. Parasitic inductive and capacitive reactances
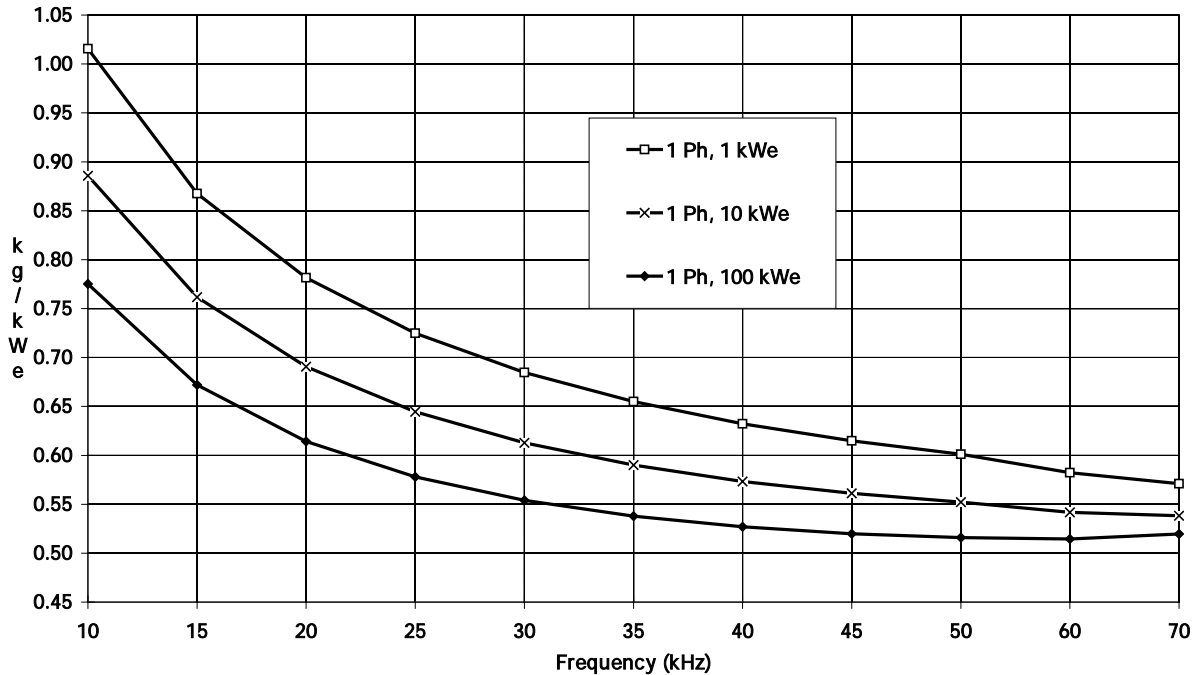
Figure 7: Chopper SPWT vs Frequency – Single Phase Designs

though, will still drive the allowable switching frequency downward as power levels rise. The point is although the model will generate a mass estimate for a high power chopper operating at a high frequency, one must consider whether the design is really practical. Table 8 is offered as a guide to assist the model user in selecting inversion frequencies appropriate for future component power levels.

Table 8: Converter Frequency Input Guide

Converter Power Level	Suggested Inversion Frequency Limit
500 Watts to 1 kWe	100 kHz
1 to 5 kWe	80 kHz
5 to 20 kWe	55 kHz
20 to 40 kWe	50 kHz
40 to 80 kWe	40 kHz
80 to 150 kWe	35 kHz
Greater than 150 kWe	30 kHz

3.3 INVERTER AND STANDARD TRANSFORMER MODELS

Two types of transformers may be used in a PMAD system depending on the architecture and user needs: inverter transformers that are an integral part of a converter circuit, and standard transformers. These transformers will be significantly different because the operating frequencies, and waveform harmonic content are different for the two applications. For this reason, it was necessary to create two model types to address the characteristics of the two designs. The inverter transformer design will be presented first because it tends to be more involved and cover a wider range of design considerations. The standard transformer discussion will rely heavily on the information and rationale presented in the inverter transformer section. The equations previously developed for the two types of transformers in 1992 still

generate masses consistent with projected transformer designs, but minor changes were made in the efficiency and frequency sections to reflect the improved efficiencies possible at high frequencies due to thinner laminations and improvements in magnetic material fabrication processes.

3.3.1 Inverter Transformer Stage Model

The inverter transformer stage is contained in the inverter, dc/dc converter, and frequency converter models. An inverter transformer follows or precedes a chopper section. It is used to step up or down the input voltage, and/or to provide isolation between the input and output.

Although transformer design guidelines have been established to deal with most operating requirements; there are many practical design and materials limitations that continue to hinder transformer fabrication. These design difficulties are more pronounced at high frequencies, and high frequency designs proposed for high power and/or high voltage levels are particularly complicated. However, established transformer design principles can provide insight into how these problems might be solved and in turn the evolution of transformer design. For this reason, design manuals and technical bulletins were frequently referred to to guide the equation development [Ref. 29, 30, 31, 32, 33]. The variables that will be used in the inverter transformer stage model discussion are shown in Table 9.

Table 9: Inverter Transformer Model Variable Definitions

1ITSM	Single-Phase Inverter Transformer Stage Mass
3ITSM	3-Phase Inverter Transformer Stage Mass
ITSE	Inverter Transformer Stage Efficiency (99.2%)
ITSAM	Inverter Transformer Stage Available Modules
ITSRM	Inverter Transformer Stage Required Modules
ITSP$_O$	Inverter Transformer Stage Power Output (kWe)
ITSV$_I$	Inverter Transformer Stage Voltage Input (Vrms)
ITSV$_O$	Inverter Transformer Stage Voltage Output (Vrms)
ITSF	Inverter Transformer Stage Frequency (kHz)

The equations used to estimate the mass of single-phase and 3-phase transformers are shown below. Sections of these equations will be discussed individually to identify the parts that correspond to specific parameters. The subsequent paragraphs will explain the development of the factors and constants contained in these equations. The factor being discussed will be underlined and accompanying graphs will be used to illustrate results and trends determined during this study.

Mass Coefficient

$$1ITSM = \underline{1.27}*((EXP(0.0048/(1-ITSE)))/1.8221)*(ITSAM/ITSRM)*ITSP_O*((ITSP_O/ITSRM)^{-0.08}$$

$$*EXP(ITSV_I/200000)*EXP(ITSV_O/200000)*ITSF^{-0.47}+(ITSF/300)^{1.4}-(200/ITSP_O)^{0.03}*$$

$$((MAX(0,ITSF-30))/300)^{1.7})$$

$$3ITSM = \underline{2.75}*((EXP(0.0048/(1-ITSE)))/1.8221)*(ITSAM/ITSRM)*ITSP_O*((ITSP_O/ITSRM)^{-0.25}$$

$$*EXP(ITSV_I/200000)*EXP(ITSV_O/200000)*ITSF^{-0.47}+(ITSF/300)^{1.4}-(200/ITSP_O)^{0.03}*$$

$$((MAX(0,ITSF-30))/300)^{1.7})$$

The constants, "1.27" and "2.75", were determined by calibrating these mass equations against the masses of known inverter transformer designs. They are designed to yield acceptable mass estimates

over the ranges specified for each of the input parameters. These constants are partially determined by the wave form factor[3] and are 10% larger than the corresponding constants contained in the standard transformer equation. Because the chopper rapidly switches a dc input to fabricate an ac output, the inverter transformer input is not a smooth sinusoid and it exhibits many square wave characteristics. Square waves have a high harmonic content; consequently, they generate higher losses in the transformer core. Calculations and design procedures contained in design manuals indicate an inverter transformer core must be sized 10% larger to lower the core flux density and manage the added losses resulting from the square wave harmonics [Ref. 29, 30, 31].

Efficiency Factor

$$1ITSM=1.27*\underline{((EXP(0.0048/(1-ITSE)))/1.8221)}*(ITSAM/ITSRM)*ITSP_O*((ITSP_O/ITSRM)^{-0.08}$$

$$*EXP(ITSV_I/200000)*EXP(ITSV_O/200000)*ITSF^{-0.47}+(ITSF/300)^{1.4}-(200/ITSP_O)^{0.03}*$$

$$((MAX(0,ITSF-30))/300)^{1.7})$$

$$3ITSM=2.75*\underline{((EXP(0.0048/(1-ITSE)))/1.8221)}*(ITSAM/ITSRM)*ITSP_O*((ITSP_O/ITSRM)^{-0.25}$$

$$*EXP(ITSV_I/200000)*EXP(ITSV_O/200000)*ITSF^{-0.47}+(ITSF/300)^{1.4}-(200/ITSP_O)^{0.03}*$$

$$((MAX(0,ITSF-30))/300)^{1.7})$$

The factor underlined above is used to estimate the mass effects that will occur when the transformer efficiency is changed. To reduce losses and increase transformer efficiency, the flux density in the core is lowered and the resistance of the windings is reduced. A lower core flux density will reduce core losses; however, Faraday's law shows the core effective cross sectional area must be increased to compensate.

$$E=4B_mA_cNfx10^{-5} \text{ (square wave)}$$

where: E = applied voltage (rms)
  4 = square wave form factor
  B_m = flux density in gauss
  A_c = core effective cross sectional area in cm^2
  N = number of primary turns
  f = frequency in kHz

This naturally increases core mass. To reduce winding resistance and losses, the winding conductor area must be increased. This can be seen from the equation used to calculate conductor electrical resistivity.

$$R=\rho l/A$$

where: R = conductor resistance
  ρ = volume resistivity ($\mu\Omega{\times}cm$)
  l = length in cm
  A = cross sectional area in cm^2

To raise the transformer efficiency from 99.2% to 99.6%, the transformer losses need to be cut in half. Core loss versus flux density tables contained in transformer design manuals indicated a 25% reduction in flux density would reduce losses 50%. To achieve this the core cross sectional area and associated mass would increase 33%. To cut the winding losses in half, the conductor area would need to double. This doubles the conductor mass. Summing only these two effects and using a ratio of about 2:1 for winding mass to core mass with a 20 kHz transformer results in a transformer mass increase of about 75%. However, increasing the core size further increases in the conductor mass due to the added length of the turns; and the larger winding size will enlarge the core window. Clearly the core and winding dimensions

---

[3] The form factor is the ratio of the root-mean-square value to the average absolute value, averaged over a full period of the waveform.

are interrelated. After including estimates for these interdependent influences, a mass increase of 85% was obtained. The trends reflected by the resulting efficiency factor are shown in Figure 8 for 10 and 20 kHz frequencies and 10 and 100 kWe transformer power levels.
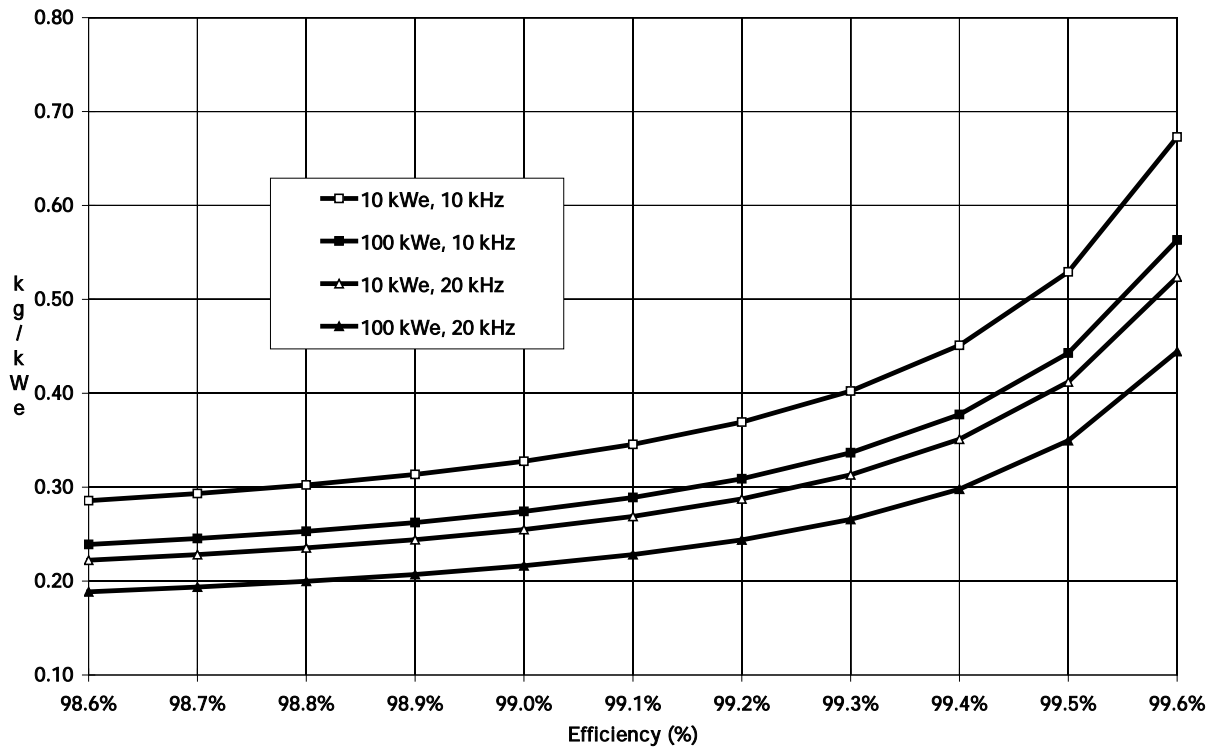
Figure 8: Inverter Transformer SPWT vs Efficiency

Redundancy Factor

$1ITSM=1.27*((EXP(0.0048/(1-ITSE)))/1.8221)*\underline{(ITSAM/ITSRM)}*ITSP_O*((ITSP_O/ITSRM)^{-0.08}$

$*EXP(ITSV_I/200000)*EXP(ITSV_O/200000)*ITSF^{-0.47}+(ITSF/300)^{1.4}-(200/ITSP_O)^{0.03}*$

$((MAX(0,ITSF-30))/300)^{1.7})$

$3ITSM=2.75*((EXP(0.0048/(1-ITSE)))/1.8221)*\underline{(ITSAM/ITSRM)}*ITSP_O*((ITSP_O/ITSRM)^{-0.25}$

$*EXP(ITSV_I/200000)*EXP(ITSV_O/200000)*ITSF^{-0.47}+(ITSF/300)^{1.4}-(200/ITSP_O)^{0.03}*$

$((MAX(0,ITSF-30))/300)^{1.7})$

The above factor addresses the mass impacts resulting from the use of a modular design to enhance reliability. The available modules is the actual number of modules present in the component; the required modules is the actual number of modules required to achieve full output power. For example, assume a design requires 4/3 redundancy to meet the reliability requirements. Each channel is rated to handle 33% of the power, but 4 channels are available. This factor shows a 4/3 redundancy design will be 33% heavier. Only 3 channels are needed to supply full power; the fourth channel represents the mass penalty incurred to enhance reliability.

Power Level Multiplier

$1ITSM=1.27*((EXP(0.0048/(1-ITSE)))/1.8221)*(ITSAM/ITSRM)*\underline{ITSP_O}*((ITSP_O/ITSRM)^{-0.08}$

$*EXP(ITSV_I/200000)*EXP(ITSV_O/200000)*ITSF^{-0.47}+(ITSF/300)^{1.4}-(200/ITSP_O)^{0.03}*$

$$((\text{MAX}(0,\text{ITSF}-30))/300)^{1.7})$$

$$3\text{ITSM}=2.75*((\text{EXP}(0.0048/(1-\text{ITSE})))/1.8221)*(\text{ITSAM}/\text{ITSRM})*\underline{\text{ITSP}_O}*((\text{ITSP}_O/\text{ITSRM})^{-0.25}$$

$$*\text{EXP}(\text{ITSV}_I/200000)*\text{EXP}(\text{ITSV}_O/200000)*\text{ITSF}^{-0.47}+(\text{ITSF}/300)^{1.4}-(200/\text{ITSP}_O)^{0.03}*$$

$$((\text{MAX}(0,\text{ITSF}-30))/300)^{1.7})$$

The equations can be used to calculate either transformer mass or transformer specific weight. When the above multiplier is included, the calculations will yield the transformer mass. To obtain the transformer specific weight, simply remove this multiplier.

Power Level Factor

$$1\text{ITSM}=1.27*((\text{EXP}(0.0048/(1-\text{ITSE})))/1.8221)*(\text{ITSAM}/\text{ITSRM})*\text{ITSP}_O*\underline{((\text{ITSP}_O/\text{ITSRM})^{-0.08}}$$

$$*\text{EXP}(\text{ITSV}_I/200000)*\text{EXP}(\text{ITSV}_O/200000)*\text{ITSF}^{-0.47}+(\text{ITSF}/300)^{1.4}-(200/\text{ITSP}_O)^{0.03}*$$

$$((\text{MAX}(0,\text{ITSF}-30))/300)^{1.7})$$

$$3\text{ITSM}=2.75*((\text{EXP}(0.0048/(1-\text{ITSE})))/1.8221)*(\text{ITSAM}/\text{ITSRM})*\text{ITSP}_O*\underline{((\text{ITSP}_O/\text{ITSRM})^{-0.25}}$$

$$*\text{EXP}(\text{ITSV}_I/200000)*\text{EXP}(\text{ITSV}_O/200000)*\text{ITSF}^{-0.47}+(\text{ITSF}/300)^{1.4}-(200/\text{ITSP}_O)^{0.03}*$$

$$((\text{MAX}(0,\text{ITSF}-30))/300)^{1.7})$$

As transformer size increases, the core can be better utilized, and the current density increased in the windings to reduce their cross sectional area. These economies of scale result in a transformer specific weight reduction at higher power levels. The "Standard Handbook for Electrical Engineers" indicated the specific weight of a 3-phase transformer would decline by the 0.25 power with power level [Ref. 34]. This was verified for 60 Hz transformers by referring to the transformer masses contained in a vendor catalogue [Ref. 35]. This factor was also assumed to hold for high frequency 3-phase transformer designs, but there wasn't any mass information available to confirm it. The same vendor catalogue showed the specific weight of a low frequency single-phase transformer would decline by the 0.08 power with power level. Mass figures obtained from another source indicated this factor also held true for high frequency single-phase transformer designs [Ref. 29]. The specific weights of single- and 3-phase transformer designs are compared in Figure 9. This figure shows a 1 kHz single-phase transformer will weigh less than a 3-phase one until a power level of about 100 kWe is reached. This value was projected from information contained in a vendor catalogue and a transformer design handbook [Ref. 35, 36]. The mass cross over point for high frequency single- and 3-phase transformers occurs at a higher power level. The mass gains achievable with a change from a single- to 3-phase design occur mainly in the core. These gains are expected to be less at higher frequencies because the core mass occupies a smaller percentage of the transformer mass. With this assumption incorporated into the equations, Figure 9 shows that a single-phase 20 kHz transformer design is more weight efficient below 250 kWe. Figure 10 shows only single-phase transformer designs and allows specific weight comparisons at several frequencies over a wide power range. Figure 11 also depicts single-phase designs, but it concentrates on the power levels and frequencies expected to be used most often in inverter transformer designs.

Voltage Level Factors

$$1\text{ITSM}=1.27*((\text{EXP}(0.0048/(1-\text{ITSE})))/1.8221)*(\text{ITSAM}/\text{ITSRM})*\text{ITSP}_O*((\text{ITSP}_O/\text{ITSRM})^{-0.08}$$

$$*\underline{\text{EXP}(\text{ITSV}_I/200000)}*\underline{\text{EXP}(\text{ITSV}_O/200000)}*\text{ITSF}^{-0.47}+(\text{ITSF}/300)^{1.4}-(200/\text{ITSP}_O)^{0.03}*$$

$$((\text{MAX}(0,\text{ITSF}-30))/300)^{1.7})$$

$$3\text{ITSM}=2.75*((\text{EXP}(0.0048/(1-\text{ITSE})))/1.8221)*(\text{ITSAM}/\text{ITSRM})*\text{ITSP}_O*((\text{ITSP}_O/\text{ITSRM})^{-0.25}$$

$$*\underline{\text{EXP}(\text{ITSV}_I/200000)}*\underline{\text{EXP}(\text{ITSV}_O/200000)}*\text{ITSF}^{-0.47}+(\text{ITSF}/300)^{1.4}-(200/\text{ITSPo})^{0.03}*$$

$((MAX(0,ITSF-30))/300)^{1.7})$

Figure 9: Inverter Transformer SPWT – 1 Phase vs 3 Phase
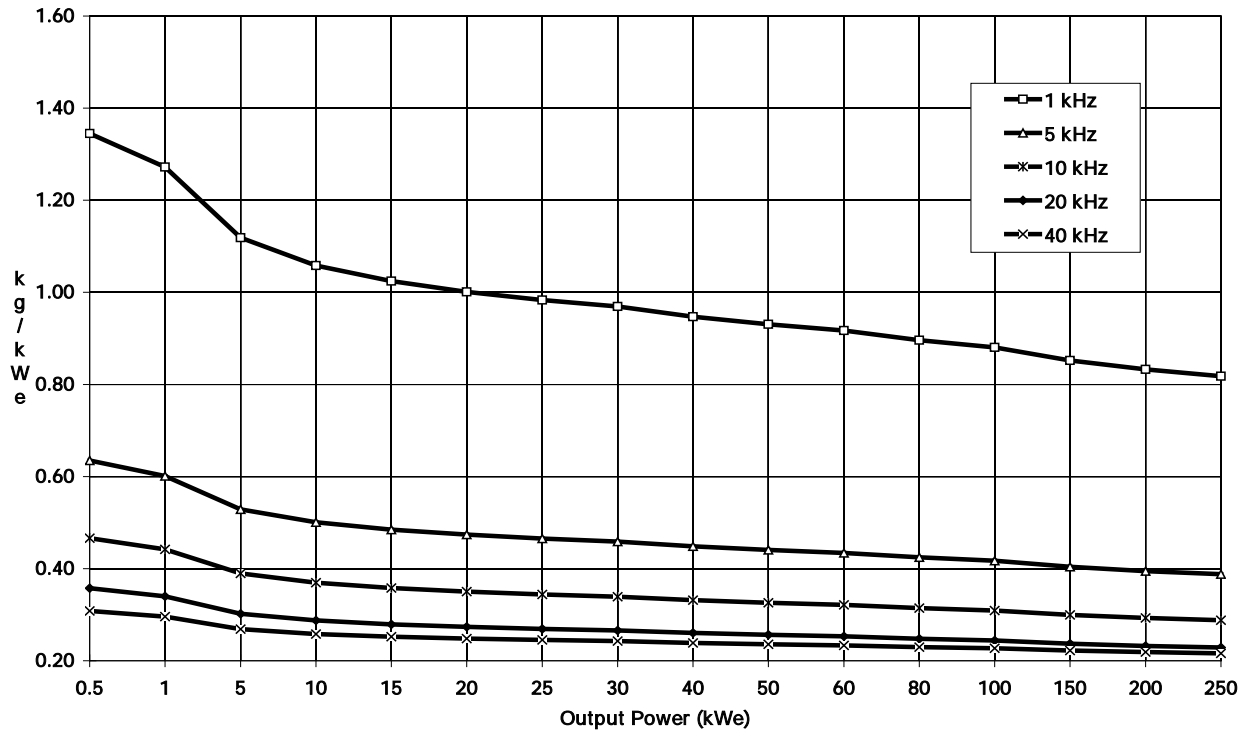
Figure 10: Inverter Transformer SPWT vs Power (Wide Range)
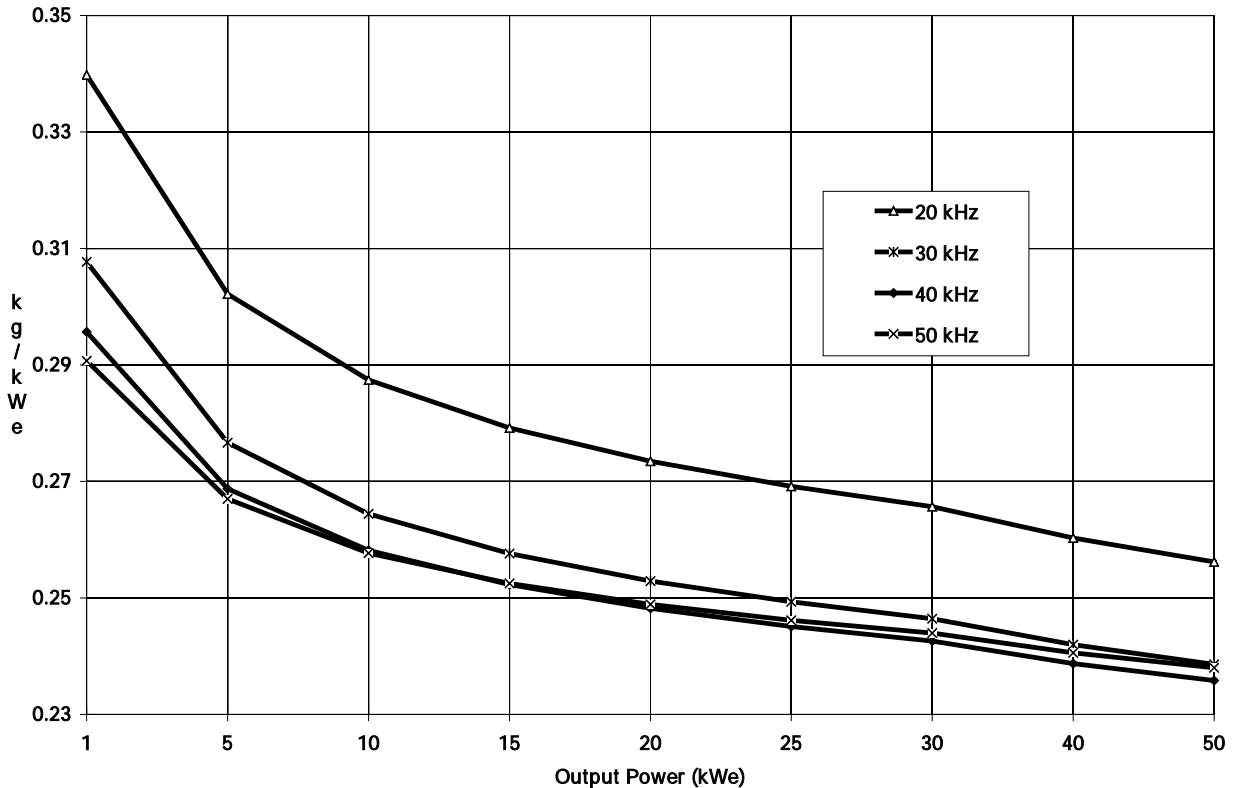
Figure 11: Inverter Transformer SPWT vs Power (Narrow Range)

The voltage factor development had to consider two factors, the influence of insulation stress on transformer mass as voltage rises, and high voltage transformer design limitations occurring as frequency rises. Only the insulation stress effects will be addressed initially. It is mainly the volts per turn not the terminal voltage that determines the stress placed on the insulation and consequently its thickness. The thickness of the insulation can be calculated from its dielectric strength, usually expressed in volts per mil. For typical operating ranges, the dielectric strength of most insulating materials is reasonably constant regardless of the transformer frequency. This information indicates the voltage mass effects occurring at low frequency also apply at higher frequencies.

This observation is important since the information on high voltage transformers is limited to low frequency designs. Low frequency, commercial transformer data showed transformer specific weight rose slowly until voltage levels approached 20 kV. This is well above the 10 kV voltage level expected to be used in most space applications. The minor increase in specific weight was attributed to the additional insulation needed to prevent insulation breakdown between windings, and the need for high voltage terminations. This added winding insulation will increase the winding cross sectional area and necessitate a slightly larger core window area. However, the impact is minor. In addition, the insulation mass is a very small percentage of the total transformer mass, so it can increase substantially and the transformer mass will only change slightly. The information obtained from this analysis was sufficient to develop a transformer voltage factor, but it was not enough to know how to properly apply it. The voltage factor determined at this point is shown for different transformer power levels in Figure 12. It shows transformer mass will only rise about 5% when the primary or secondary voltage is increased from 20 to 10,000 Vrms.

It was previously stated that the volts per turn determined the insulation thickness and that the dielectric strength of an insulating material is basically independent of frequency. However, frequency does influence the calculated volts per turn and this ultimately impacts the voltage characteristics of the com-

plete transformer. Referring back to Faraday's law and rearranging the terms, one can see that the volts per turn is a function of frequency.
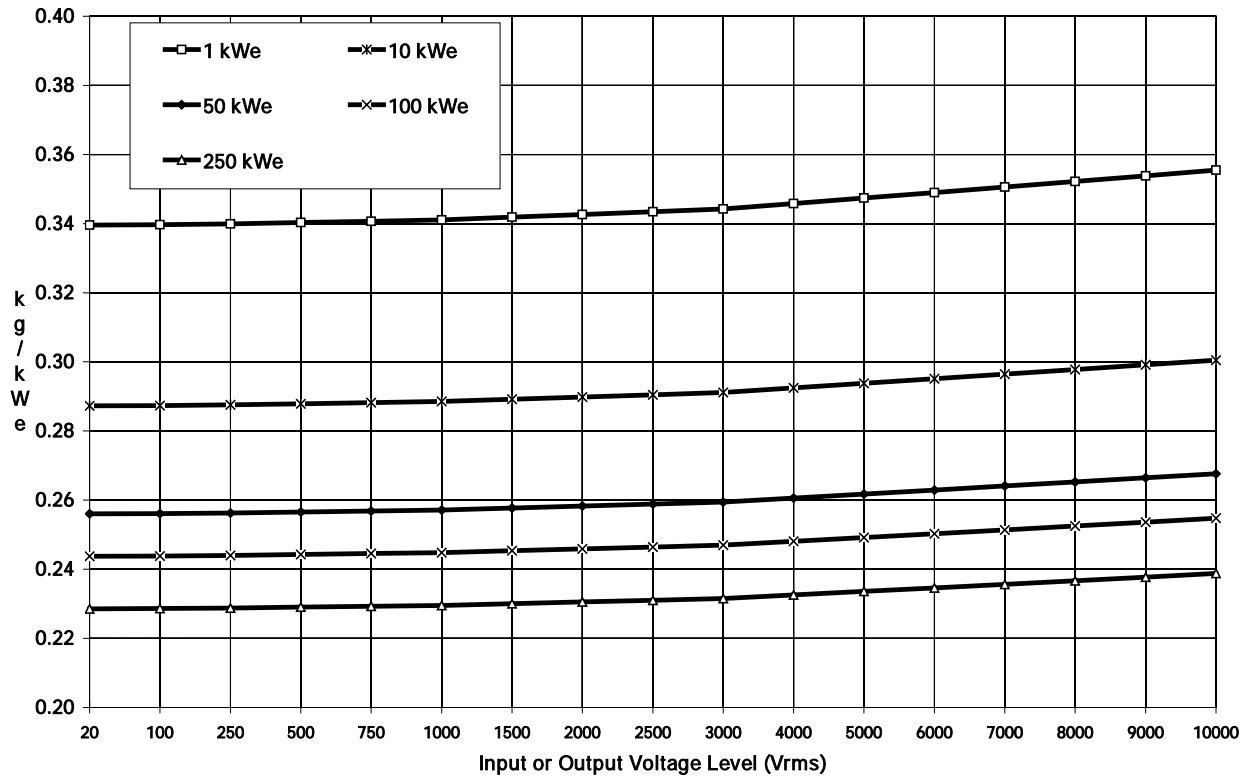
Figure 12: **Inverter Transformer SPWT vs Voltage**

$$E/N = \ (K, B_m, A_c, f)$$

where: E = applied voltage (rms)
        K = form factor constant
        B_m = flux density
        A_c = core effective cross sectional area
        N = number of primary turns
        f = frequency

Because of nonlinearities in transformer design, particularly in core material characteristics, the product of core cross sectional area and flux density can not be linearly changed to accommodate an increasing frequency. This situation indicates a designer will encounter voltage restraints as frequency rises. To verify this conclusion, a transformer design analysis was conducted and transformer point designs were evaluated. They showed that the volts per turn will increase significantly when moving from 60 Hz to 20 kHz, possibly enough to increase the insulation level on the turns. Thicker insulation will lead to greater separation distances between the primary and secondary windings, and reduce transformer coupling. This results in higher leakage flux. Because leakage flux increases if additional winding insulation is needed and the effects attributable to turn-to-turn capacitance rise with frequency, a high frequency transformer tends to have more reactance. High voltage transformers have more turns, which increases the total turn-to-turn or winding capacitance. Although these effects are compounding, they are not enough to preclude the design of a high voltage, high frequency transformer. But they do complicate its design and emphasize the need to minimize turn-to-turn capacitance.

It was already mentioned that a high voltage transformer has a higher winding capacitance; and transformer coupling is poorer if thicker winding insulation is required. Leakage inductance also rises as

the distance between the windings increases. To maximize transformer coupling and minimize leakage inductance, the primary and secondary windings must be in close proximity. However, this is difficult to accomplish in a transformer that has a high voltage ratio because thick insulation levels are required to prevent primary to secondary voltage breakdown. Most loads require a relatively low voltage; therefore, the voltage will need to be stepped down further in a system that uses high voltage transmission. This forces the distribution transformers to utilize higher voltage ratios and leads to higher leakage inductance.

Oscillations in the power system, a phenomenon known as ringing, may result from the leakage capacitance and inductance present in high voltage transformers. Ringing occurs because the parasitic capacitive and inductive reactances transfer energy back and forth during operation and after turn off until it is damped out by element resistances. This increases transformer losses and may cause damage if high voltage spikes result. Ringing is frequency related because the effects attributable to parasitic capacitive and inductive reactances grow as frequency rises. Power may also be a factor because it may make it more difficult to limit stray capacitance and inductance due to fabrication constraints resulting from the transformer's larger physical size.

Ringing limits the acceptable voltage ratio of the transformer. In a discussion with John Beiss, he indicated the step ratio of a present 20 kHz transformer is probably limited to about 6 or 7 due to ringing. However, a transformer design generated by Space Power Incorporated exhibited a voltage ratio of 10, 180 divided by 18 Vrms. Its demonstrated efficiency of 99.1% indicates this step ratio is feasible, although it will be harder to achieve good operating characteristics at higher voltages [Ref. 37]. Commercial transformer data indicates a step ratio of 145 is obtainable with a 60 Hz transformer. Using these two values, an empirical relationship was developed to estimate reasonable step ratios for transformers at several different frequencies. This relationship is shown below and it was used to generate the values shown in Table 10. This table is only offered as a guide; its main intent is to point out the need to include step ratio effects when evaluating a high voltage power transmission design. It shows that it may be necessary to connect transformers in series to utilize a high voltage transmission system with input or output components that require fairly low voltages, especially if high frequency distribution is employed.

$$SR = 39.7 * f^{-0.46}$$

where: SR = acceptable step ratio
        f = frequency in kHz

Table 10: Transformer Step Ratio Guidelines

Transformer Frequency (kHz)	Suggested Step Ratio Limit
0.060	145
0.070	135
0.400	60
1	40
5	19
10	14
15	11
20	10
25	9
30	8
35	8
40	7
45	7
50	7

Frequency Factors

$$1ITSM=1.27*((EXP(0.0048/(1-ITSE)))/1.8221)*(ITSAM/ITSRM)*ITSP_O*((ITSP_O/ITSRM)^{-0.08}$$

$$*EXP(ITSV_I/200000)*EXP(ITSV_O/200000)*\underline{ITSF^{-0.47}+(ITSF/300)^{1.4}-(200/ITSP_O)^{0.03}*}$$

$$\underline{((MAX(0,ITSF-30))/300)^{1.7})}$$

$$3ITSM=2.75*((EXP(0.0048/(1-ITSE)))/1.8221)*(ITSAM/ITSRM)*ITSP_O*((ITSP_O/ITSRM)^{-0.25}$$

$$*EXP(ITSV_I/200000)*EXP(ITSV_O/200000)*\underline{ITSF^{-0.47}+(ITSF/300)^{1.4}-(200/ITSP_O)^{0.03}*}$$

$$\underline{((MAX(0,ITSF-30))/300)^{1.7})}$$

Transformer core mass declines with increasing frequency. Faraday's law shows the flux density required to generate a voltage is lower at a higher frequency. Because the flux density is lower, the transformer core volume and mass are reduced. Winding mass also declines because the mean length of the turns is less. However, core mass does not decrease linearly with frequency as Faraday's law appears to indicate. Alternate core materials must be employed at higher frequencies to hold down losses. While these materials are more efficient, they must be operated at lower flux densities. For transformer operating frequencies ranging from 10 to 60 kHz, the selected core materials might progress from 50-50 Ni-Fe, to Permalloy, to Supermalloy, to Metglas. During this materials progression, the allowable flux density will roughly decline from about 10,000 to 2,000 Gauss.

In addition to material limitations, other factors must be addressed during a transformer design. Thermal management considerations may limit how much the core size can be reduced. The surface area of a transformer must be sufficient to allow internally generated heat to be conducted away. At high frequencies, roughly above 60 kHz, another set of effects begins to dictate the size of a power transformer core. The eddy current and hysteresis losses become high enough to actually drive the core volume and mass upward. This seems to be where the greatest advancement has been in recent years and it has allowed circuit designers to use higher switching frequencies to lower transformer mass. This has enabled higher power inverter transformer frequencies to increase from 20 to 50 kHz, to 30 to 60 kHz. At high power levels, 50 kWe and above for example, the preferred frequency is probably in the range of 30 to 40 kHz. For power levels below 20 kWe, the optimum frequency can range from 40 kHz all the way up to 80 kHz for a 1 to 2 kWe transformer.

To determine how transformer mass declines as frequency is increased, inverter transformer mass estimates were examined at 1, 2, 5, 10, 20, 40, and 60 kHz [Ref. 14, 17, 29, 30, 31, 32]. Based on these designs, the mass gains occurring as frequency is increased are shown in Figure 13 for several power levels. Figure 14 concentrates on the frequencies envisioned to be used for most spaced based inverter transformer designs. It shows the optimum design frequency shifts downward as the transformer power level rises. This reflects a feature that has been incorporated into the transformer mass equations.

3.3.2 Standard Transformer Stage Model

The standard transformer stage is contained in the transformer, and transformer/static rectifier models. Standard ac transformers will be used in ac power transmission systems primarily at the user end to step down a high transmission voltage to a level suitable for secondary distribution. Standard ac transformers may also follow an alternator or inverter output in certain cases. However, this will not be as common because alternators can provide nearly any voltage desired and inverters and frequency converters will probably contain their own integral inverter transformer stage. Transformers following an alternator will experience frequencies less than 5 kHz. If the system utilizes inverters or frequency converters to change the characteristics of the power source, the transformers will probably be designed for frequencies between 20 and 50 kHz. The type of ac waveform encountered should be a smooth sinusoid with a low harmonic content. A pure sinusoid minimizes transformer core losses because the added eddy current and hysteresis losses resulting from high frequency harmonics are not present.
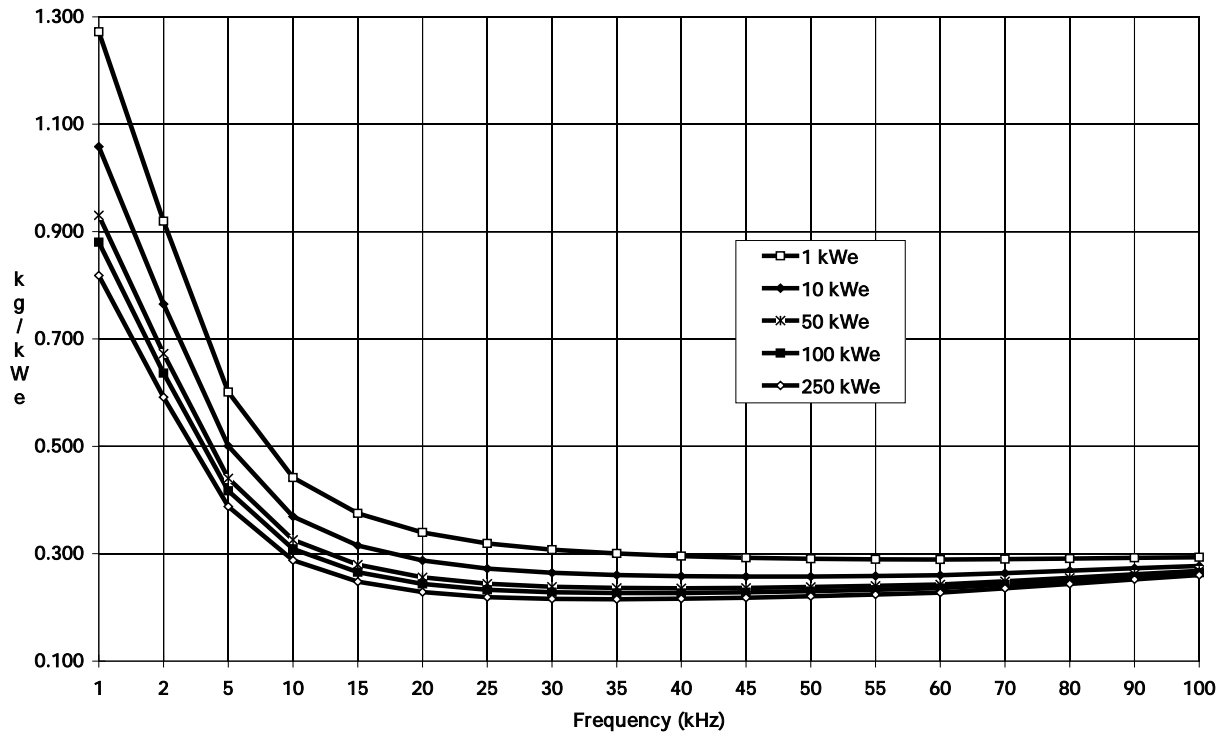
Figure 13: Inverter Transformer SPWT vs Frequency (Wide Range)
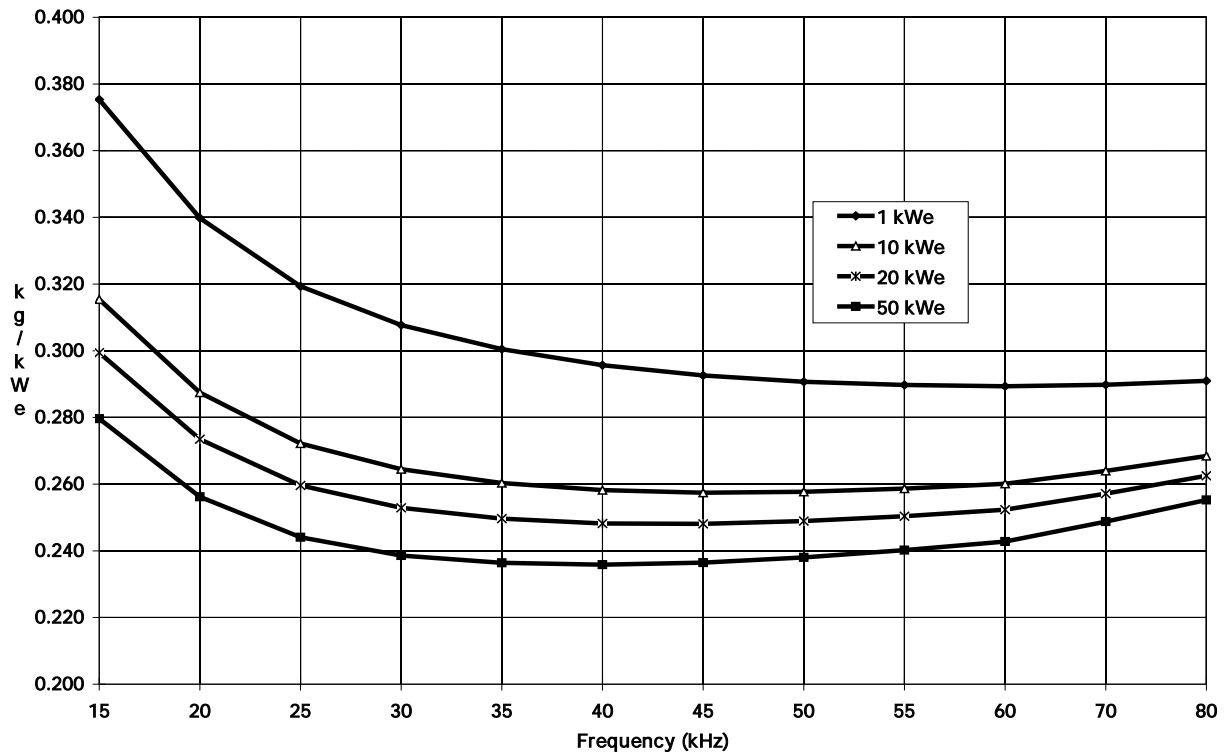
Figure 14: Inverter Transformer SPWT vs Frequency (Narrow Range)

Because a fine transformer design manual existed, especially for low frequency transformer designs, it was frequently referred to assist in the equation development [Ref. 36]. The variables used in the standard transformer stage model discussion are shown in Table 11.

Table 11: Standard Transformer Model Variable Definitions

1STSM	Single-Phase Standard Transformer Stage Mass
3STSM	3-Phase Standard Transformer Stage Mass
STSE	Standard Transformer Stage Efficiency (98%)
STSAM	Standard Transformer Stage Available Modules
STSRM	Standard Transformer Stage Required Modules
STSP$_O$	Standard Transformer Stage Power Output (kWe)
STSV$_I$	Standard Transformer Stage Voltage Input (Vrms)
STSV$_O$	Standard Transformer Stage Voltage Output (Vrms)
STSF	Standard Transformer Stage Frequency (kHz)

The equations used to estimate the mass of single-phase and 3-phase standard transformers are shown below. Only the mass coefficient will be discussed here since the rest of the factors are identical to those contained in the section on inverter transformers. To see how the specific weight or mass of a standard transformer changes with efficiency, power level, voltage, and frequency refer to the graphs contained in the inverter transformer section and subtract 10% from each value. The shape of the curves will be identical for both designs, the standard transformer curves are simply shifted downward a slight amount.

Mass Coefficient

$$1STSM = \underline{1.15}*((EXP(0.0048/(1-STSE)))/1.8221)*(STSAM/STSRM)*STSP_O*((STSP_O/STSRM)^{-0.08}$$

$$*EXP(STSV_I/200000)*EXP(STSV_O/200000)*STSF^{-0.47}+(STSF/300)^{1.4}-(200/STSP_O)^{0.03}*$$

$$((MAX(0,STSF-30))/300)^{1.7})$$

$$3STSM = \underline{2.5}*((EXP(0.003/(1-STSE)))/1.35)*(STSAM/STSRM)*STSP_O*((STSP_O/STSRM)^{-0.25}$$

$$*EXP(STSV_I/200000)*EXP(STSV_O/200000)*STSF^{-0.47}+(STSF/300)^{1.4}-(200/STSP_O)^{0.03}*$$

$$((MAX(0,STSF-30))/300)^{1.7})$$

The constants, "1.15" and "2.5", were determined by calibrating these mass equations against the masses of standard transformer designs--minus their enclosures--contained in vendor catalogues [Ref. 35]. Initially, an individual might feel the mass of a terrestrial transformer would be heavier than a space-based transformer. However, the masses of low frequency commercial and space-based transformers were felt to be comparable. Most of the transformer mass is concentrated in the transformer core and windings, and this will be nearly equivalent in both designs. Because the space-based transformer mounting hard-ware needs to be stronger than similar earth-based mounting hardware to withstand the launch environment, the mass reductions possible by using alternate materials and space type packaging approaches will be largely offset. Terrestrial transformers mainly rely on convection for cooling, a space-based unit must include thermal management hardware and use conduction. Finally, the enclosure mass is calculated by a separate algorithm and not included in this equation.

These constants are designed to produce reasonably accurate mass estimates for the specified input parameters contained in the component models. They are 10% less than those shown in the inverter transformer section because the wave form factors of the power inputs differ. The waveform encountered by a standard transformer is a smooth sinusoid with a low harmonic content. A pure sinusoid minimizes

transformer core losses because the added eddy current and hysteresis losses resulting from high frequency harmonics are not present. The square wave input of an inverter transformer has a high harmonic content; consequently, it generates higher losses in the transformer core. The design equations contained in design manuals indicate a standard transformer core can be 10% smaller due to these improved waveform characteristics [Ref. 29, 32].

3.4 RECTIFIER STAGE MODEL

The rectifier stage converts ac into dc. It is contained in the rectifier, transformer/rectifier, dc/dc converter, and frequency converter models. Two basic operating types of rectifiers are available, diode and switching. The diode rectifier is a static device that simply converts ac into dc. The switching rectifier is essentially a simplified chopper operating in reverse. Since it uses active switching devices such as SCRs or MOSFETs it can regulate the output voltage. This is done by adjusting the commutation angle, the point at which the switch is turned on to allow conduction. The equations presented here are for diode rectifiers.

The rectification stage consists of a diode network. Mass breakdowns for a circa 1992, present 2002 and projected post 2005 diodes capable of handling 1 kWe are shown in Table 12. Note this breakdown is similar to the previous switch module breakdown contained in the chopper section. The main differences are the snubber circuitry, gate drive circuitry, and switch control logic have been removed because diodes aren't active switching devices and the mass of the packaging and mounting hardware has been reduced because there are fewer parts. The original mass values were estimated from briefing packages prepared by Rocketdyne, Ford Aerospace, and TRW in support of SSF [Ref. 14, 15, 16]. Projected mass improvements were obtained from by comparing 1992 diode characteristics with present diode characteristics and extrapolating to post 2005 [Ref. 38].

Table 12: 1 kWe Diode Module Mass Breakdown

Hardware Element	Circa 1992 Mass (grams)	Present 2002 Mass (grams)	Projected Post 2005 Mass (grams)
Diode Element	7	6	5
Heat Sink, Thermal Management	48	40	35
Packaging and Mounting	<u>40</u>	<u>30</u>	<u>25</u>
Total Switch Module	95	76	65

Two full wave rectifier configurations are available, a center-tapped full-wave rectifier, or a bridge rectifier circuit. The center-tapped rectifier construction is simpler, but bridge rectifiers appear to be more attractive for high voltage applications because the peak inverse voltage imposed across each diode is half the center-tapped case. Bridge rectifiers also make better use of transformers. A center-tapped rectifier requires two 1 kWe diodes, each weighing 65 grams; a bridge rectifier uses four 500 watt diodes, each weighing 33 grams. The total mass in each case is 130 grams. Based on this assessment, the total mass of a future 1 kWe rectifier is projected to be about 130 grams.

The subsequent paragraphs will explain the development of the single-phase and 3-phase rectifier stage equations in detail. These sections will use the format presented earlier in the chopper stage discussion since the items are comparable in many respects. The variables that will be used during this discussion are shown in Table 13.

Table 13: Rectifier Stage Model Variable Definitions

1RSM Single-Phase Rectifier Stage Mass

3RSM Three-Phase Rectifier Stage Mass

RSE Rectifier Stage Efficiency (98.7%)

RSAM Rectifier Stage Available Modules

RSRM Rectifier Stage Required Modules

RSP_O Rectifier Stage Power Output (kWe)

RSV_I Rectifier Stage Voltage Input (Vrms)

Mass Coefficient

$$1RSM = \underline{0.1175}*((EXP(0.005/(1-RSE)))/1.469)*(RSAM/RSRM)*RSP_O*(RSV_I/(RSV_I-2))^6$$

$$3RSM = \underline{0.12}*((EXP(0.005/(1-RSE)))/1.469)*(RSAM/RSRM)*RSP_O*(RSV_I/(RSV_I-2))^6$$

To calculate the rectifier stage mass coefficients, the equations were calibrated to yield values consistent with the above 1 kWe mass breakdown and actual component designs [Ref. 14, 15, 17].

The diodes comprising three single-phase full wave rectifiers are interconnected to form a 3-phase full wave rectifier. Six diodes are required and each processes a third of the power. The 3-phase rectifier design was judged to be slightly heavier because of the added number of diodes. This would probably enlarge the mounting area and increase the interconnecting wiring weight. Figure 15 compares the specific weights of single- and 3-phase rectifiers.
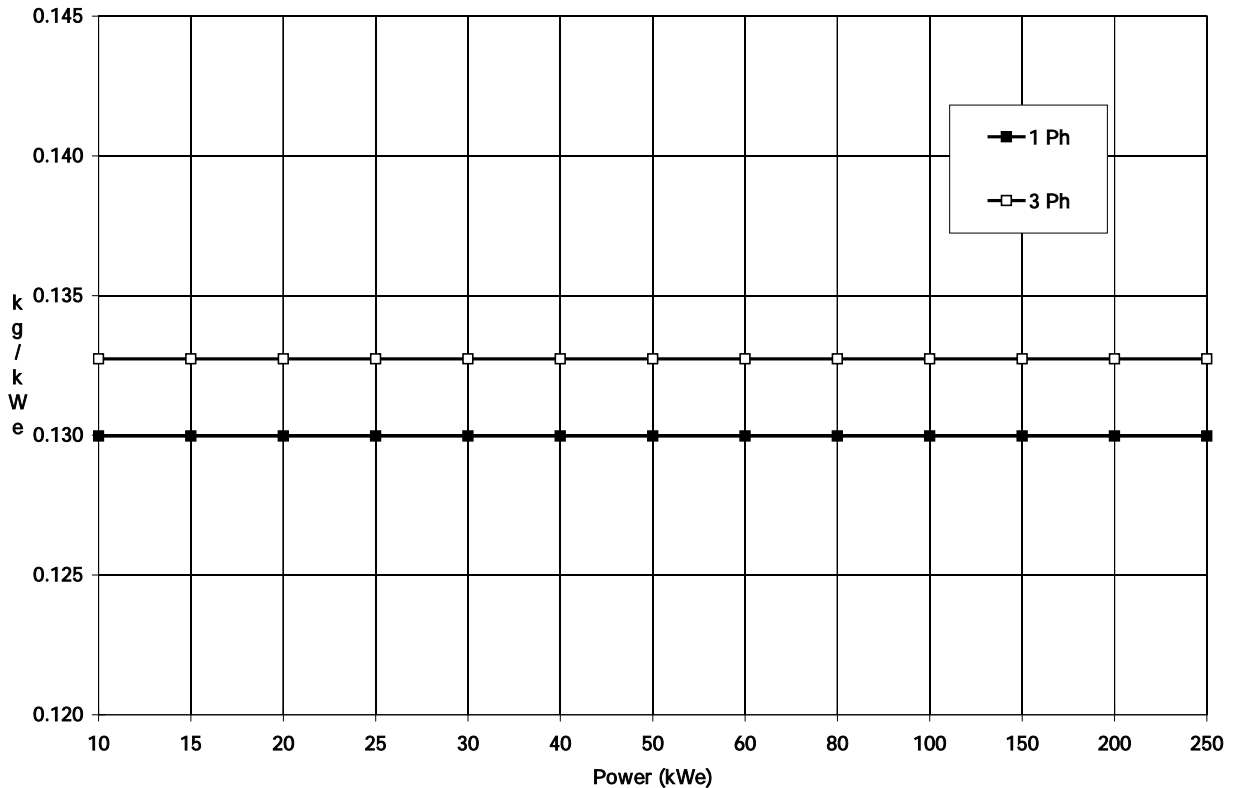
Figure 15: Rectifier SPWT – 1 Phase vs 3 Phase

Efficiency Factor

1RSM=0.1175*$\underline{((EXP(0.005/(1-RSE)))/1.469)}$*(RSAM/RSRM)*$RSP_O$*$(RSV_I/(RSV_I-2))^6$

3RSM=0.12*$\underline{((EXP(0.005/(1-RSE)))/1.469)}$*(RSAM/RSRM)*$RSP_O$*$(RSV_I/(RSV_I-2))^6$

The factor underlined above estimates the specific weight values associated with a range of rectifier efficiencies. Within reason, the interconnecting wiring and the diode conduction losses can be reduced by increasing the size of the wiring and the diode die area. An improved efficiency allows a reduction in the heat sink mass. The effect of power losses on individual elements within a diode module were assessed to develop rectifier mass estimates for efficiencies ranging from 98.3 to 99.1%. From this analysis, an efficiency factor was calculated and incorporated into the rectifier mass equation. Figure 16 shows a graph of the resulting specific weight versus efficiency values that were developed with this approach. Note that the depicted rectifier efficiency range is relatively narrow. Rectifier efficiencies higher than about 99.5% are not considered practical due to diode fabrication limitations. Lower efficiencies are undesirable because of the additional radiator mass. Because silicon diodes require a forward bias voltage of about 0.7 V before they will conduct, their efficiency is considerably less at lower operating voltages. This will be addressed later in the section on voltage factors.
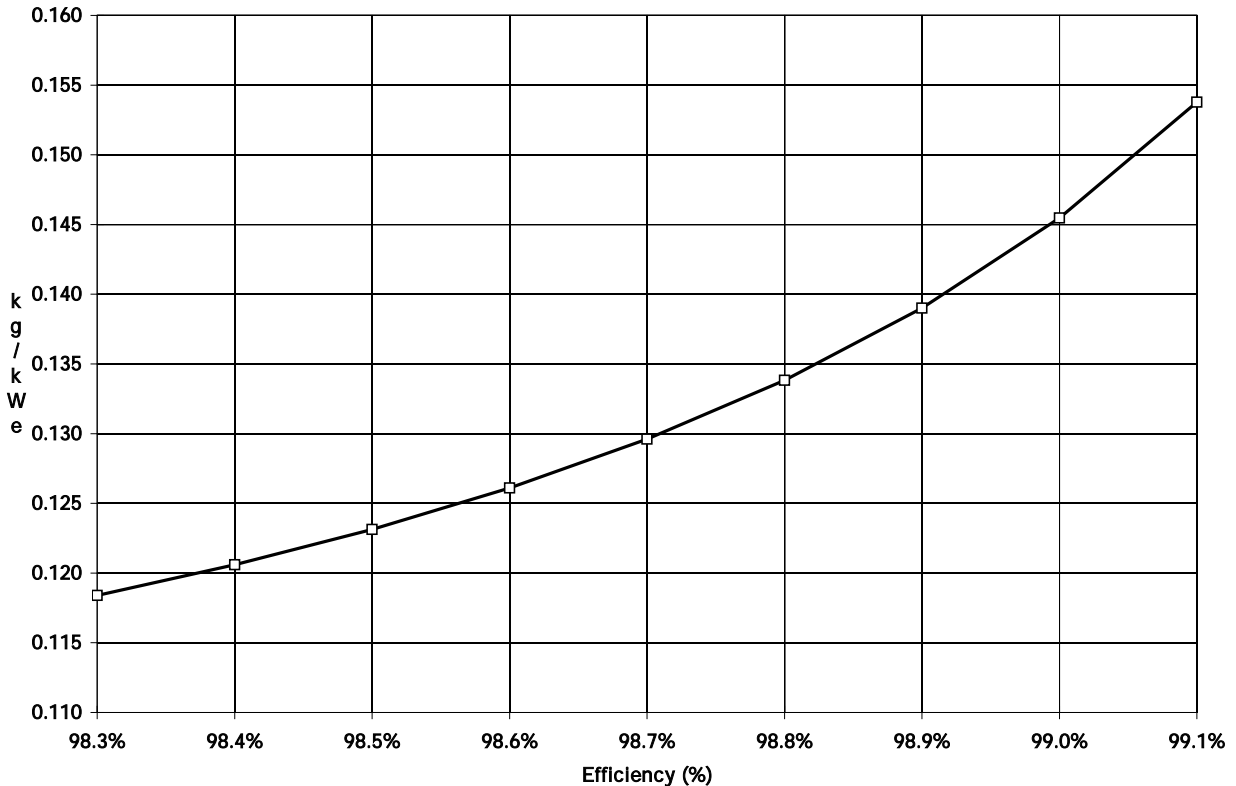
Figure 16: Rectifier SPWT vs Efficiency

Redundancy Factor

1RSM=0.1175*((EXP(0.005/(1-RSE)))/1.469)*$\underline{(RSAM/RSRM)}$*RSP_O*$(RSV_I/(RSV_I-2))^6$

3RSM=0.12*((EXP(0.005/(1-RSE)))/1.469)*$\underline{(RSAM/RSRM)}$*RSP_O*$(RSV_I/(RSV_I-2))^6$

The above factor computes the redundancy mass impacts occurring when a modular design approach is used to improve reliability. The "available modules" number is the actual number of modules present in the

component; the "required modules" value is the actual number of modules required to achieve full output power. If a design requires 4/3 redundancy to meet the reliability requirements, each channel will be rated to carry 33% of the power. 4 channels are available, but only 3 channels are needed to supply full power. The mass of the fourth channel is the penalty paid to obtain a higher reliability.

Power Level Multiplier

$$1RSM=0.1175*((EXP(0.005/(1-RSE)))/1.469)*(RSAM/RSRM)*\underline{RSP_O}*(RSV_I/(RSV_I-2))^6$$

$$3RSM=0.12*((EXP(0.005/(1-RSE)))/1.469)*(RSAM/RSRM)*\underline{RSP_O}*(RSV_I/(RSV_I-2))^6$$

The equations can be used to calculate the mass or specific weight of the rectifier. When the above multiplier is included, the value that results is a rectifier mass estimate. To obtain the specific weight of the rectifier, remove this multiplier.

A power factor was not included in the rectifier equation to improve the specific weight at higher power levels. As the rectifier power level increases, a slight reduction in specific weight may occur because it is possible to package larger sized units more compactly; however, this minor effect was considered to be to small to warrant the inclusion of an additional factor.

Frequency Factor

Although it may be necessary to incorporate fast recovery diodes in a high frequency design, the effect of frequency on rectifier mass was considered to be minor. In fact it may even be desirable to incorporate fast recovery diodes in lower frequency designs to gain an improvement in efficiency. For these reasons, it was not considered necessary to include a frequency factor in the equations.

Voltage Level Factors

$$1RSM=0.1175*((EXP(0.005/(1-RSE)))/1.469)*(RSAM/RSRM)*RSP_O*\underline{(RSV_I/(RSV_I-2))}^6$$

$$3RSM=0.12*((EXP(0.005/(1-RSE)))/1.469)*(RSAM/RSRM)*RSP_O*\underline{(RSV_I/(RSV_I-2))}^6$$

The low voltage impacts on rectifier and chopper mass were judged to be similar; therefore, the approaches used to define the low voltage factor are comparable. Two primary effects cause the rectifier efficiency to decline as the voltage level is reduced: the bias voltage imparted across the diode, and the conduction losses. Silicon diodes require a forward bias voltage of about 0.7 V before they will conduct. At lower voltage levels this bias voltage is a larger percentage of the device voltage; therefore, the efficiency is reduced. Conduction losses are calculated with the equation I^2R. Since current levels rise as voltage declines, the rectifier efficiency is poorer at lower voltage levels. Methods are available to partially offset these losses, but they have associated mass penalties. The resistances of circuit elements can be lowered by increasing the cross sectional areas of the conductors and leads, but it causes their mass to increase. Increasing the diode die area and reducing its current density will lower the conduction losses, but a heavy mass penalty can be incurred. An alternate approach is to replace these standard diodes with Schottky diodes or germanium rectifiers [Ref. 39]. Schottky rectifiers have a lower forward voltage drop, but they generally are not as rugged. The bias voltage of a germanium rectifier is about 0.3 V, but it is more limited in temperature and has a lower breakdown voltage.

Because of these factors, the efficiency parameter input for rectifier stage calculations should be decreased in accordance with Table 14. These values reflect the increase in mass and reduction in efficiency that occurs at lower voltages. These values will yield a smoothly increasing mass curve. The rectifier specific weight curve generated with these values is shown in Figure 17.

Table 14: Efficiency Corrections for Lower Voltage Rectifier Mass Estimates

Input Voltage (Vrms)	Input Rectifier Efficiency (percent)
120	98.70
110	98.70
100	98.68
90	98.66
80	98.62
70	98.56
60	98.50
50	98.38
40	98.20
30	97.95
20	96.70

Presently, diodes are available that can withstand reverse voltages up to 24000 V and are rated for ac supply voltages up to 9000 Vrms [Ref. 38]. This should be adequate for most space based power conditioning needs and further improvements are likely over the next few years. Because of the availability of these extremely high voltage diodes it isn't necessary to use a pancake configuration consisting of diodes stacked in series to achieve high voltage capabilities. As a result the mass penalties associated with maintaining proper voltage sharing across the diodes in these stacks don't have to be incurred and the previously included high voltage segment of these equations was removed.
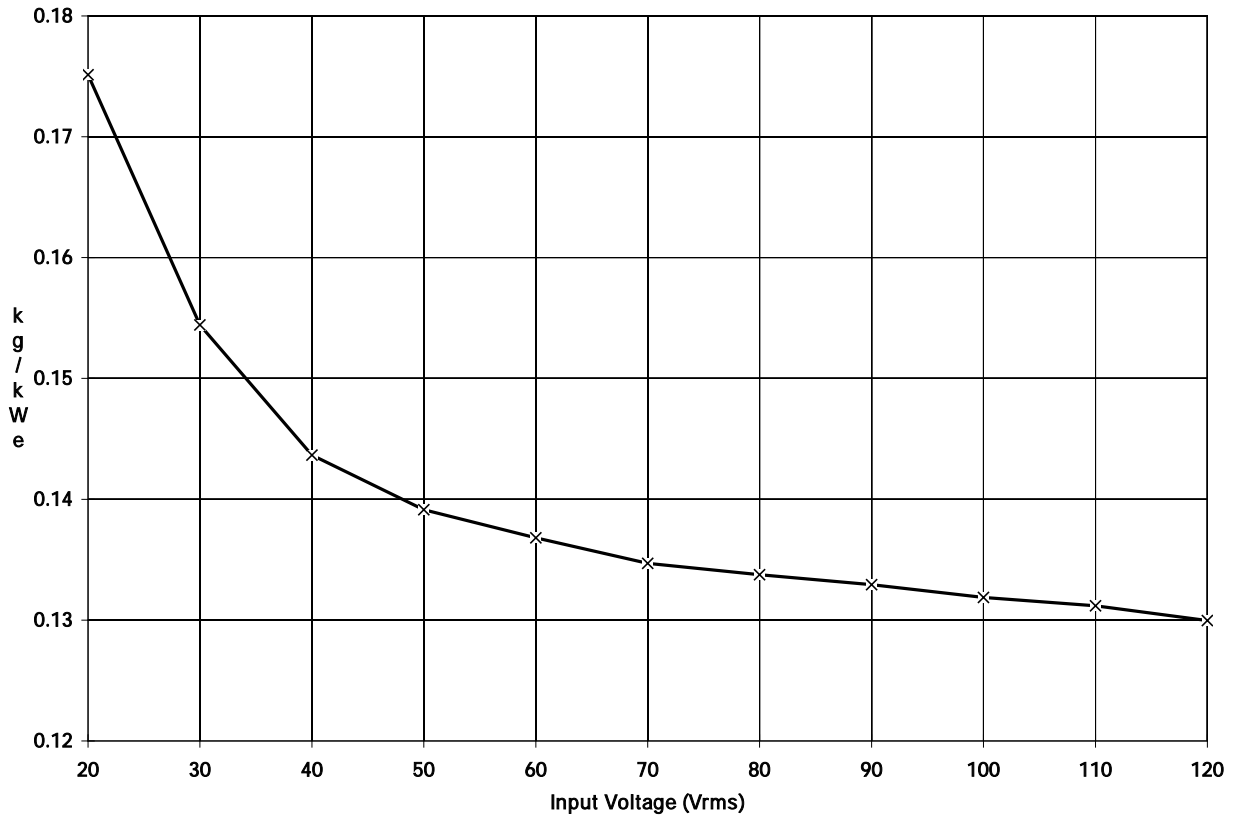
Figure 17: Rectifier SPWT vs Low Voltages

3.5 DC FILTER STAGE MODEL

The dc filter stage conditions the dc voltage to obtain the power quality required by the system. Two dc filters may be required for a component, one on the input and another on the output. Most components containing a chopper or rectifier will require dc filtering; therefore, dc filter stages are contained in the rectifier, dc/dc converter, and inverter models. Filtering mass is difficult to estimate. The power quality requirements for future applications are vague or nonexistent, and the design of a filter is a complex process that is heavily influenced by the circuit topology. The filter stage equations presented here are generalized and only intended to provide rough mass estimates to facilitate component comparisons. For more accurate mass estimates, power quality requirements must be defined and specific filter designs generated.

A single-stage filter design was assumed to precede the chopper and follow the rectifier. This configuration is relatively simple, consisting of a series inductor and a parallel capacitor. Since the input to a chopper and the output from a rectifier are periodically discontinuous and they have a high ripple content, filtering is needed to smooth the dc level and suppress voltage and current spikes. The masses of the filter hardware elements preceding the chopper and following the rectifier were assumed to be comparable because they are both performing similar functions, providing energy to smooth the dc level during discontinuous conduction periods. Due to the approximations and inaccuracies already inherent in these models, it was not considered practical to identify differences in the two filter designs and develop alternate equations for both applications.

Based on space station documentation [Ref. 14, 17], the mass of a dc filter following a 1 kWe, 120 Vdc single-phase rectifier, designed to reduce the output ripple content to 0.4%, was estimated to be 470 grams. This rectifier was assumed to follow a Weinberg converter operating at 40 kHz. The ripple frequency of a 3-phase rectifier is three times higher than a single-phase design. This decreases the energy that must be stored in the filter hardware to one-third of the single phase value and proportionally reduces the filter mass. Consequently, the mass of a dc filter following a 3-phase rectifier also designed to reduce the output ripple to 0.4% is 157 grams. Filter inductor and capacitor masses aren't projected to decline significantly, but gradual improvements in their manufacture and materials are expected to allow them to operate at higher frequencies without exhibiting higher losses. This capability will lower filter mass.

Internal model development studies conducted after the delivery of the original Task Order 15 report [Ref. 1] showed the mass per farad of a capacitor rises as the voltage level it is designed for is increased [Ref. 40, 41, 42, 43, 44]. Both the dielectric thickness and capacitor plate area must be increased at higher voltages. This effect partially offsets the reduction in filter mass that occurs because of the ability to use a smaller capacitor value and it was incorporated into the dc filter equations presented in this report.

To develop the dc filter stage mass equations, power conditioning model analyses by Gilmour, Moriarty, and TRW were referred to for guidance [Ref. 45, 46, 47). The equations developed by TRW under contract NAS3-19690 were especially valuable since they allowed dc filter masses to be calculated for numerous conditions. The variables contained in the dc filter stage equations are shown in Table 15.

Table 15: DC Filter Model Variable Definitions

1FSM	Single-Phase Dc Filter Stage Mass
3FSM	3-Phase Dc Filter Stage Mass
FSRF	Dc Filter Stage Ripple Factor (0.1 to 5%)
FSE	Dc Filter Stage Efficiency (99.8%)
FSAM	Dc Filter Stage Available Modules
FSRM	Dc Filter Stage Required Modules
FSP$_O$	Dc Filter Stage Power Output (kWe)
FSV$_O$	Dc Filter Stage Voltage Output (Vdc)
FSF	Dc Filter Stage Frequency (kHz)

The equations developed for the single-phase and 3-phase dc filter mass estimates are shown below. Each factor in the equations will be discussed separately. The factor being discussed will be underlined and accompanying graphs will be used to display the values generated by the equations.

Mass Coefficient

$1FSM=\underline{22.05}*(1/(FSRF/0.01)^{0.5})*((1-0.998)/(1-FSE))*(FSAM/FSRM)*FSP_O*$

$(FSV_O^{-0.9}+0.000015)*(40/FSF)$

$3FSM=\underline{22.05}*(1/(FSRF/0.01)^{0.5})*((1-0.998)/(1-FSE))*(FSAM/FSRM)*FSP_O*$

$(FSV_O^{-0.9}+0.000015)*(13.33/FSF)$

A four step process was used to calculate the mass coefficient contained in the above dc filter equations. First, masses of actual LC filter designs were located in technical reports [Ref. 14, 15, 17, 48]. Because the filter masses identified in these reports were under widely varying conditions, it allowed the later developed filter equations to be verified in different applications. The next step was to calculate filter masses using equations developed by TRW during a component mass optimization study [Ref. 47]. The parameters input into these filter mass equations were obtained from values contained in the reference reports. The third step compared the calculated filter masses with masses listed in reports. Finally, discrepancies were noted and investigated.

The TRW equations generally appeared to be quite accurate and seemed to correctly reflect the dc filter mass trends associated with voltage, frequency, and efficiency. Using a mass coefficient value of "22.05" yielded good dc filter mass estimates for filters preceding a Weinberg converter and following a static rectifier. However, because a resonant converter switches at the zero current crossing point, it doesn't generate as much electromagnetic interference during switching. This translates into a lower filter mass, but there wasn't enough information available to calculate the mass of a filter for a resonant converter designed to meet the same requirements as a Weinberg converter filter. Conservatively, it was estimated this filter would be 5% lighter than the filters used with a Weinberg converter and a static rectifier, which resulted in a mass coefficient of "20.9". Since this is the only difference in the filter equations, only the filter equation designed for a Weinberg converter will be displayed throughout the filter discussion.

Ripple Factor

$1FSM=22.05*\underline{(1/(FSRF/0.01)^{0.5})}*((1-0.998)/(1-FSE))*(FSAM/FSRM)*FSP_O*$

$(FSV_O^{-0.9}+0.000015)*(40/FSF)$

$3FSM=22.05*\underline{(1/(FSRF/0.01)^{0.5})}*((1-0.998)/(1-FSE))*(FSAM/FSRM)*FSP_O*$

$(FSV_O^{-0.9}+0.000015)*(13.33/FSF)$

The ripple factor measures the amount of ripple existing on the dc waveform. It is calculated with the following equation:

$$RF=(V_R)/Vdc$$

where: RF is the ripple factor expressed as a percentage
V_R is the ripple voltage level expressed as a rms value
Vdc is the dc voltage level.

The dc filter mass will increase as the ripple requirements get more demanding. Equations derived by Gilmore and later verified by the TRW calculations showed that the mass would change by the reciprocal of the square root of the increase in the ripple factor. This led to the factor underlined above. Figure 18 shows the rise in dc filter mass occurring as the ripple factor is reduced. To obtain filter masses consistent with the ISS DDCU design requirements, set the ripple factor to 0.4%. For utility power applications, such as following a large alternator based power source or feeding drive motors, a value of

5% is suggested. The subsequent graphs on filter characteristics use a ripple factor of 0.4% unless otherwise noted.
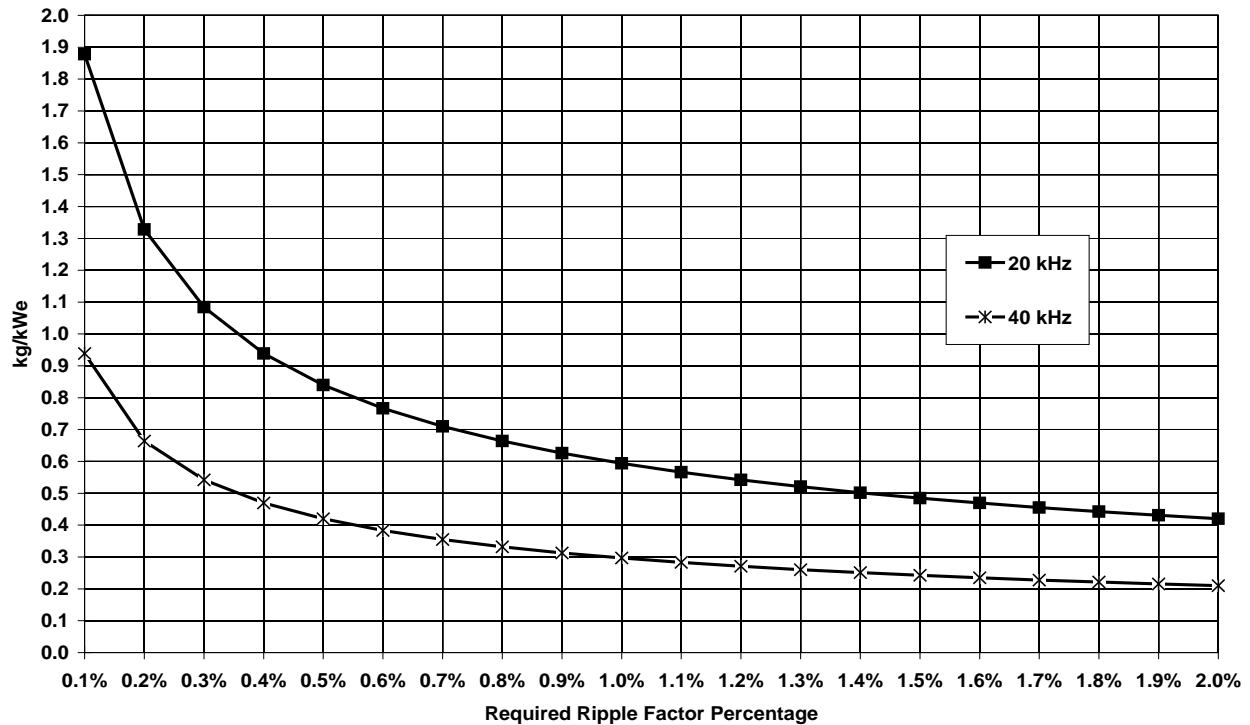
Figure 18: DC Filter SPWT vs Ripple Factor

Efficiency Factor

$$1FSM = 22.05*(1/(FSRF/0.01)^{0.5})*\underline{((1-0.998)/(1-FSE))}*(FSAM/FSRM)*FSP_O*$$

$$(FSV_O^{-0.9}+0.000015)*(40/FSF)$$

$$3FSM = 22.05*(1/(FSRF/0.01)^{0.5})*\underline{((1-0.998)/(1-FSE))}*(FSAM/FSRM)*FSP_O*$$

$$(FSV_O^{-0.9}+0.000015)*(13.33/FSF)$$

The efficiency of an LC filter network is determined by the equivalent series resistance (ESR) of the inductor and capacitor. To reduce the ESRs of these devices the inductor winding and core size, and the capacitor dielectric cross sectional area must be increased. This increases filter mass. The TRW equations were used to calculate filter masses for efficiency values ranging from 99.7 to 99.9%. An equation based curve was then matched to those data points. The equation segment underlined above was computed during that exercise and used to generate Figure 19. It shows the change in dc filter specific weight occurring with a change in efficiency.

Redundancy Factor

$$1FSM = 22.05*(1/(FSRF/0.01)^{0.5})*((1-0.998)/(1-FSE))*\underline{(FSAM/FSRM)}*FSP_O*$$

$$(FSV_O^{-0.9}+0.000015)*(40/FSF)$$

$$3FSM = 22.05*(1/(FSRF/0.01)^{0.5})*((1-0.998)/(1-FSE))*\underline{(FSAM/FSRM)}*FSP_O*$$

$$(FSV_O^{-0.9}+0.000015)*(13.33/FSF)$$

The redundancy factor underlined above addresses the mass penalty associated with a more reliable system. The actual number of modules in the assembly is defined by the "available modules" value. The number of modules needed to provide full power is defined by the "required modules" value. If a design requires 4/3 redundancy to meet the reliability requirements, four 33% rated channels will be used. This increases the mass of the assembly at least 33%. The mass of the fourth channel is the penalty incurred to achieve a higher reliability.
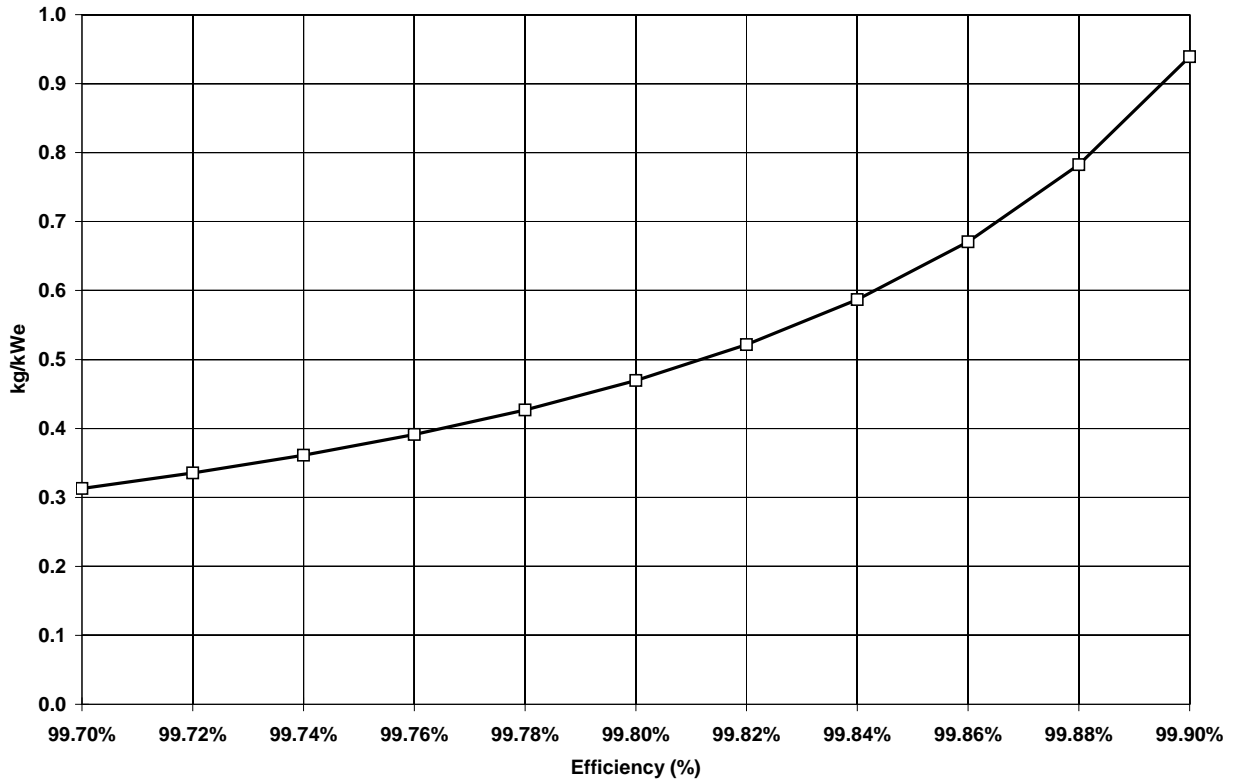
Figure 19: DC Filter SPWT vs Efficiency

Power Level Multiplier

$1FSM = 22.05*(1/(FSRF/0.01)^{0.5})*((1-0.998)/(1-FSE))*(FSAM/FSRM)*\underline{FSP_O}*$

$\quad (FSV_O^{-0.9}+0.000015)*(40/FSF)$

$3FSM = 22.05*(1/(FSRF/0.01)^{0.5})*((1-0.998)/(1-FSE))*(FSAM/FSRM)*\underline{FSP_O}*$

$\quad (FSV_O^{-0.9}+0.000015)*(13.33/FSF)$

The equations can calculate filter mass or specific weight. When the power level multiplier is included, the equations determine the mass of the dc filter. Remove this multiplier to obtain the dc filter specific weight.

A power level factor is not included in the dc filter mass equations because the TRW equations indicated the filter specific weight remained constant with power level. This is shown in Figure 20 for single- and 3-phase filter designs. Because the energy density of the capacitors and inductors in the filter network remains constant regardless of the power level, the filter specific weight does not change. The gains that might be realized in packaging density as the size of the filter element was increased were considered to be minor. After some consideration it was decided a power level factor wasn't necessary.
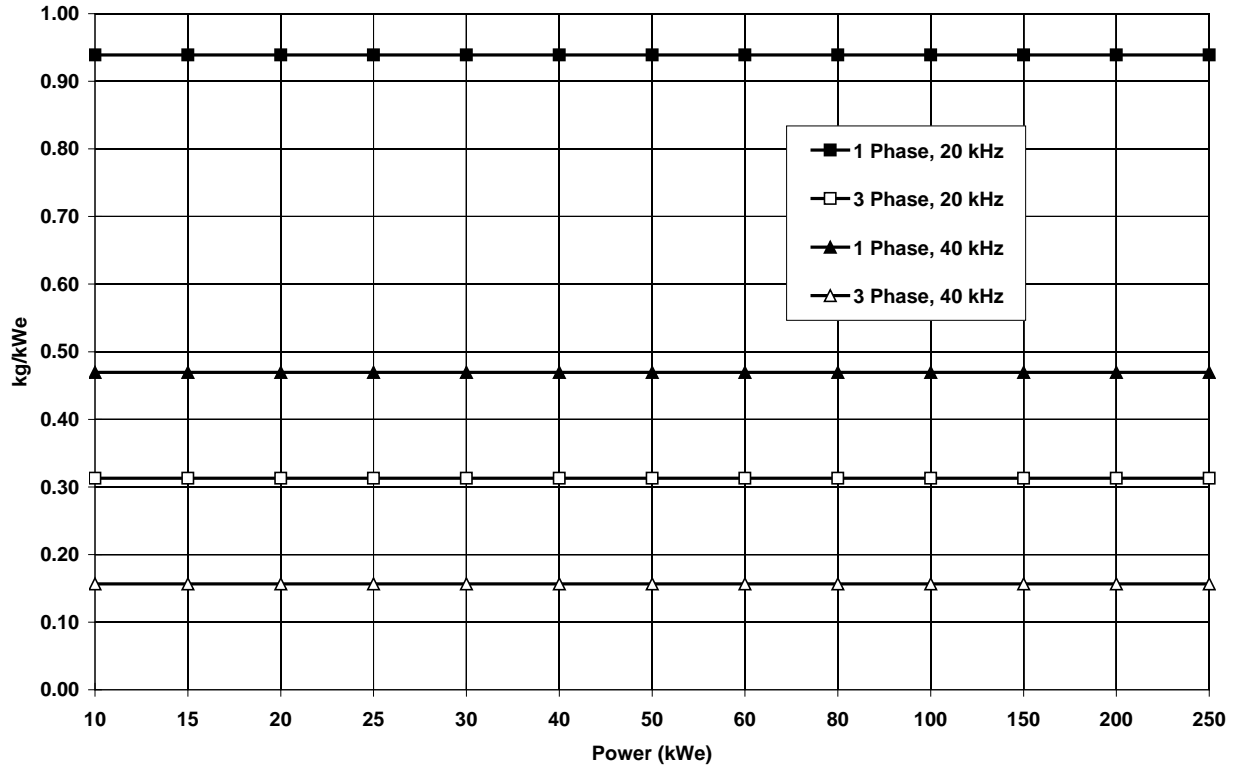
Figure 20: DC Filter SPWT vs Power – Single–Phase and 3-Phase

Voltage Level Factors

$1FSM=22.05*(1/(FSRF/0.01)^{0.5})*((1-0.998)/(1-FSE))*(FSAM/FSRM)*FSP_O*$

$\underline{(FSV_O^{-0.9}+0.000015)}*(40/FSF)$

$3FSM=22.05*(1/(FSRF/0.01)^{0.5})*((1-0.998)/(1-FSE))*(FSAM/FSRM)*FSP_O*$

$\underline{(FSV_O^{-0.9}+0.000015)}*(13.33/FSF)$

In most LC filter designs, the mass of the capacitor is the largest portion of the filter mass. To determine the changes that will occur in filter mass as the voltage level rises, the changes occurring in capacitor mass must be identified. For a given power level and frequency, the energy that must be stored in the filter is constant regardless of the voltage level, but filter capacitance is not. The energy stored in a capacitor is defined by the equation:

$$E=\tfrac{1}{2}CV^2$$

where: C is the capacitance in farads
              V is the voltage level in volts.

By inspection, one can see that the energy stored in a capacitor rises with the voltage squared. If the voltage level is doubled, the capacitance can be reduced to one-fourth of its previous value and the amount of energy that is stored will remain the same. If one could assume a constant mass per farad, the capacitor mass would drop to one-fourth of its previous value. However, an increase in voltage will necessitate a thicker dielectric to withstand the electric field being imparted between the plates. Furthermore, the following equation shows that the capacitor plate area must also be increased to maintain the same level of capacitance.

$$C = \varepsilon_o \varepsilon A / t$$

where: C is the capacitance in farads

ε_o is the dielectric constant of a vacuum (0.0884 x10^{-12} F/cm)

ε is the relative dielectric constant of the dielectric material

A is the capacitor plate area in cm^2

t is the thickness of the dielectric material in cm

The fact that both the dielectric thickness and capacitor plate area must be increased at higher voltages causes the mass per farad to rise as the voltage level is increased. This partially offsets the reduction in filter mass that occurs because of the ability to use a lower capacitor rating. Mass versus voltage data was obtained for high voltage tantalum capacitors, ceramic surface mount, disc and multilayer capacitors, and two types of polyester/polypropylene dielectric capacitors [Ref. 41, 42, 43, 44]. This data showed capacitor mass rises at an exponential rate of 0.3 for ceramic disc capacitors and up to 1.1 for polyester/polypropylene capacitors. Ceramic disc capacitors are only available in picofarad sizes, too small for high power filters. The ceramic surface mount and polyester/polypropylene capacitors, with exponents of 0.9 and 1.1, were judged the best for this application. The types reviewed are specifically designed for dc filtering applications and they have the high voltage capability and are available in the range of sizes required for this application. Based on this analysis an exponent of 1.1 was used to calculate the change in capacitor mass as a function of voltage. Since the capacitance in a dc filter declines according to the voltage squared (-2 exponent), while per this analysis its mass is rising at an exponential rate of 1.1, the two factors must be multiplied together to obtain the total effect. Adding the two exponents together (the exponents are added when two factors are multiplied) resulted in the final exponent value of -0.9. Because the mass of the capacitor dominates the filter mass over the voltages of interest, almost all of the change in filter mass results from a change in capacitor mass. At lower voltages this correlation appears quite accurate. Figure 21 shows the relationship between filter mass and voltage for voltage levels below 120 Vdc.
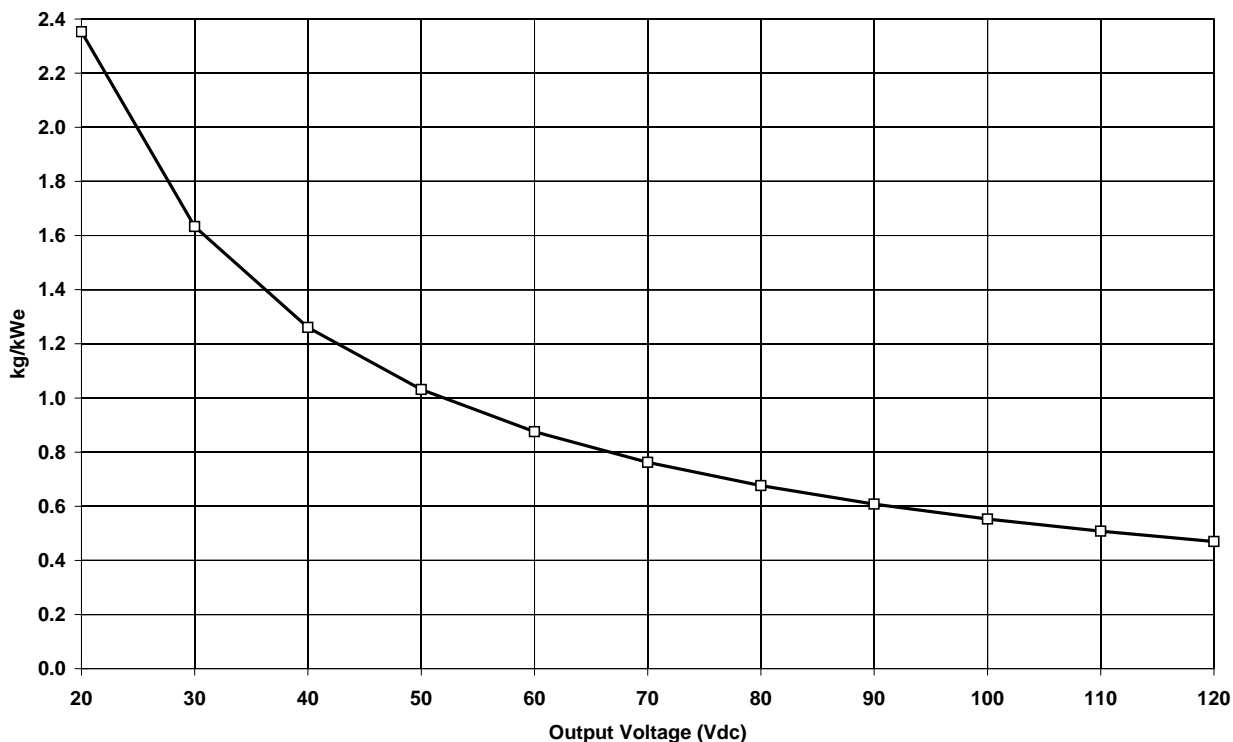
Figure 21: DC Filter SPWT vs Voltage – Low Voltage Region

Because capacitor mass declines with voltage, the inductor mass becomes a noticeable fraction of the filter mass at higher voltages. This is the reason for the constant "0.000015". For voltages above a approximately 5000 Vdc, the reduction in capacitor mass that occurs with a rising voltage is largely offset by the capacitor's rising mass per farad and a larger percentage of inductor mass in the filter. This causes the filter specific weight to approach a constant value, as shown in Figure 22. The voltage factor under-lined above is designed to cover a voltage range of 20 to 10000 Vdc, and it was developed by integrating the data from these analyses.
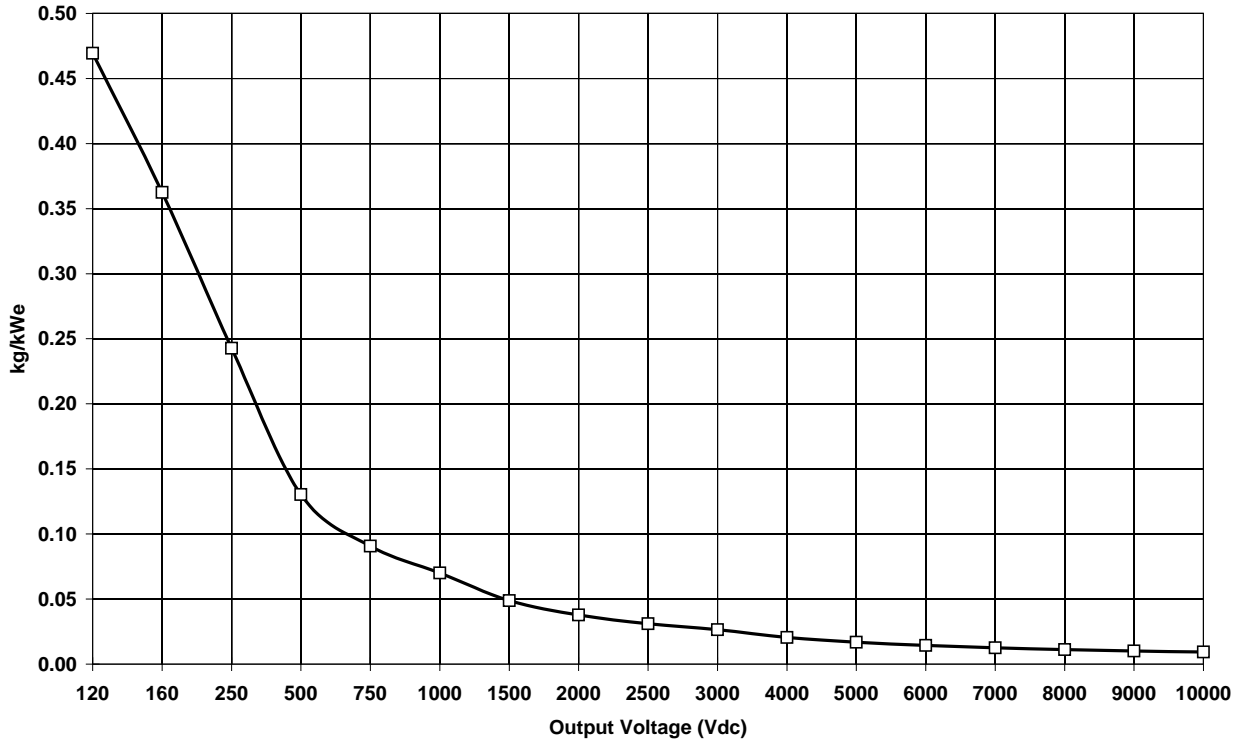
Figure 22: DC Filter SPWT vs Voltage – High Voltage Region

Frequency Factor

1FSM$=22.05*(1/(\text{FSRF}/0.01)^{0.5})*((1-0.998)/(1-\text{FSE}))*(\text{FSAM}/\text{FSRM})*\text{FSP}_O*$

$(\text{FSV}_O^{-0.9}+0.000015)*\underline{(40/\text{FSF})}$

3FSM$=22.05*(1/(\text{FSRF}/0.01)^{0.5})*((1-0.998)/(1-\text{FSE}))*(\text{FSAM}/\text{FSRM})*\text{FSP}_O*$

$(\text{FSV}_O^{-0.9}+0.000015)*\underline{(13.33/\text{FSF})}$

The mass of a dc filter is primarily determined by the amount of energy it must store. The energy storage requirements are in turn proportional to the ripple frequency. The further apart the wavecrests of the ripple voltage are, the more energy a filter must provide to the system to maintain a smooth dc output. The ripple frequency of a full wave rectified single-phase waveform is twice the input frequency. Because the three phases of a 3-phase system are superimposed after rectification, the output ripple frequency is six times the operating frequency. This is why the factor "13.33" in the 3-Phase filter equation is one-third the size of the single-phase value, "40". Because the best mass data available was for the ISS DDCU, which has a 40 kHz switching frequency, the filter masses were referenced to a 40 kHz frequency. Figure 43 shows how much the filter mass declines as the switching frequency of a dc/dc converter is increased. These masses are consistent with filters following single-phase rectifiers that are designed to meet a ripple requirement of 0.4%.
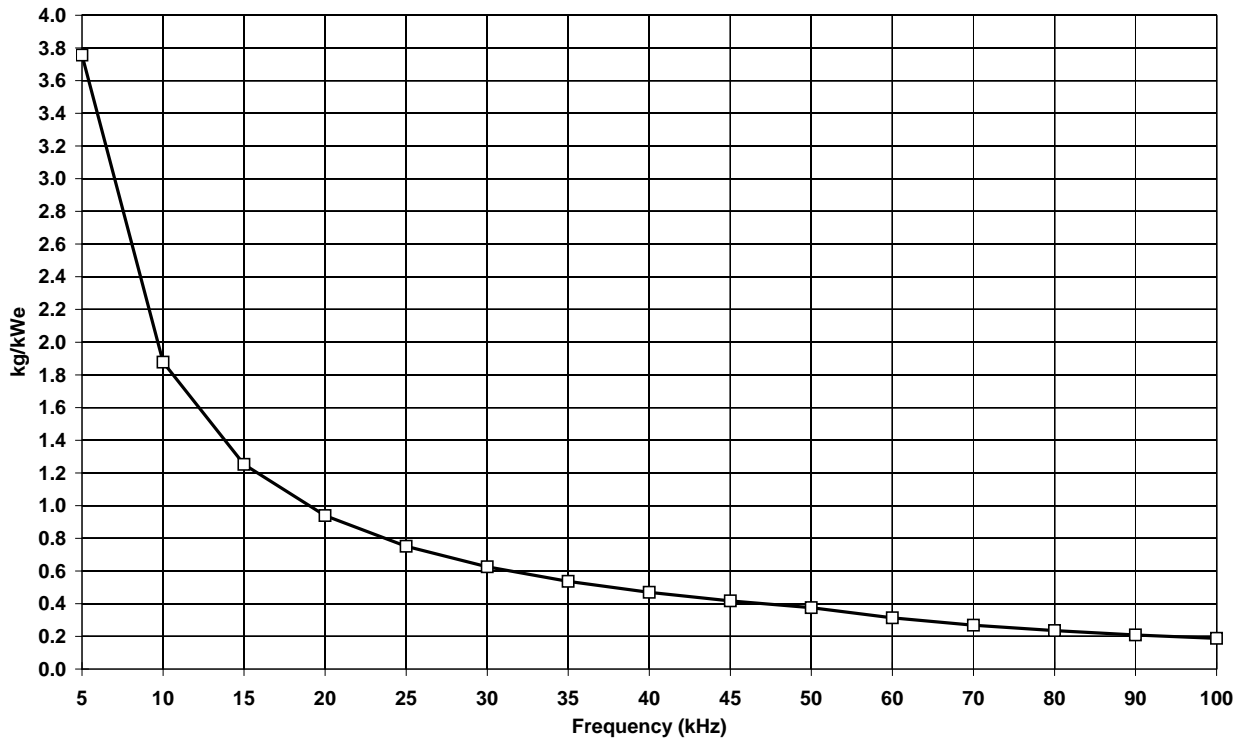
Figure 23: DC Filter SPWT vs Frequency

3.6 AC FILTER STAGE MODEL

Resonant converters can typically achieve less than 5% total harmonic distortion without filtering. This is adequate for most PMAD applications; however, a series harmonic trap is required to prevent external harmonics from being amplified within the converter. The mass of a harmonic filter is difficult to estimate. In discussions held with converter designers familiar with the design of harmonic filters, they indicated present harmonic filter designs are not optimized and quite a bit of improvement is expected. Many articles discuss harmonic distortion, but none were found that described a method for calculating the mass of a harmonic filter. Consequently, the following equations are approximate since there is very little concrete data. It is recommended that further work be done in this area when additional information becomes available. If more accurate mass estimates are required, it will be necessary to define power quality requirements and have a knowledgeable designer generate a specific filter design.

A harmonic filter is located before the converter input or after its output, and it is connected in series with the source or load. The equations in this report are based on a series resonant circuit tuned to the inversion frequency of the converter. The filter configuration itself consists of a current transformer that is connected in parallel with a resistor, and a series connected inductor and capacitor combination [Ref. 49]. The current transformer is required to obtain reasonable values for the inductor and capacitor and to reflect adequate resistance into the line to inhibit harmonics [Ref. 23]. Much of the filter mass is concentrated in this current transformer and it can not be eliminated.

A technical presentation compiled by TRW indicated the mass of a harmonic filter placed on the output of a 5 kWe, 20 kHz inverter would weigh 1071 grams [Ref. 15]. The specific weight of this filter is about 0.21 kg/kWe. In a discussion held at the "High Frequency Power Distribution and Controls Technology Conference" in June 1991, John Biess indicated it might be possible to reduce this filter design to one-third of its present weight with extensive analysis and optimization. This would result in a specific weight of about 0.07 kg/kWe [Ref. 23]. However, he also indicated this value might be optimistic. Based on this discussion, it was decided to use a value of 0.1 kg/kWe for a harmonic filter following a single-phase 1

kWe, 20 kHz inverter. The harmonic filter used for a 3-phase inverter was assumed to consist of three single-phase inverter filters each rated to carry one-third of the power. Its mass would be just slightly heavier due to economies of scale. The estimated masses of filters following single-phase and 3-phase, 1 kWe inverters was estimated to be 100 and 105 grams respectively.

The variables used in the ac filter stage equations are shown in Table 16.

Table 16: AC Filter Model Variable Definitions

1FSM	Single-Phase Ac Filter Stage Mass
3FSM	3-Phase Ac Filter Stage Mass
FSE	Ac Filter Stage Efficiency (99.5%)
FSAM	Ac Filter Stage Available Modules
FSRM	Ac Filter Stage Required Modules
FSP_O	Ac Filter Stage Power Output (kWe)
FSF	Ac Filter Stage Frequency (kHz)

The equations generated to estimate the masses of single-phase and 3-phase ac filters follow. The factors in the equations will be discussed separately and underlined. Graphs will be used to depict the effects calculated by the equations.

Mass Coefficient

$1FSM = \underline{0.1}*((1-0.998)/(1-FSE))*(FSAM/FSRM)*FSP_O*(FSP_O/FSRM)^{-0.03}*(FSF/20)^{-0.6}$

$3FSM = \underline{0.105}*((1-0.998)/(1-FSE))*(FSAM/FSRM)*FSP_O*(FSP_O/FSRM)^{-0.03}*(FSF/20)^{-0.6}$

The single- and 3-phase ac filter stage mass coefficients were calibrated to yield specific weights of 0.1 and 0.105 kg/kWe respectively, when placed after a 1 kWe, 20 kHz inverter. The inverter filter specific weights are based on the previously discussed conversation with John Biess [Ref. 23]. The mass coefficient for the 3-phase design is larger because it consists of three single-phase filters, each carrying one-third of the power. Economies of scale are lost in the current transformer as the filter power level declines. This causes the mass of the 3-phase filter to be slightly greater. The difference in masses of single- and 3-phase ac filters is illustrated in Figure 24. This figure compares the specific weights of inverter filter designs at 20 and 40 kHz resonant frequencies.

Efficiency Factor

$1FSM = 0.1*\underline{((1-0.998)/(1-FSE))}*(FSAM/FSRM)*FSP_O*(FSP_O/FSRM)^{-0.03}*(FSF/20)^{-0.6}$

$3FSM = 0.105*\underline{((1-0.998)/(1-FSE))}*(FSAM/FSRM)*FSP_O*(FSP_O/FSRM)^{-0.03}*(FSF/20)^{-0.6}$

The ac filter design presented in this study uses a series resonant circuit. This circuit has the largest influence on filter efficiency and its efficiency is determined by the ESRs of the inductor and capacitor composing it. These ESRs can only be decreased by enlarging the inductor winding and core, the capacitor dielectric area, and the interconnecting lead wires. A larger filter mass will result. Since this same process occurred in the dc filter case, the efficiency factors were assumed to be the same. This factor lead to the relationship for ac filter efficiency shown graphically in Figure 25.
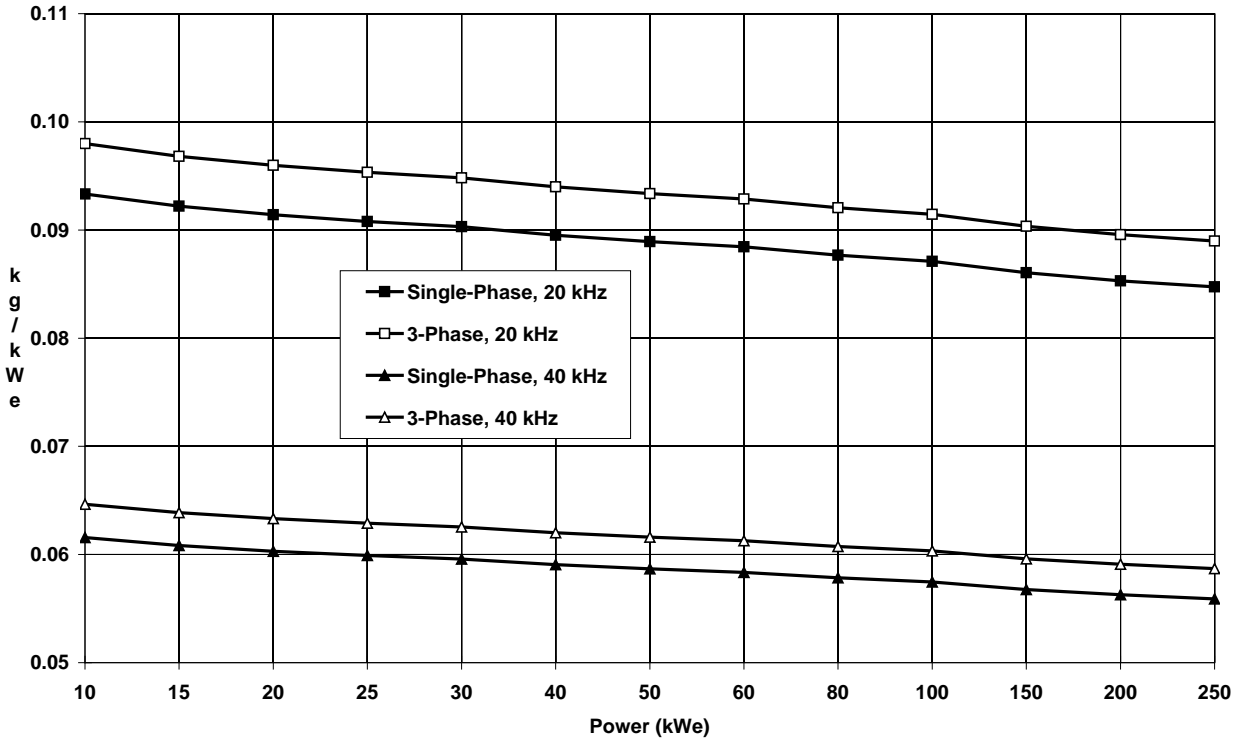
Figure 24: AC Filter SPWT vs Power - Single Phase & 3 Phase
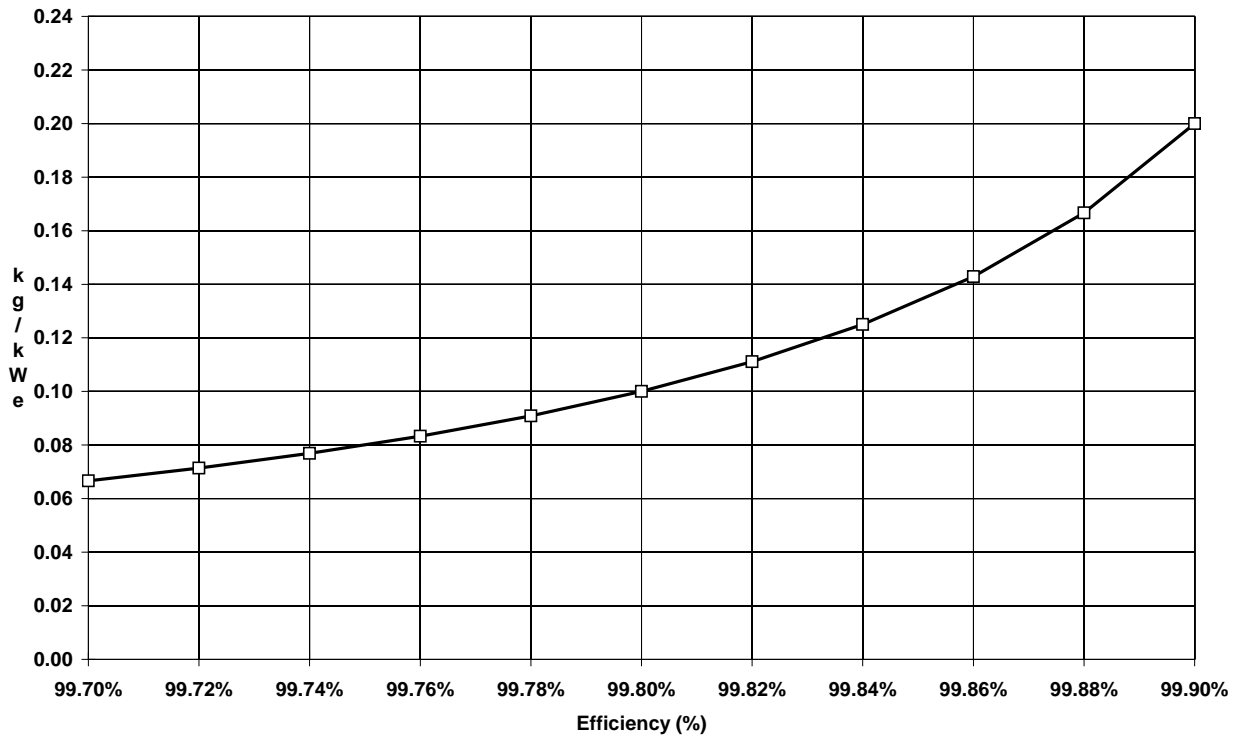
Figure 25: AC Filter SPWT vs Efficiency

Redundancy Factor

$$1FSM = 0.1*((1-0.998)/(1-FSE))*\underline{(FSAM/FSRM)}*FSP_O*(FSP_O/FSRM)^{-0.03}*(FSF/20)^{-0.6}$$

$$3FSM = 0.105*((1-0.998)/(1-FSE))*\underline{(FSAM/FSRM)}*FSP_O*(FSP_O/FSRM)^{-0.03}*(FSF/20)^{-0.6}$$

A redundancy factor accounts for the additional mass needed to realize a more reliable system. The actual number of modules in the assembly is defined by the "available modules" value. The number of modules needed to provide full power is defined by the "required modules" value. A design requiring 4/3 redundancy has four 33% rated channels. The mass of this assembly will be at least 33% heavier and the mass of the fourth channel is part of the penalty associated with this higher reliability requirement.

Power Level Multiplier

$$1FSM = 0.1*((1-0.998)/(1-FSE))*(FSAM/FSRM)*\underline{FSP_O}*(FSP_O/FSRM)^{-0.03}*(FSF/20)^{-0.6}$$

$$3FSM = 0.105*((1-0.998)/(1-FSE))*(FSAM/FSRM)*\underline{FSP_O}*(FSP_O/FSRM)^{-0.03}*(FSF/20)^{-0.6}$$

These equations can calculate the mass or specific weight of the ac filter. If the power level multiplier is included, the mass of the ac filter will be calculated; removing it produces the filter's specific weight.

Power Level Factor

$$1FSM = 0.1*((1-0.998)/(1-FSE))*(FSAM/FSRM)*FSP_O*\underline{(FSP_O/FSRM)^{-0.03}}*(FSF/20)^{-0.6}$$

$$3FSM = 0.105*((1-0.998)/(1-FSE))*(FSAM/FSRM)*FSP_O*\underline{(FSP_O/FSRM)^{-0.03}}*(FSF/20)^{-0.6}$$

The heaviest element in the ac filter is the current transformer. As the filter power level increases and the size of this transformer grows, its core is better utilized, and the winding current density increases slightly. These economies of scale reduce the current transformer specific weight by the 0.08 power as the filter power level rises. Similar evaluations of the inductor, capacitor, and resistor specific weights indicated they did not change with power level. Combining the specific weight contributions of all the elements in the ac filter indicated the specific weight of the complete filter declined at the 0.03 power as the ac filter power level grew. This effect is shown in Figure 26 for 10, 20, and 40 kHz single-phase ac filter designs.

The "required modules" figure is included in this factor to address the use of a modular design approach. The total output power of the assembly must be divided by the required number of modules since each module processes just a portion of this power. Because the specific weight of an ac filter changes with power, its mass must be calculated at the power level of the individual modules and not the power level of the complete assembly.

Frequency Factor

$$1FSM = 0.1*((1-0.998)/(1-FSE))*(FSAM/FSRM)*FSP_O*(FSP_O/FSRM)^{-0.03}*\underline{(FSF/20)^{-0.6}}$$

$$3FSM = 0.105*((1-0.998)/(1-FSE))*(FSAM/FSRM)*FSP_O*(FSP_O/FSRM)^{-0.03}*\underline{(FSF/20)^{-0.6}}$$

The combined impact of frequency on ac filter mass was determined by evaluating the influence frequency had on the current transformer, the series resonant circuit, and the resistor masses. The mass of the current transformer core will decline with increasing frequency because the flux density needed to generate a given voltage declines as frequency rises. This lower flux density reduces the transformer core volume and mass. A smaller core means less winding mass because the mean length of the turns is
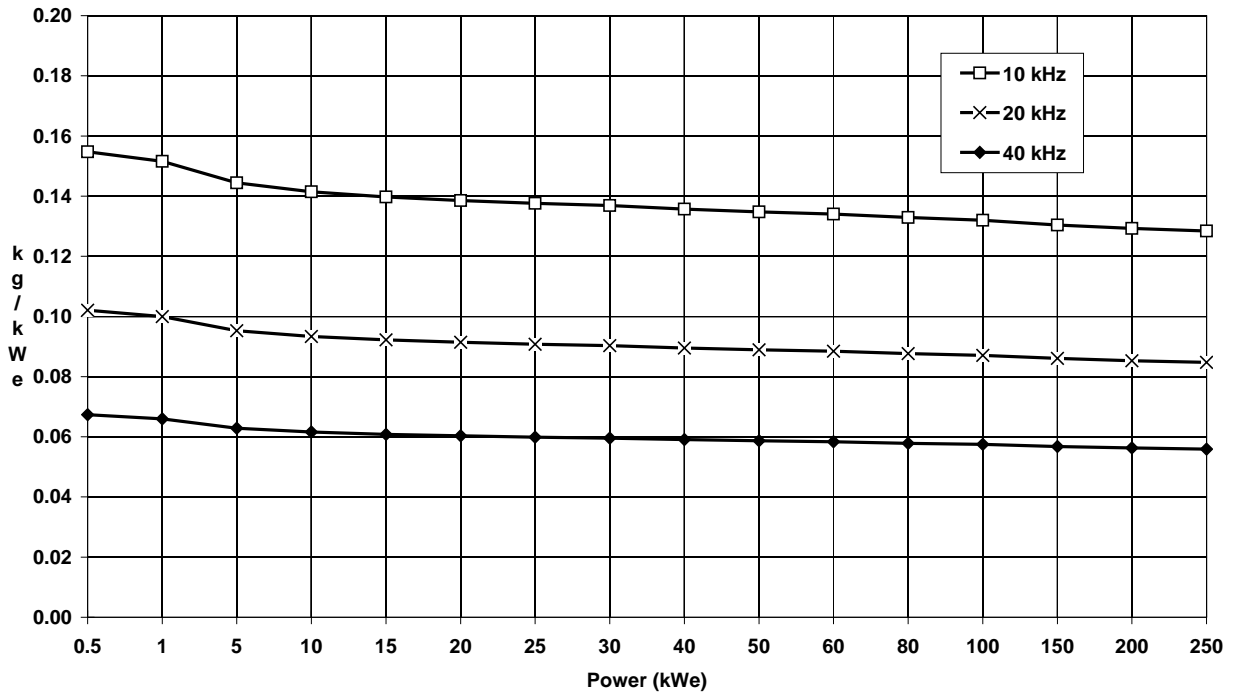
Figure 26: AC Filter SPWT vs Power

less. By totaling the overall effect, it was determined that the current transformer specific weight declined at the 0.47 power as frequency rose.

The resonant frequency of the series resonant circuit is calculated with the following equation.

$$F_R = 1/(LC)^{0.5}$$

Where: F_R is the resonant frequency,
L is the circuit inductance in Henries,
C is the circuit capacitance in Farads.

By inspection one can see the circuit inductance and capacitance must double if the resonant frequency is cut in half. This causes the inductor and capacitor mass to double and shows that the mass of a series resonant circuit is inversely proportional to frequency. The final element in the filter, the resistor, is unaffected by frequency. By adding these individual frequency effects together, a frequency factor was generated for the complete ac filter. This calculation indicated the specific weight of an ac filter would decline at the 0.6 power as its resonant frequency rose. The combined influence of frequency on filter mass is shown in Figure 27 for 1 and 100 kWe single-phase ac filter designs.

Voltage Factor

The current transformer contained in the ac filter is necessary to obtain reasonable values for the inductor and capacitor and to reflect adequate resistance into the line to inhibit harmonics. Consequently, the effects of different operating voltages on the resonant circuit elements and the resistor can be offset by selecting the proper turns ratio for this transformer. This means the only item that will be impacted by varying the voltage level is the current transformer itself. The effect of voltage on a transformer was previously investigated in section 3.1.2.1 and it was shown to be fairly minor. Since the transformer is only one element in the filter, the cumulative effect will be even less. After a short analysis, it was considered negligible and a factor was not included in the equations.
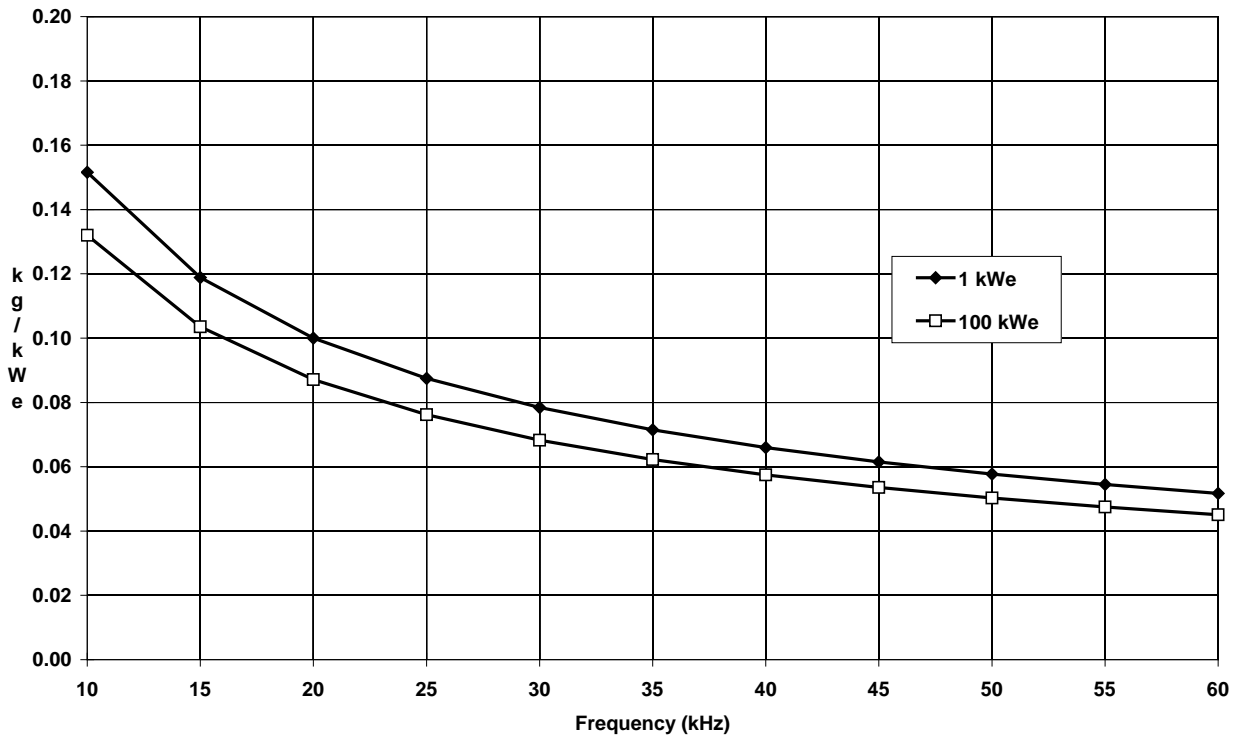
Figure 27: AC Filter SPWT vs Frequency

3.7 DC RBI MODEL

Dc remote bus isolators (RBIs) are smart circuit protection devices that incorporate current sensors and are used to switch dc power and interrupt fault currents. They are located in dc switchgear units. This section discusses the equations developed to estimate their masses as a function of power, efficiency, and voltage.

The latest dc RBI switchgear design uses a channelized approach because the card cage assembly that controls and monitors the dc RBI operation can be shared among several units. Three basic design approaches are available for a single RBI channel, a mechanical relay, a hybrid arrangement consisting of a mechanical relay paralleled with a semiconductor switch, or a semiconductor switch. The ISS RBIs use a mechanical relay and add a snubber circuit to suppress voltage transients occurring during opening and closing periods. A hybrid arrangement has certain advantages because the relay and semiconductor switch can function together to improve the operating characteristics of the RBI switch. The relay carries the bulk of the current during normal operation; this results in a high efficiency switch. The main need for the semiconductor switch is during opening and closing times. It closes immediately before relay closing to quell relay chatter transients, and it opens after the relay to suppress opening transients. The opening rate of the semiconductor can be varied to obtain the best opening characteristics. A design that only uses a semiconductor switch exhibits very good opening and closing characteristics. However, the conduction resistance of a semiconductor is much higher than a relay contact; therefore, the switch losses are significantly higher during normal operating periods.

The dc RBI model described in this report is based on a hybrid switch configuration. This design was considered to provide the best combination of mass, efficiency, and switching characteristics. However, as the RBI voltage rises the switch design will probably change from a relay in parallel with a single semiconductor to a vacuum switch in parallel with a number of series connected semiconductors. At the present time, the semiconductor devices in a dc RBI would likely be MOSFETs or insulated gate bipolar transistors (IGBTs). Future RBI designs will probably use MCTs. Mass breakdowns were generated for two sizes of dc RBIs. These mass estimates were derived from a SSF RBI mass breakdown that was

adjusted to be consistent with the as-built flight DC Switching Unit (DCSU) and information obtained from a Ford Aerospace briefing package [Ref. 14, 17, 50]. The original RBI efficiency was calculated from RBI loss information contained in a Rocketdyne SSF document [Ref. 51]. During this review, the previously calculated efficiency value determined for the dc RBIs was checked against the Electrical Power System On-Orbit Performance (EPSOP) Modeling Data report, which showed the original efficiency value, 99.85%, was consistent with the flight design [Ref. 52]. These mass and efficiency values were utilized as a basis for the subsequent equation development.

The following paragraphs explain the dc RBI equation development. Graphs are used in conjunction with technical descriptions to explain the equation rationale. The variables used in this discussion are shown in Table 17.

Table 17: DC RBI Model Variable Definitions

DRBM	Dc RBI Mass
DRBE	Dc RBI Efficiency (99.85%)
DRBAM	Dc RBI Available Modules
DRBRM	Dc RBI Required Modules
DRBP$_O$	Dc RBI Power Output (kWe)
DRBV$_O$	Dc RBI Voltage Output (Vdc)

Mass Coefficient

$$DRBM = \underline{0.12} * ((EXP(0.0008/(1-DRBE)))/1.7) * (DRBAM/DRBRM) * DRBP_O * (DRBP_O/DRBRM)^{-0.15} *$$
$$(DRBV_O/200)^{0.13}$$

The dc RBI mass coefficient was developed from SSF DC RBI mass breakdowns. To be consistent with the previously discussed future design, the design of the SSF dc RBI was revised to include a semiconductor switch in parallel with the mechanical relay, the snubber circuitry was removed since it was no longer required, and mass benefits obtained from minor hardware advancements were incorporated. The mass coefficient was calibrated to yield values consistent with these mass breakdowns.

Efficiency Factor

$$DRBM = 0.12 * \underline{((EXP(0.0008/(1-DRBE)))/1.7)} * (DRBAM/DRBRM) * DRBP_O * (DRBP_O/DRBRM)^{-0.15} *$$
$$(DRBV_O/200)^{0.13}$$

The above underlined factor estimates the change in specific weight occurring with a change in dc RBI efficiency. The efficiency of an RBI is quite high and it does not appear practical to change it much. However, it can be increased by reducing the resistances of the relay contacts and semiconductor. To accomplish this, the conduction areas of these elements must be enlarged. Basically, doubling the masses of the relay contacts and semiconductor switch will cut their losses in half. Since the losses are cut in half, the thermal management hardware changes likewise. The rest of the RBI elements will also change slightly to conform to the new relay, semiconductor, and thermal management hardware designs. The variation in RBI mass was estimated for efficiencies ranging from 99.8 to 99.9% and it was used to generate the above efficiency factor. A graph of RBI specific weights that shows the results of this analysis is contained in Figure 28. Note that the depicted dc RBI efficiency range is relatively narrow. Efficiencies higher than about 99.9% are not considered viable because the relay contact and semiconductor switch size will become impractical. It is not feasible to cut the RBI mass below a certain level because the relay contacts, semiconductor switch, and structural hardware simply will not be strong enough to withstand the stresses encountered while interrupting a fault current.
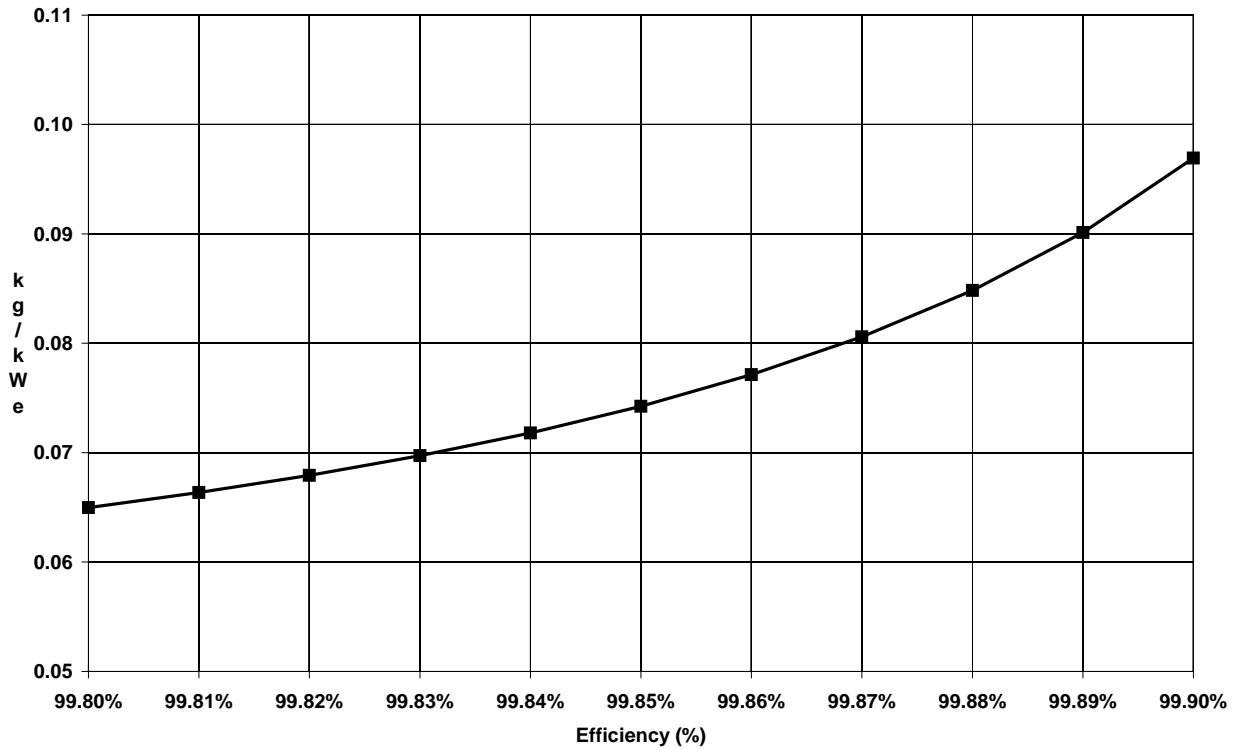
Figure 28: DC RBI SPWT vs Efficiency

Redundancy Factor

$$DRBM=0.12*((EXP(0.0008/(1-DRBE)))/1.7)*\underline{(DRBAM/DRBRM)}*DRBP_O*(DRBP_O/DRBRM)^{-0.15}*$$

$$(DRBV_O/200)^{0.13}$$

The mass of a dc RBI network will rise if a modular design approach is used to enhance reliability. The mass increase is estimated by the factor above. The "available modules" number is the actual number of modules present in the component; the "required modules" value is the actual number of modules required to provide the full output power level. If the reliability requirements of a system force a design to use 4/3 redundancy, each channel is designed to carry 33% of the power. Although 4 channels are available, only 3 channels are needed to supply full power. The mass of the fourth channel is the penalty paid to obtain the higher specified reliability.

Power Level Multiplier

$$DRBM=0.12*((EXP(0.0008/(1-DRBE)))/1.7)*(DRBAM/DRBRM)*\underline{DRBP_O}*(DRBP_O/DRBRM)^{-0.15}*$$

$$(DRBV_O/200)^{0.13}$$

The equation can be used to calculate the mass or specific weight of the dc RBI. When the above multiplier is included, the value that results estimates the RBI mass. To obtain the specific weight of the RBI, remove this multiplier.

Power Level Factor

$$DRBM=0.12*((EXP(0.0008/(1-DRBE)))/1.7)*(DRBAM/DRBRM)*DRBP_O*\underline{(DRBP_O/DRBRM)^{-0.15}}*$$

$$(DRBV_O/200)^{0.13}$$

The masses of the power conducting parts of the dc RBI, which are the relay contacts and the semiconductor switch, will increase nearly linearly with a rise in power. However, the mass of supporting hardware elements, such as driver modules, sensors, and control logic devices, grows at a slower rate. This results in some economies of scale as the dc RBI power level rises and causes its specific weight to decline. The change in the specific weight of a dc RBI as the power level rises is shown in Figure 29.
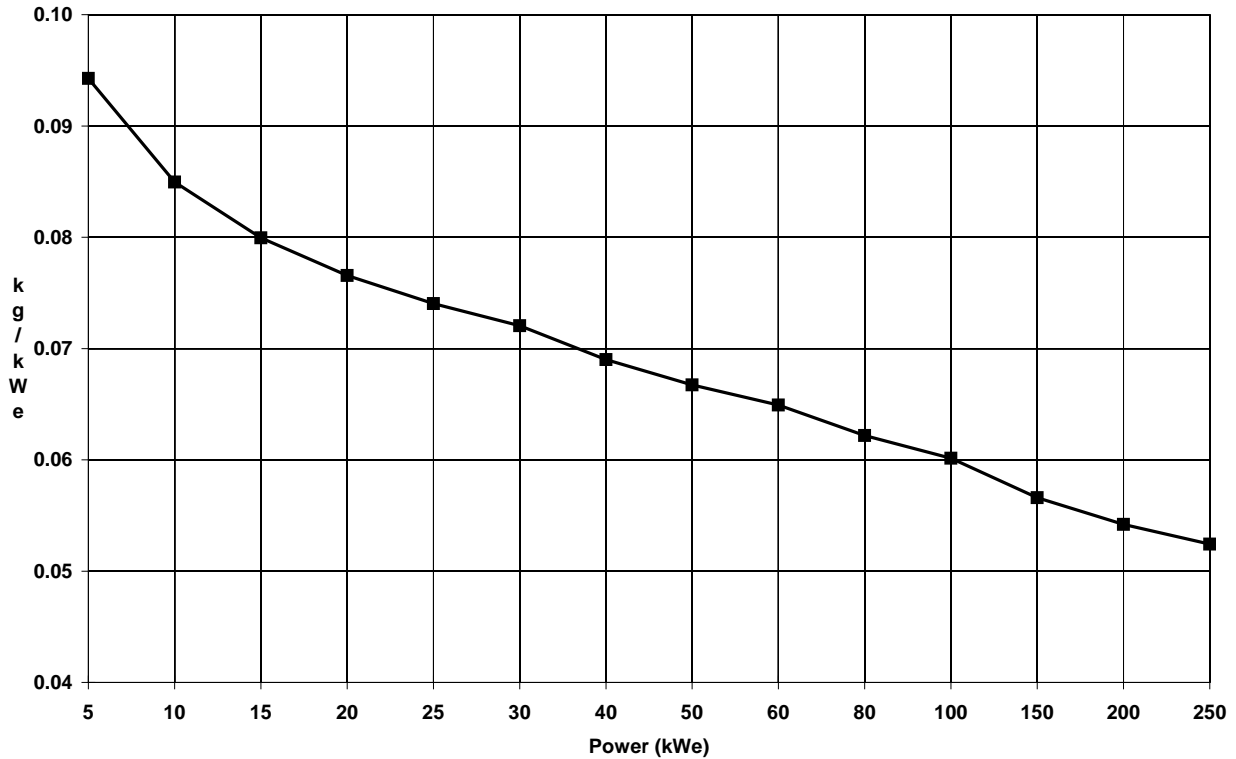
Figure 29: DC RBI SPWT vs Power Level

Voltage Level Factor

$$DRBM=0.12*((EXP(0.0008/(1-DRBE)))/1.7)*(DRBAM/DRBRM)*DRBP_O*(DRBP_O/DRBRM)^{-0.15}*$$

$$(DRBV_O/200)^{0.13}$$

As the voltage across a dc RBI increases, its mass was expected to rise at a slightly higher rate. This is because the elements in the RBI must be further isolated, more insulation is required, and the stresses are higher. The separation distance between the relay contacts in a dc RBI will need to increase as the voltage level rises to prevent vacuum breakdown and arcing. The mass of the semiconductor switch in parallel with the relay is also expected to rise. The semiconductor devices will need to be connected in series to handle higher voltages; however, series connected semiconductors do not inherently share voltages evenly. Additional hardware is needed to make them voltage share and protect them in case they do not. Finally, dc systems normally require capacitors to maintain voltage stability. Unfortunately, the capacitors will discharge into a fault and greatly increase the initial fault current. The RBI must be structurally strong enough to withstand the added stress of this discharge. Each of these factors increases the mass of the complete RBI. By referring to terrestrial RBI designs, an estimate of this mass increase was developed and it was utilized to generate the factor shown above. The results of this exercise are shown in Figure 30.
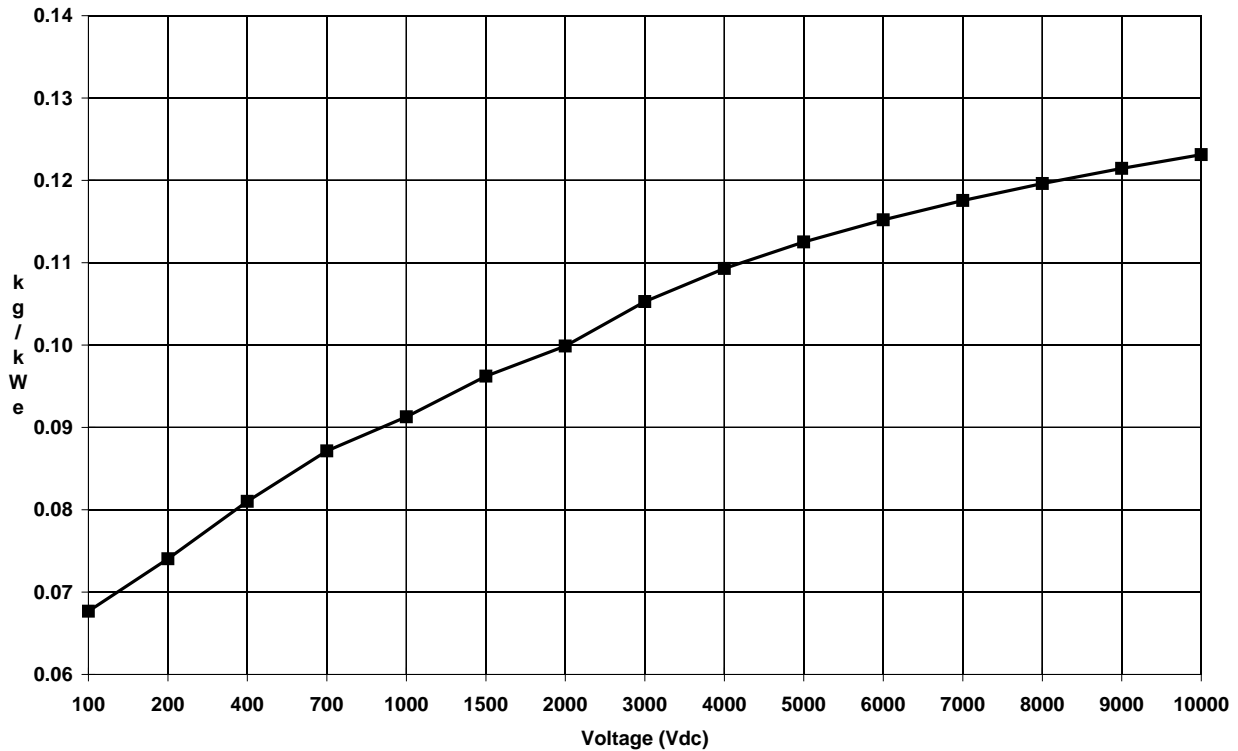
Figure 30: DC RBI SPWT vs Voltage

3.8 AC RBI MODEL

Ac RBIs are smart circuit protection switches with current sensors. They are used to switch major ac power feeds and interrupt faults. They are located in ac switchgear units. The equations developed to estimate ac RBI mass as it varies with power and voltage are discussed in this section.

The ac RBI design will be similar in many respects to the dc RBI design. An ac RBI switchgear unit will also use a channelized approach because the card cage assembly that controls and monitors ac RBI operation can be shared between several RBIs. Two configurations are practical for an ac RBI channel, a hybrid arrangement consisting of a fast acting mechanical relay that is paralleled with a back-to-back pair of semiconductor switches, or just a back-to-back pair of semiconductor switches. A solitary mechanical relay is not fast enough to open during the zero current crossing; consequently, this configuration is not practical.

The hybrid arrangement is preferred because the relay and semiconductor switch can work together to improve the operating characteristics of the RBI switch. During normal power delivery periods, the relay carries the bulk of the current. The mechanical relay contacts greatly reduce conduction losses and allow high efficiency operation. The semiconductor switches are primarily required during opening and closing times. Only semiconductor switches can operate fast enough to close or open within the zero current crossing point limits. The semiconductor switches are closed immediately before relay closing to quell relay chatter transients, and opened after the relay to suppress opening transients. An RBI design using just semiconductor switches exhibits very good opening and closing characteristics; however, its con-duction losses are much higher than a hybrid design with a relay. Consequently, the efficiency of this ac RBI design would be much poorer.

The ac RBI model described in this report is based on a hybrid switch configuration. This design was considered to provide the best combination of mass, efficiency, and switching characteristics. However, as the RBI voltage rises the RBI switch design will probably change from a relay in parallel with a single

semiconductor to a vacuum switch in parallel with a number of series connected semiconductors. At the present time, the semiconductor devices in an ac RBI would probably be SCRs. Future RBI designs may use MCTs. In a telephone conversation with Dave Fox of Westinghouse, he indicated that ac and dc RBIs rated to conduct the same amount of power would have similar masses (Ref. 53). The data bus interface and control elements in the ac RBIs would probably be the same as those in the dc units. The relay in an ac RBI would be lighter because the existence of a zero current crossing point eases fault current interruption; however, the mass of the ac RBI must include the mass of a back-to-back pair of semiconductor switches and their drivers. Based on this discussion the masses of many of the elements in an ac RBI were obtained from the SSF dc RBI mass breakdown [Ref. 14].

The ensuing paragraphs explain the development of single-phase and 3-phase ac RBI equations in detail. The equation formulation is explained via technical descriptions and graphs. The variables used in succeeding discussions are listed in Table 18.

Table 18: AC RBI Model Variable Definitions

1ARB	Single-Phase ac RBI Mass
3ARB	Three-Phase ac RBI Mass
ARBE	Ac RBI Efficiency (99.85%)
ARBAM	Ac RBI Available Modules
ARBRM	Ac RBI Required Modules
ARBP$_O$	Ac RBI Power Output (kWe)
ARBV$_O$	Ac RBI Voltage Output (Vrms)

Mass Coefficient

$$1ARB = \underline{0.1} * ((EXP(0.0008/(1-ARBE)))/1.7) * (ARBAM/ARBRM) * ARBP_O * (ARBP_O/ARBRM)^{-0.13} *$$

$$(ARBV_O/200)^{0.05}$$

$$3ARB = \underline{0.135} * ((EXP(0.0008/(1-ARBE)))/1.7) * (ARBAM/ARBRM) * ARBP_O * (ARBP_O/ARBRM)^{-0.15} *$$

$$(ARBV_O/200)^{0.05}$$

The SSF dc RBI mass breakdowns were used as a starting point to generate mass breakdowns for ac RBIs. The resulting ac RBI mass breakdowns were then used to determine the mass coefficients underlined above. Many elements in dc and ac RBIs will be equivalent; therefore, the masses of these dc RBI elements were also used in the ac RBI case. The size of the relay in an ac RBI is smaller, but an ac RBI requires a back-to-back pair of semiconductor switches. The reduced relay mass and the mass of these semiconductor switches and their drivers was included in the ac RBI mass breakdowns. The ac RBI mass breakdown was completed by removing the snubber circuitry included in the SSF dc RBI design and incorporating the mass gains resulting from minor hardware advancements expected over the next ten years. The mass breakdowns generated for future ac RBIs are located in Appendix A on pages A-8 and A-9. The mass coefficients contained in the ac RBI mass equations were calculated to yield values consistent with these mass breakdowns.

The mass of the relay in a 3-phase ac RBI design was estimated to be about 50% heavier due to the need for two additional contact and semiconductor switch pairs. However, because the mass of the control logic and thermal management hardware is similar in both designs and the packaging weight difference becomes less as the RBI size grows, the relative difference in mass between the two designs also declines as the power level rises. The specific weights of single- and 3-phase ac RBI designs are compared in Figure 31.
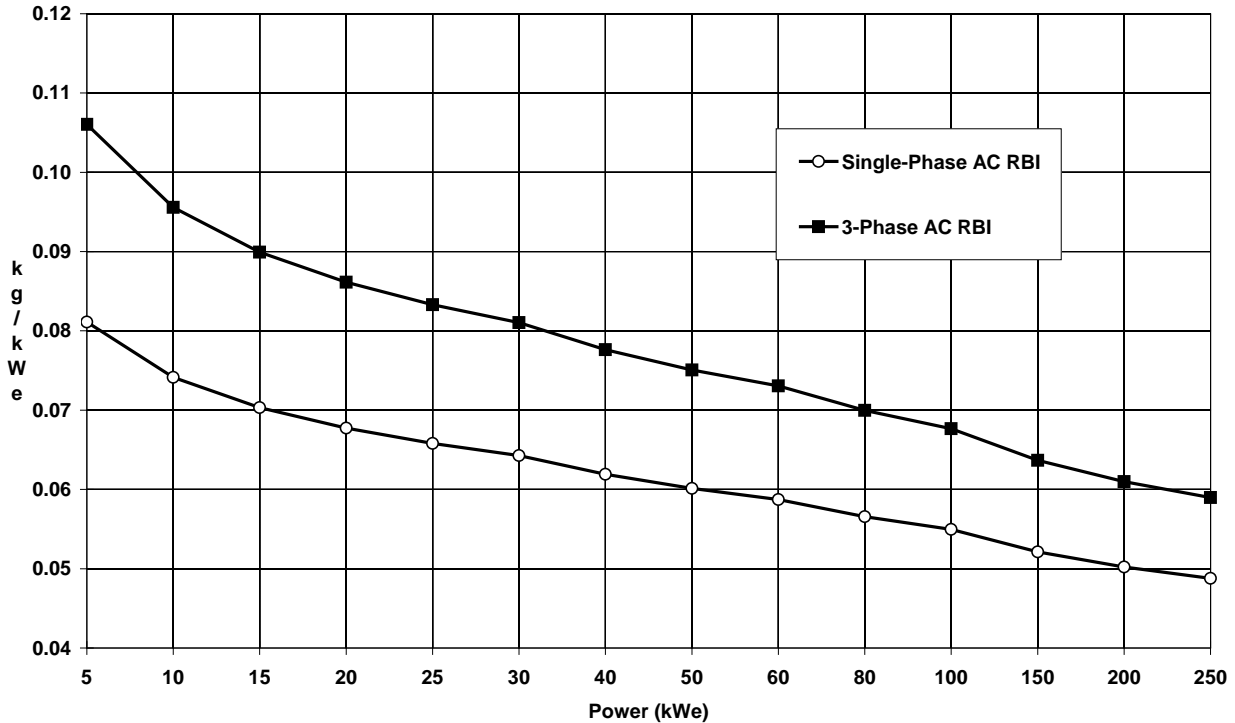
Figure 31: AC RBI SPWT - 1 Phase vs 3 Phase

Efficiency Factor

$1ARB = 0.1 * \underline{((EXP(0.0008/(1-ARBE)))/1.7)} * (ARBAM/ARBRM) * ARBP_O * (ARBP_O/ARBRM)^{-0.13} *$

$(ARBV_O/200)^{0.05}$

$3ARB = 0.135 * \underline{((EXP(0.0008/(1-ARBE)))/1.7)} * (ARBAM/ARBRM) * ARBP_O * (ARBP_O/ARBRM)^{-0.15} *$

$(ARBV_O/200)^{0.05}$

The efficiency of an ac RBI was expected to be the same as a dc RBI; the reactive parasitics associated with ac operation were expected to be negligible. The efficiency of an ac RBI can be increased by enlarging the conduction area of the relay contacts and semiconductor switches to reduce their resistance. Doubling the mass of the relay contacts and semiconductor switches should cut conduction losses in half. The mass of the thermal management hardware should decline proportionally. Other RBI elements will change slightly to conform to the new relay, semiconductor, and thermal management hardware designs. Changes in RBI mass were estimated for efficiencies ranging from 99.8 to 99.9%. Efficiencies higher than 99.9% are not considered practical because the relay contact and semiconductor switch sizes would become too large. Below an efficiency of 99.8% the structural integrity of the RBI, and the strength of its relay contacts and semiconductor switches would be suspect. RBI mass breakdowns generated during this process were used to create the above efficiency factor. A graph of ac RBI specific weights as a function of efficiency is shown in Figure 32.
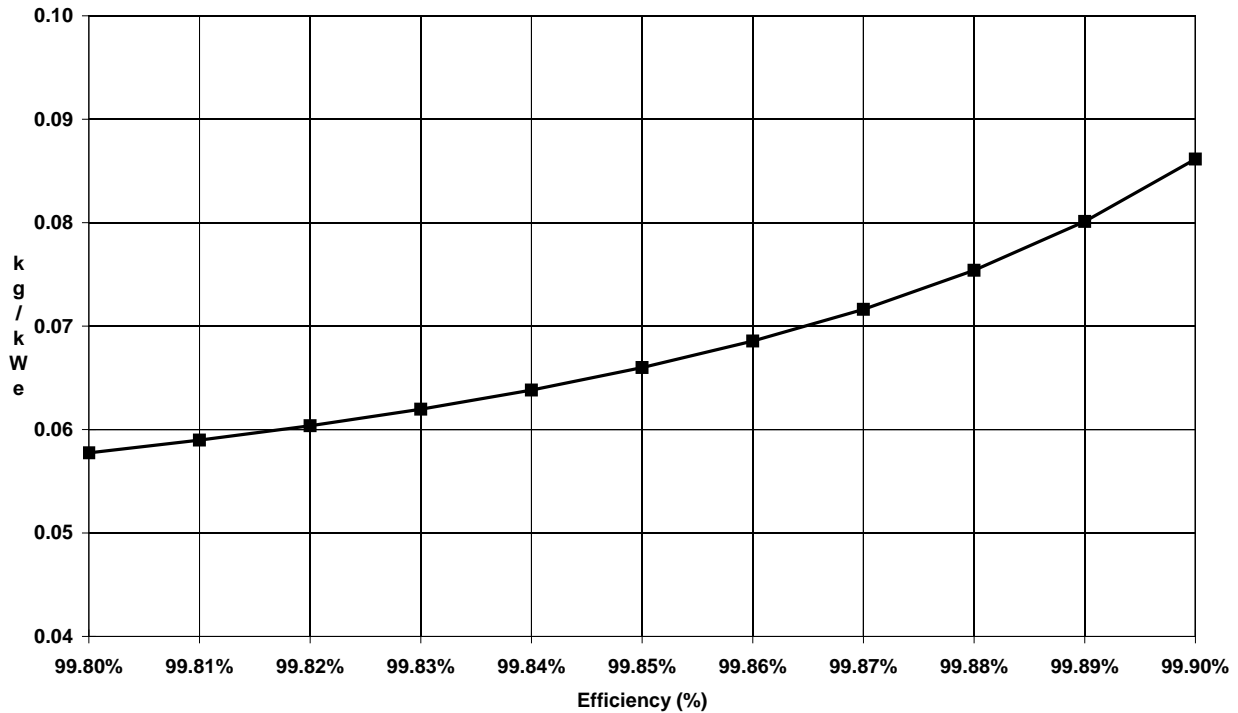
Figure 32: AC RBI SPWT vs Efficiency

Redundancy Factor

$1ARB=0.1*((EXP(0.0008/(1-ARBE)))/1.7)*\underline{(ARBAM/ARBRM)}*ARBP_O*(ARBP_O/ARBRM)^{-0.13}*$

$(ARBV_O/200)^{0.05}$

$3ARB=0.135*((EXP(0.0008/(1-ARBE)))/1.7)*\underline{(ARBAM/ARBRM)}*ARBP_O*(ARBP_O/ARBRM)^{-0.15}*$

$(ARBV_O/200)^{0.05}$

If a modular design approach is used to enhance reliability, the total mass of the ac RBI units will rise. The above factor estimates this mass increase. The actual number of modules present in the system is defined by the "available modules" number; the number of modules required to deliver full power is specified by the "required modules" value. If a system is designed with 4/3 redundancy, each channel is capable of carrying 33% of the power. The fourth channel is not required to provide full power and its mass is the penalty paid to obtain a higher reliability.

Power Level Multiplier

$1ARB=0.1*((EXP(0.0008/(1-ARBE)))/1.7)*(ARBAM/ARBRM)*\underline{ARBP_O}*(ARBP_O/ARBRM)^{-0.13}*$

$(ARBV_O/200)^{0.05}$

$3ARB=0.135*((EXP(0.0008/(1-ARBE)))/1.7)*(ARBAM/ARBRM)*\underline{ARBP_O}*(ARBP_O/ARBRM)^{-0.15}*$

$(ARBV_O/200)^{0.05}$

The equations can be used to calculate the mass or specific weight of the ac RBI. When the above multiplier is included, the value that results is an estimate of the RBI mass. To obtain the specific weight of the RBI, remove this multiplier.

Power Level Factor

1ARB=0.1*((EXP(0.0008/(1-ARBE)))/1.7)*(ARBAM/ARBRM)*ARBP_O*$\underline{(\text{ARBP}_O/\text{ARBRM})^{-0.13}}$*

$(\text{ARBV}_O/200)^{0.05}$

3ARB=0.135*((EXP(0.0008/(1-ARBE)))/1.7)*(ARBAM/ARBRM)*ARBP_O*$\underline{(\text{ARBP}_O/\text{ARBRM})^{-0.15}}$*

$(\text{ARBV}_O/200)^{0.05}$

The mass of the relay contacts and semiconductor switches will rise nearly linearly with an increase in power because they are the power conducting elements in the ac RBI. However, the masses of the drivers, sensors, and logic devices do not rise as fast. These trends result in some economies of scale as ac RBI power levels rise and they cause specific weights to decline. Because the mass of the ancillary hardware in a 3-phase ac RBI occupies a larger percentage of its total mass, the gains in specific weight that occur with power are greater in this RBI design than in the single-phase RBI design. This explains the difference between the single- and 3-phase power level multiplier exponents, -0.18 and -0.21. The difference in mass growth rates between single- and 3-phase ac RBIs can be seen by referring back to Figure 31. An expanded view of only the single-phase ac RBI is shown in Figure 33.
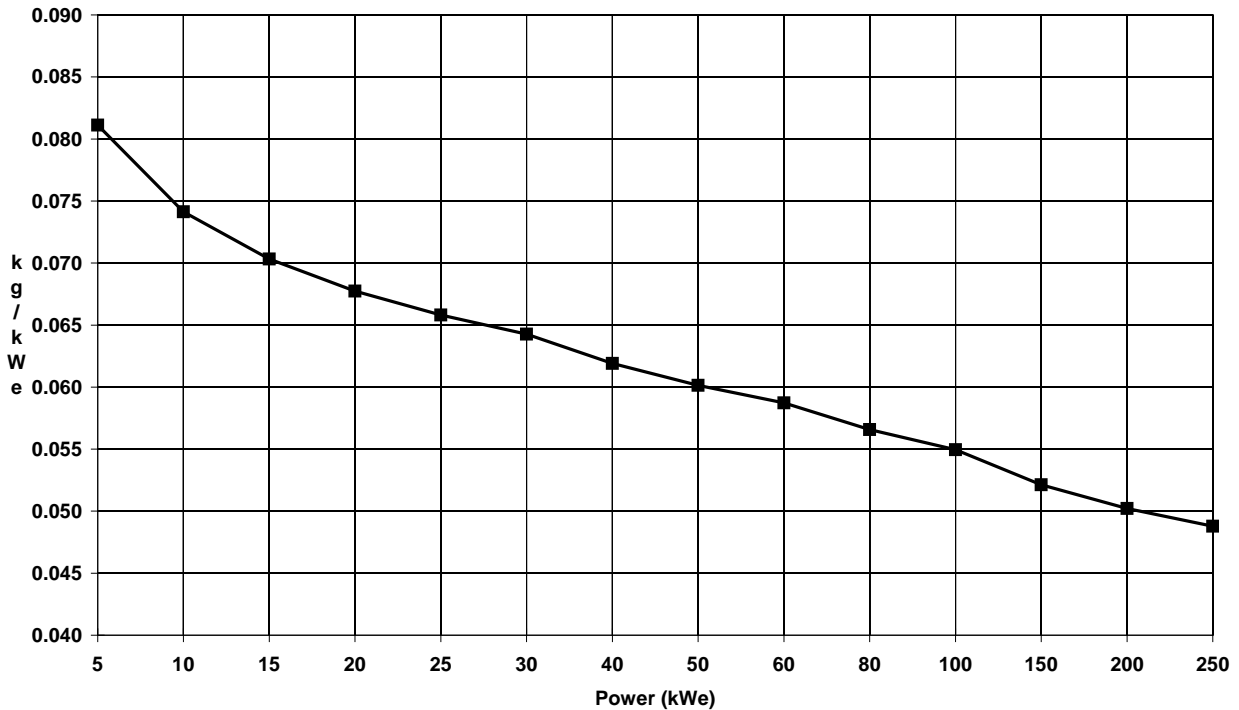
Figure 33: AC RBI SPWT vs Power Level

Voltage Level Factor

1ARB=0.1*((EXP(0.0008/(1-ARBE)))/1.7)*(ARBAM/ARBRM)*ARBP_O*$(\text{ARBP}_O/\text{ARBRM})^{-0.13}$*

$\underline{(\text{ARBV}_O/200)^{0.05}}$

3ARB=0.135*((EXP(0.0008/(1-ARBE)))/1.7)*(ARBAM/ARBRM)*ARBP_O*$(\text{ARBP}_O/\text{ARBRM})^{-0.15}$*

$\underline{(\text{ARBV}_O/200)^{0.05}}$

A number of effects, some of them offsetting, occur as the voltage across an ac RBI increases. The internal RBI wiring and its devices will require more insulation to withstand the added voltage stresses. The relay contacts will need to be separated further to prevent vacuum breakdown. These effects tend to increase the RBI mass, especially the relay mass. However, assuming the RBI power level remains the same, the current conducted by the contacts will decline as the voltage rises. This reduces the mass of the relay contacts and the relay driver. Since the mechanical parts of the relay are heavier than insulation, the overall effect should be a slight reduction in relay mass as the ac RBI voltage increases. The mass of the semiconductor switches in parallel with the relay, however, is expected to rise as voltage increases. Semiconductor devices must be connected in series to switch higher voltages; however, series connected semiconductors will not naturally share voltages evenly. Additional hardware is needed to make them voltage share and protect them in case they do not. These factors increase the mass of the RBI. After weighing the increase in semiconductor mass against the reduction in relay mass, it appears the mass of a complete ac RBI will slowly rise as voltage levels rise. Figure 34 displays the results of this evaluation.
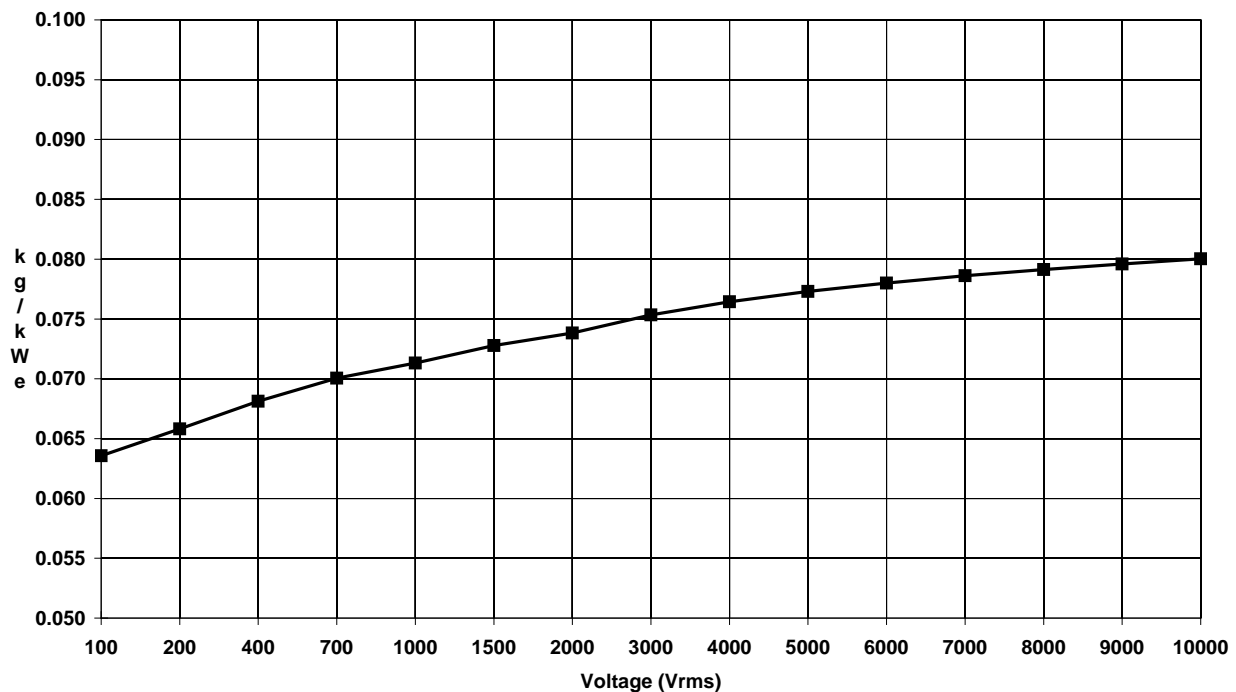
Figure 34: AC RBI SPWT vs Voltage

3.9 DC RPC MODEL

Dc remote power controllers (RPCs) are used to switch and monitor individual dc load circuits and provide circuit protection. These devices will be located in dc power distribution racks. This section explains the equation developed to estimate their masses as a function of power, efficiency, and voltage. This equation provides rough mass estimates for component comparison purposes. For more accurate mass estimates specific component designs must be developed.

The present ISS dc RPC module design uses a channelized approach similar to the dc RBI configuration since the card cage assembly that controls and monitors the operation of a dc RPC can be shared among several units. Two types of RPCs are employed depending on the current rating. The 65 amp rated RPC uses a relay, while the 25 amp and lower rated RPCs utilize semiconductor switches. An alternative would be an RPC channel with a hybrid arrangement consisting of a mechanical relay paralleled with a semiconductor switch. A hybrid arrangement is attractive because the relay and semiconductor switch can function together to yield a high efficiency switch that also exhibits good opening and closing characteristics. However, because the semiconductor only switch design is lighter and semiconductor switches,

especially MOSFETs, have lower "on" resistances then past generations of semiconductor switches the dc RPC equation described in this section is based on a semiconductor only switch configuration. Since a dc RPC is essentially a lower power dc RBI in many respects and most of their characteristics are similar, the paragraphs describing the RPC equation development and rationale will rely heavily on the previous dc RBI discussion. Explanations will be succinct to reduce the amount of repetition. If additional information is desired please refer back to the dc RBI discussion.

It was mentioned that the dc RBI and RPC configurations are similar; however, there are some differences that cause their specific weights to vary. The mass of the thermal management hardware occupies a larger percentage of the RPC mass. This is partially because an RPC is less efficient, but mainly because thermal management hardware does not scale linearly down to these smaller power levels. The mass of the housing and structure of an RPC also assumes a greater portion of the total mass for the same reason. The effect of these two items causes the specific weight of an RPC to be considerably higher than a RBI. Dc RPC mass breakdowns are contained in Appendix A on page A-10 and A-11. They were derived from SSF RPC mass breakdowns, adjusted to reflect the flight unit masses [Ref. 14, 17]. The efficiency of the dc RPC was calculated using the ISS RPC Interface Control Document (ICD), which indicated the value previously calculated during Task Order 15, 99.85%, was too high and it was reduced to 99.7% [Ref. 54]. These values were used as a basis for the subsequent equation development.

The dc RPC equation development is explained in the following paragraphs. Graphs are used in conjunction with technical descriptions to explain the equation rationale. Variables used in this discussion are shown in Table 19.

Table 19: DC RPC Model Variable Definitions

DRPM	Dc RPC Mass
DRPE	Dc RPC Efficiency (99.7%)
DRPAM	Dc RPC Available Modules
DRPRM	Dc RPC Required Modules
DRPP$_O$	Dc RPC Power Output (kWe)
DRPV$_O$	Dc RPC Voltage Output (Vdc)

Mass Coefficient

$DRPM = \underline{0.135} * ((EXP(0.0006/(1-DRPE)))/1.2214) * (DRPAM/DRPRM) * DRPP_O * (DRPP_O/DRPRM)^{-0.12} *$

$(DRPV_O/120)^{0.04}$

The dc RPC mass breakdowns located in Appendix A were derived from SSF dc RPC mass breakdowns. The mass totals obtained from these breakdowns were checked against the latest flight unit masses and were found to be in close agreement. The SSF RPC mass breakdowns and those used for this equation development are based on a semiconductor switch configuration. Mass gains originating from technology improvements are incorporated into the dc RPCM rack model and the breakdowns in Appendix A and they reflect a 2 to 3% reduction in total RPC mass depending on its configuration. An RPC with more channels, 16 channels versus one for instance, tends to be slightly heavier due to the mass overhead for more switch gate drives, sensors, and additional control elements. The above mass coefficient was calculated to yield values consistent with these mass breakdowns.

Efficiency Factor

$DRPM = 0.135 * \underline{((EXP(0.0006/(1-DRPE)))/1.2214)} * (DRPAM/DRPRM) * DRPP_O * (DRPP_O/DRPRM)^{-0.12} *$

$(DRPV_O/120)^{0.04}$

The above underlined factor estimates the change in specific weight occurring with a change in dc RPC efficiency. The efficiency of an RPC can be raised by enlarging the contact and semiconductor conduction area to reduce their resistance. The mass of the semiconductor switch will increase, but the sensor, control logic and gate drive circuitry mass doesn't change significantly, and the thermal management hardware mass will decline slightly. RPC mass estimates were generated for efficiencies ranging from 99.65 to 99.75% and they were used to generate the above efficiency factor. A graph of these RPC specific weights is shown in Figure 35.
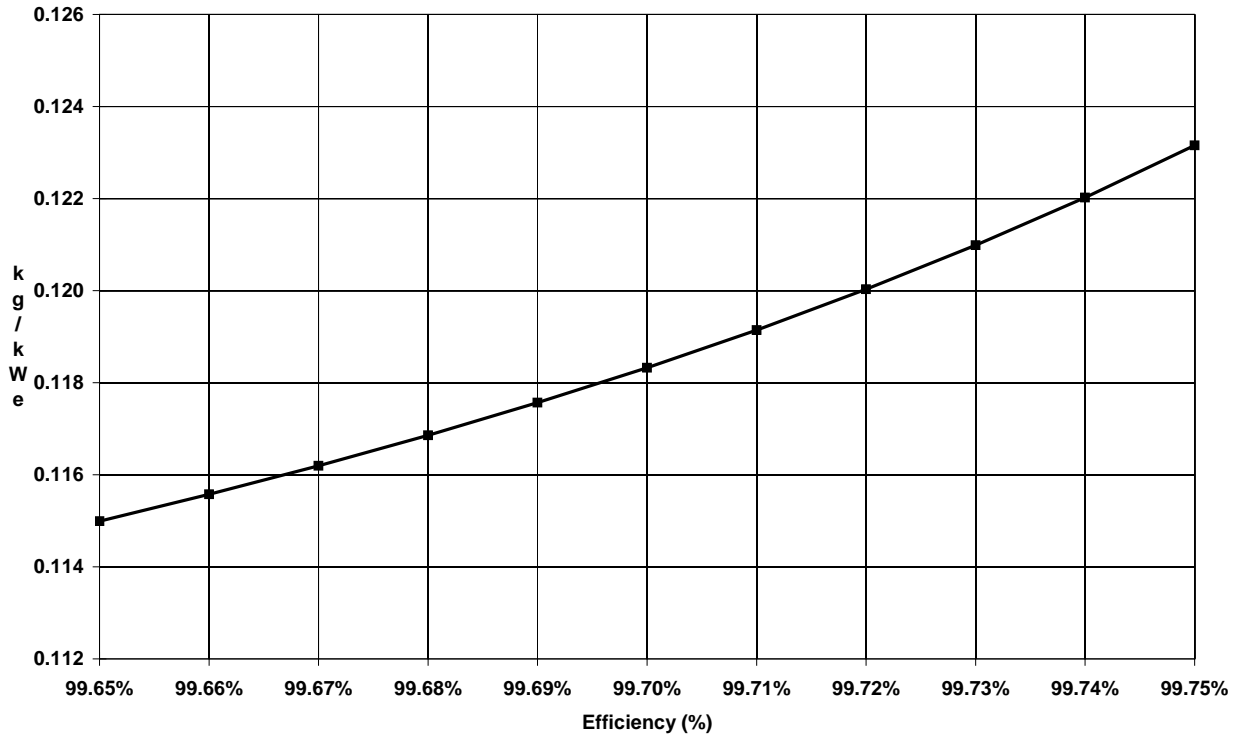
Figure 35: DC RPC SPWT vs Efficiency

Redundancy Factor

$$DRPM = 0.135 * ((EXP(0.0006/(1-DRPE)))/1.2214) * \underline{(DRPAM/DRPRM)} * DRPP_O * (DRPP_O/DRPRM)^{-0.12} *$$

$$(DRPV_O/120)^{0.04}$$

The mass of a dc RPC network rises if a modular design approach is used to enhance reliability. The factor underlined above estimates this mass increase. The "available modules" number is the actual number of modules present in the component; the "required modules" number is the actual number of modules required to provide full output power. Assume the system reliability requirements necessitate the use of 4/3 redundancy. Each channel will be designed to carry 33% of the power. 4 channels will be available, but only 3 are needed to supply full power. The mass of the fourth channel is the penalty paid to obtain the higher specified reliability.

Power Level Multiplier

$$DRPM = 0.135 * ((EXP(0.0006/(1-DRPE)))/1.2214) * (DRPAM/DRPRM) * \underline{DRPP_O} * (DRPP_O/DRPRM)^{-0.12} *$$

$$(DRPV_O/120)^{0.04}$$

The equation can be used to calculate the mass or specific weight of the dc RPC. When the above multiplier is included, the RPC mass is estimated. To obtain the specific weight of the RPC, remove this multiplier.

Power Level Factor

$$DRPM=0.135*((EXP(0.0006/(1-DRPE)))/1.2214)*(DRPAM/DRPRM)*DRPP_O*\underline{(DRPP_O/DRPRM)^{-0.12}}*$$

$$\underline{(DRPV_O/120)^{0.04}}$$

The mass of the dc RPC semiconductor switch will increase proportionally with a rise in power. However, the masses of supporting hardware elements, such as gate drive circuits, sensors, and control logic devices, will grow at a slower rate. This results in some economies of scale as the RPC power level rises and causes its specific weight to decline. The change in the specific weight of a dc RPC as the power level rises is shown in Figure 36.
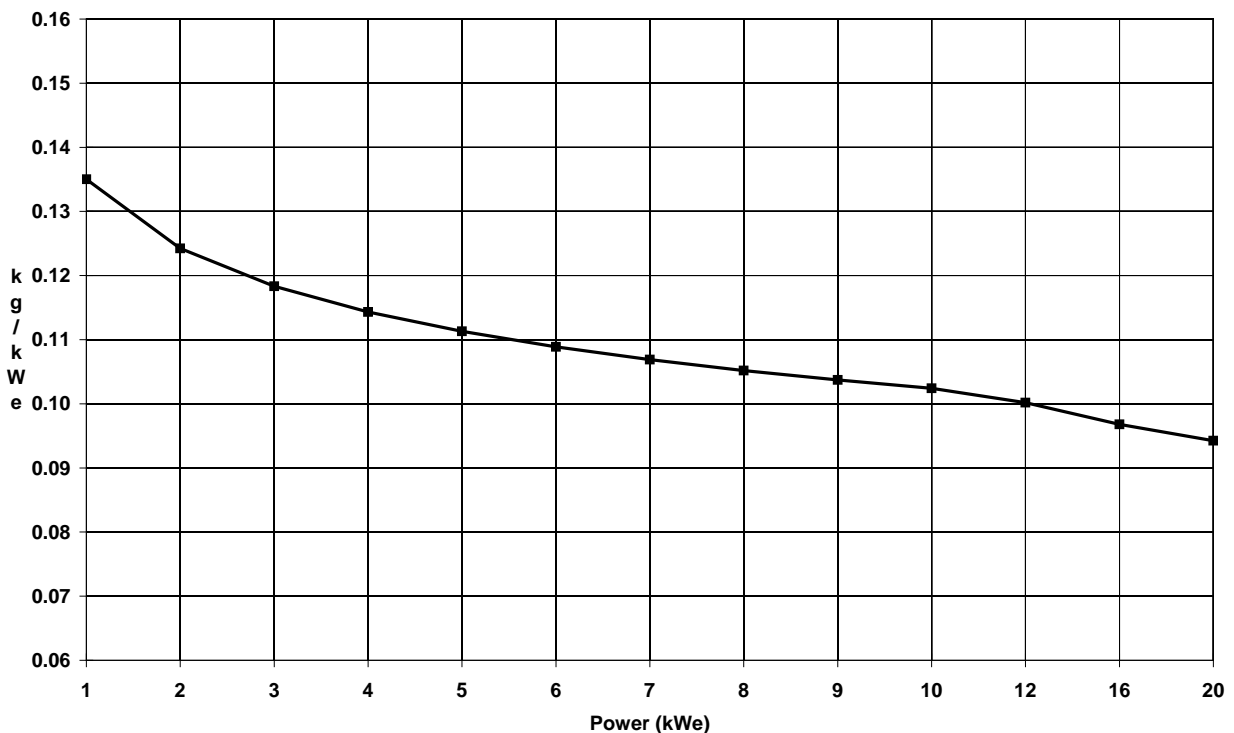
Figure 36: DC RPC SPWT vs Power Level

Voltage Level Factor

$$DRPM=0.135*((EXP(0.0006/(1-DRPE)))/1.2214)*(DRPAM/DRPRM)*DRPP_O*(DRPP_O/DRPRM)^{-0.12}*$$

$$\underline{(DRPV_O/120)^{0.04}}$$

The mass of an RPC was expected to rise slowly as the voltage across it was increased. However, RPCs are located near the loads and experience voltages that are much lower than RBIs. Consequently, many effects identified with high voltage operation, such as vacuum relay breakdown, presumably will not be a factor. RPC voltages also are not high enough to warrant connecting semiconductor switches in series. This means the problems associated with this form of operation will not occur and the mass of the semiconductor switches should not rise much with voltage. Finally, the largest capacitors contained in dc systems are normally located in the primary power distribution components near the power source.

These capacitors will be isolated from the RPCs by dc/dc converters that are likely equipped with current limiting. This will greatly reduce the effects of capacitor discharge into a load fault and mitigate the stress imposed on the RPC. The main item that will increase the mass of the RPC is added insulation. This is needed to withstand higher voltages, but its effect on RPC mass should be minor. Figure 37 displays the results of this analysis.
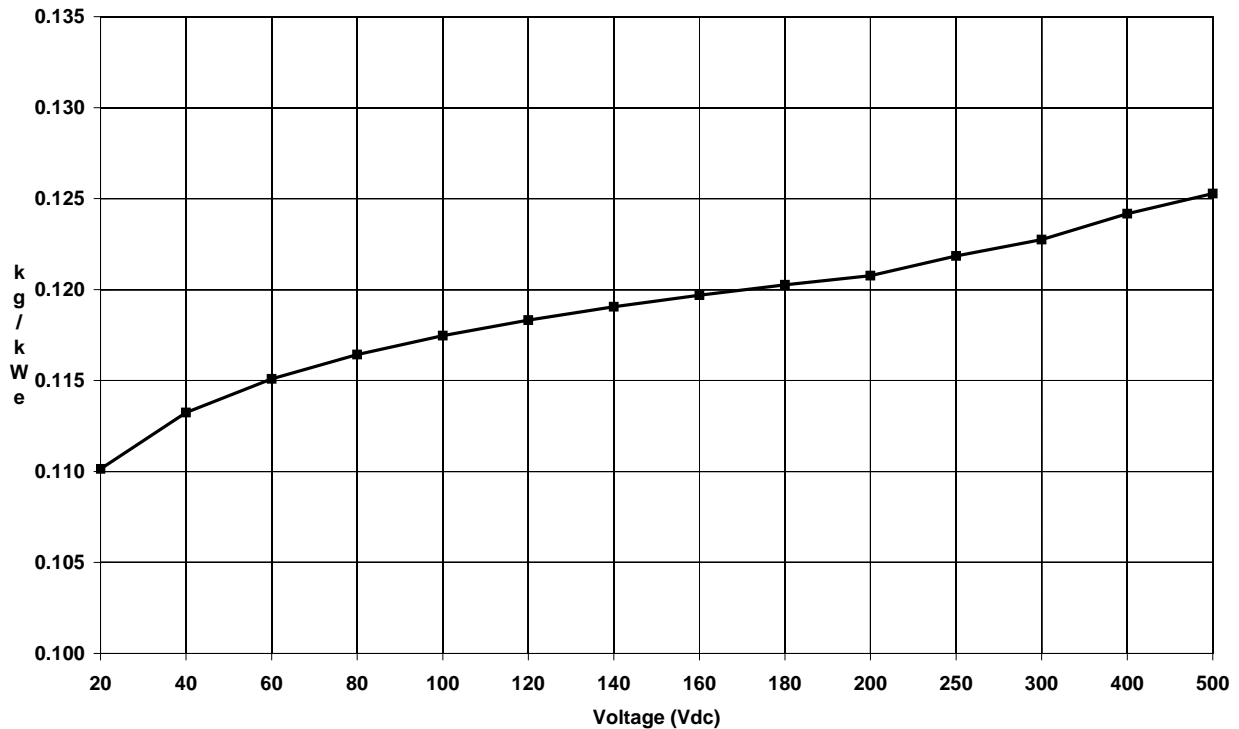
Figure 37: DC RPC SPWT vs Voltage

3.10 AC RPC MODEL

Ac RPCs are used to switch and monitor individual ac load circuits and provide circuit protection. These devices will be located in ac power distribution racks. The following paragraphs explain the equations generated to estimate the masses of single- and 3-phase RPCs as a function of power, efficiency, and voltage. These equations generate rough mass estimates for component comparison purposes. Specific component designs must be developed for more accurate mass estimates.

It is anticipated the ac RPC module design will use a channelized approach like the ac RBI configuration. This allows the card cage assembly that controls and monitors ac RPC operation to be shared among several units. The ac RPC equations described here are based on switch configurations consisting of back-to-back semiconductor switch pairs. This design is lighter and semiconductor switches, especially MOSFETs, have lower "on" resistances then previous devices. This enables high efficiency operation without the use of a parallel relay contact. Since an ac RPC is basically a low power ac RBI in many respects and most features are similar, the information presented in the ac RBI section will be relied on while describing the RPC equation development. The ac RPC discussion is shortened to reduce the amount of repetition. If additional information is desired please refer back to the ac RBI discussion.

The ac RPC and RBI configurations are similar; however, certain differences will cause their specific weights to differ considerably. The mass of the thermal management hardware, housing, and structure will assume a greater percentage of the RPC mass because it does not scale linearly down to the smaller RPC power levels. This results in the specific weight of an RPC being much higher than a RBI. In a telephone conversation with Dave Fox of Westinghouse, he indicated that comparably rated ac and dc RPCs

should have similar masses [Ref. 53]. The data bus interface and control elements in the ac RPCs would probably be like those in the dc units. However, the mass of the ac RPC must include the masses of two gate drives for the back-to-back semiconductor switch pairs, and additional logic to control and coordinate the operation of the two devices. The masses of many of the elements in an ac RPC were obtained from the SSF dc RPC mass breakdowns that were adjusted to reflect the flight unit masses [Ref. 14, 17]. These masses were used as a basis for the following equation development.

The following paragraphs explain the development of the single-phase and 3-phase ac RPC equations. The variables used in these discussions are listed in Table 20.

Table 20: AC RPC Model Variable Definitions

1ARP	Ac RPC Mass
3ARP	Ac RPC Mass
ARPE	Ac RPC Efficiency (99.7%)
ARPAM	Ac RPC Available Modules
ARPRM	Ac RPC Required Modules
ARPP$_O$	Ac RPC Power Output (kWe)
ARPV$_O$	Ac RPC Voltage Output (Vrms)

Mass Coefficient

$$1ARP = \underline{0.15} * ((EXP(0.0007/(1-ARPE)))/1.2628) * (ARPAM/ARPRM) * ARPP_O * (ARPP_O/ARPRM)^{-0.14} *$$

$$(ARPV_O/120)^{0.03}$$

$$3ARP = \underline{0.21} * ((EXP(0.0007/(1-ARPE)))/1.2628) * (ARPAM/ARPRM) * ARPP_O * (ARPP_O/ARPRM)^{-0.22} *$$

$$(ARPV_O/120)^{0.03}$$

The ac RPC mass breakdowns used the SSF dc RPC mass breakdowns as a starting point. Many items in dc and ac RPCs will be the same, so dc RPC component masses were also used for the ac RPC case. The ac RPC requires a back-to-back pair of semiconductor switches to conduct an alternating current. The mass effects resulting from this design difference were incorporated into the ac RPC mass break-downs. To complete the ac RPC mass breakdowns, mass gains occurring as a result of minor hardware advancements were also included. The above mass coefficients were determined from these ac RPC mass breakdowns.

The mass of a 3-phase ac RPC will be higher than a single-phase RPC because the 3-phase design requires two more back-to-back pairs of semiconductor switches with gate drive circuits and two additional sets of sensors. However, the control logic and thermal management hardware masses are similar in both designs and the packaging weight difference becomes less as the RPC size grows, so the relative difference in mass becomes less as the power level rises. Single- and 3-phase RPC specific weights are compared in Figure 38.
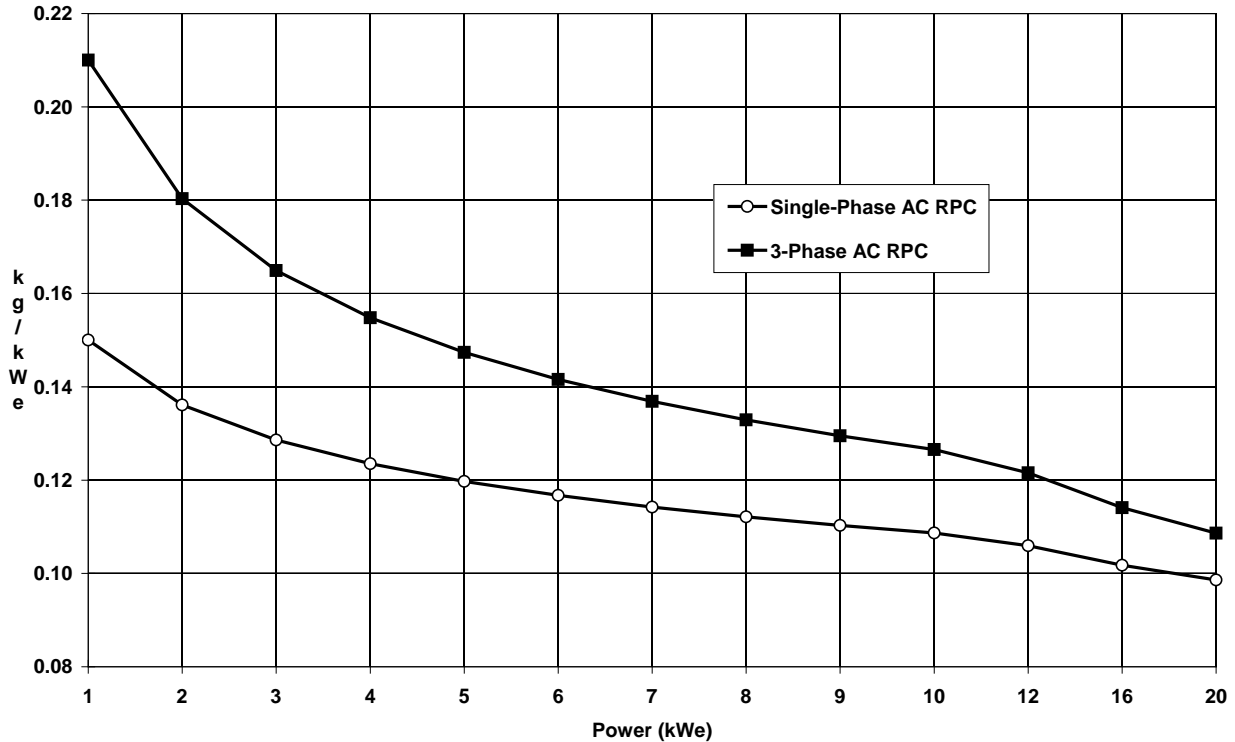
Figure 38: AC RPC SPWT - 1 Phase vs 3-Phase

Efficiency Factor

$1\text{ARP} = 0.15 * \underline{((\text{EXP}(0.0007/(1-\text{ARPE})))/1.2628)} * (\text{ARPAM}/\text{ARPRM}) * \text{ARPP}_O * (\text{ARPP}_O/\text{ARPRM})^{-0.14} *$

$(\text{ARPV}_O/120)^{0.03}$

$3\text{ARP} = 0.21 * \underline{((\text{EXP}(0.0007/(1-\text{ARPE})))/1.2628)} * (\text{ARPAM}/\text{ARPRM}) * \text{ARPP}_O * (\text{ARPP}_O/\text{ARPRM})^{-0.22} *$

$(\text{ARPV}_O/120)^{0.03}$

The factor underlined above estimates the change in specific weight occurring with a change in ac RPC efficiency. The efficiency of an ac RPC was assumed to be the same as a dc RPC; the reactive parasitics associated with ac operation were expected to be negligible. Because the efficiency of the dc RPC was lowered to agree with an efficiency of 99.7%, derived from the RPC ICD, the nominal efficiency of the ac RPC was also correspondingly lowered. The efficiency of an ac RPC can be increased by enlarging the conduction area of the semiconductor switches. This will reduce their resistance. The mass of the semiconductor switches will increase, but the sensor, control logic and gate drive circuitry mass doesn't change significantly, and the thermal management hardware mass will decline slightly. RPC mass estimates were generated for efficiencies ranging from 99.65 to 99.75%. They were used to calculate the efficiency equation element. A graph showing how RPC specific weights vary with efficiency is shown in Figure 39.
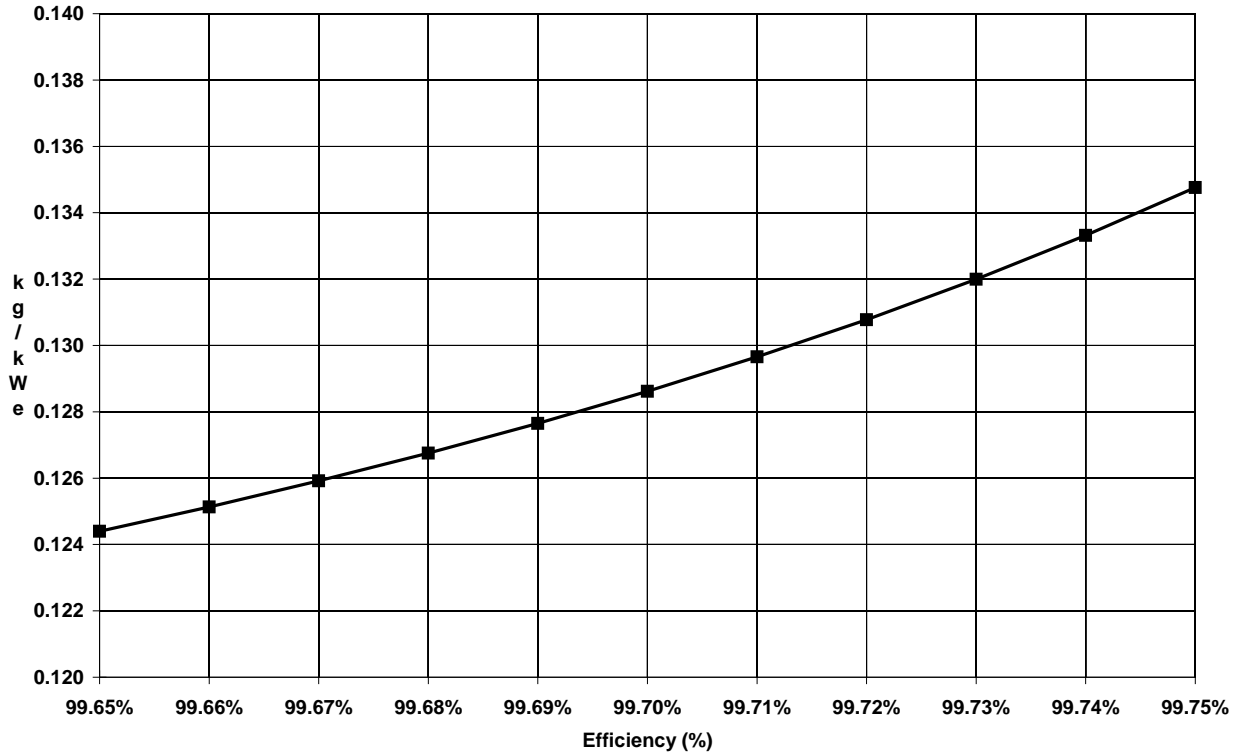
Figure 39: AC RPC SPWT vs Efficiency

Redundancy Factor

$$1ARP=0.15*((EXP(0.0007/(1-ARPE)))/1.2628)*\underline{(ARPAM/ARPRM)}*ARPP_O*(ARPP_O/ARPRM)^{-0.14}*$$

$$(ARPV_O/120)^{0.03}$$

$$3ARP=0.21*((EXP(0.0007/(1-ARPE)))/1.2628)*\underline{(ARPAM/ARPRM)}*ARPP_O*(ARPP_O/ARPRM)^{-0.22}*$$

$$(ARPV_O/120)^{0.03}$$

A modular design approach used to improve reliability will cause the total mass of an ac RPC assembly to rise. This mass increase is estimated by the above factor. The actual number of modules present in the assembly is specified by the "available modules" number; the number of modules required to deliver full power is defined by the "required modules" value. If a system is designed with 4/3 redundancy, each channel can carry up to 33% of the power. The fourth channel is included solely to improve reliability and its mass is the penalty paid to obtain the higher reliability.

Power Level Multiplier

$$1ARP=0.15*((EXP(0.0007/(1-ARPE)))/1.2628)*(ARPAM/ARPRM)*\underline{ARPP_O}*(ARPP_O/ARPRM)^{-0.14}*$$

$$(ARPV_O/120)^{0.03}$$

$$3ARP=0.21*((EXP(0.0007/(1-ARPE)))/1.2628)*(ARPAM/ARPRM)*\underline{ARPP_O}*(ARPP_O/ARPRM)^{-0.22}*$$

$$(ARPV_O/120)^{0.03}$$

The equations can be used to calculate the mass or specific weight of the ac RPC. When the above multiplier is included, the value that results estimates the RPC mass. To obtain the specific weight of the RPC, remove this multiplier.

Power Level Factor

$1ARP=0.15*((EXP(0.0007/(1-ARPE)))/1.2628)*(ARPAM/ARPRM)*ARPP_O*\underline{(ARPP_O/ARPRM)}^{-0.14}*$

$(ARPV_O/120)^{0.03}$

$3ARP=0.21*((EXP(0.0007/(1-ARPE)))/1.2628)*(ARPAM/ARPRM)*ARPP_O*\underline{(ARPP_O/ARPRM)}^{-0.22}*$

$(ARPV_O/120)^{0.03}$

The masses of the semiconductor switches in an ac RPC increase fairly linearly with a rise in power. However, the masses of supporting hardware elements, such as driver modules, sensors, and control logic devices, grow at a much slower rate. This results in some economies of scale as the RPC power level rises and it causes its specific weight to decline. Because the mass of the control logic and gate drive circuits, and the sensors in a 3-phase ac RPC occupies a greater portion of its total mass, the reductions in specific weight occurring with power are greater in this RPC design than in the single-phase design. This causes the difference in the single- and 3-phase power level multiplier exponents, -0.14 and -0.22. The difference in mass growth rates between single- and 3-phase ac RPCs can be seen by referring back to Figure 38. An expanded view of only the single-phase ac RPC is shown in Figure 40.
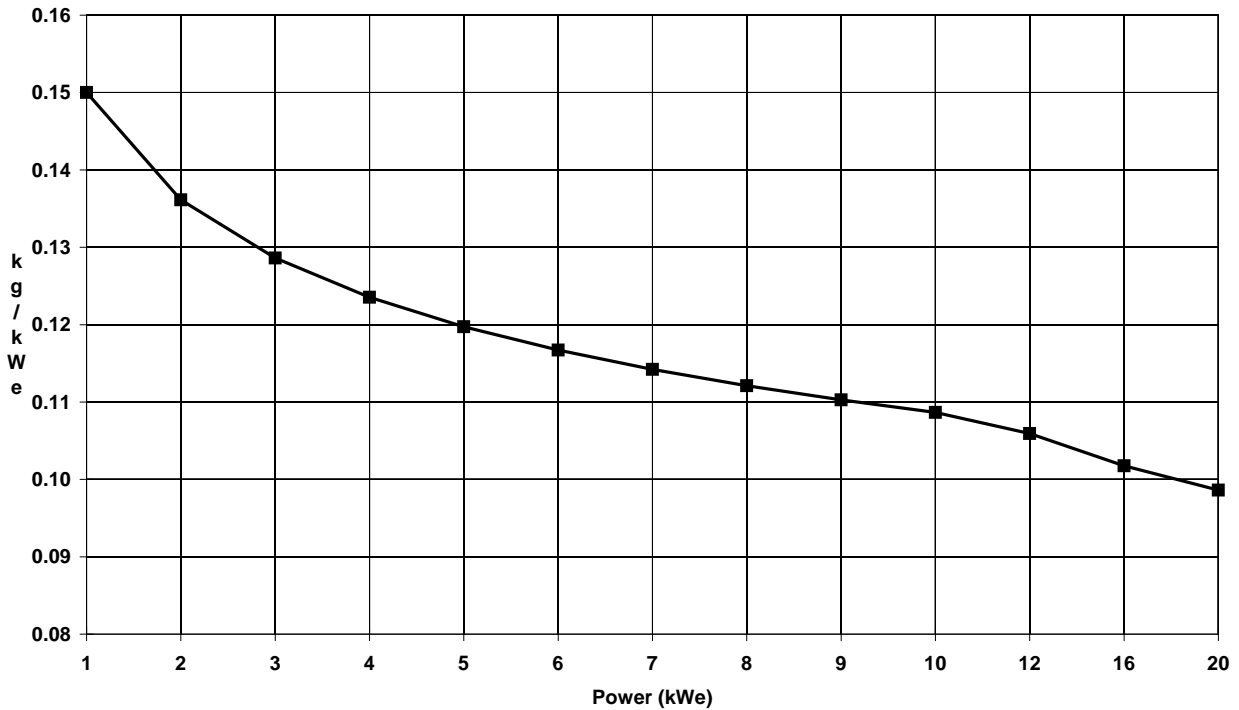
Figure 40: AC RPC SPWT vs Power Level

Voltage Level Factor

$1ARP=0.15*((EXP(0.0007/(1-ARPE)))/1.2628)*(ARPAM/ARPRM)*ARPP_O*(ARPP_O/ARPRM)^{-0.14}*$

$\underline{(ARPV_O/120)}^{0.03}$

$$3ARP=0.21*((EXP(0.0007/(1-ARPE)))/1.2628)*(ARPAM/ARPRM)*ARPP_O*(ARPP_O/ARPRM)^{-0.22}*$$

$$(ARPV_O/120)^{0.03}$$

The ac RPCs will be located near the loads; consequently, the voltages they will experience will be lower than RBIs. This means that many effects associated with high voltage operation, such as vacuum relay breakdown, presumably will not occur. The RPC devices and internal wiring will require additional insulation to withstand the higher voltage stresses. While the RPC voltages are not high enough to warrant connecting the semiconductor switches in series, their masses will probably rise slowly to maintain adequate operating margins at higher voltages. The combined effects of additional insulation, conformal coatings, and other voltage related design features will cause the mass of the RPC to rise slightly as voltage levels rise. The results of this evaluation are displayed in Figure 41.
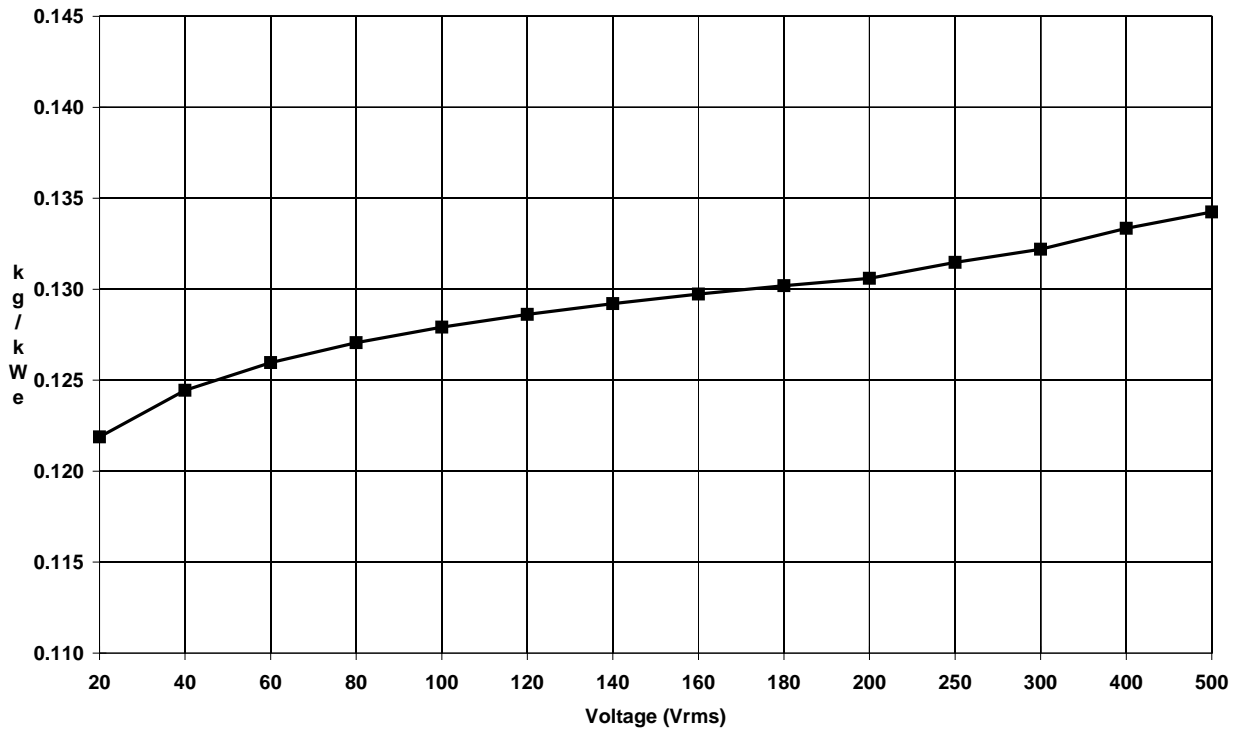
Figure 41: AC RPC SPWT vs Voltage

3.11 ANCILLARY HARDWARE EQUATIONS

Every power conditioning component requires additional ancillary hardware to enable it to perform its functions, protect it from the environment, dissipate excess generated heat, and mount and support the internal circuit elements and devices. In this report, the component ancillary hardware is considered to consist of the following items: conductors and connectors, a control and monitoring subsystem, an enclosure and baseplate collectively called a box, and a thermal management system consisting of a coldplate and radiator. These items are addressed separately in the following sections.

3.11.1 Conductor and Connector Equations

Within a power conditioning component, conductors are required for internal power distribution and the transmission of control and monitoring commands and data. This section establishes a mass for the input and output power conductors, the conductors that transfer power from one stage to the next, the control and monitoring harnesses, and the power and control and monitoring connectors. This conductor mass doesn't include the wiring within a particular stage, for example the wiring in the chopper stage that connects its switches and tank hardware. This wiring is included as part of the stages ancillary hardware.

The information used to develop the following equations was obtained from SSF documentation (Ref. 14, 16, 17, 50). Table 21 defines the variables used in the equations. These equations are based on copper power conductors because copper is more ductile and occupies a smaller volume than aluminum. However, the model allows the selection of copper or fiber optic conductors within the control and monitoring cable harnesses. Separate equations are provided for single- and 3-phase systems because the conductor sizes and control and monitoring harness masses are calculated differently.

Table 21: Conductor and Connector Equation Variable Definitions

1CCM	Single-Phase Conductor and Connector Mass
3CCM	3-Phase Conductor and Connector Mass
CE	Component Efficiency
AM	Available Modules
RM	Required Modules
P_O	Power Output (kWe)
V_I	Voltage Input (Vrms$_{L-L}$ or Vdc)
V_O	Voltage Output (Vrms$_{L-L}$ or Vdc)
EL	Packaged Electronics Length (meters)
EW	Packaged Electronics Width (meters)
EH	Packaged Electronics Width (meters)

Finned Heat Exchanger Box with Copper Control & Monitoring Conductors

Single-Phase, 1 Voltage: $1CCM=(AM/RM)*58.6*(0.5*(EL+EW)+EH)*(P_O/V_O)$
$+AM*(5.22*(0.5*(EL+EW)+EH)+0.238*(P_O/RM)^{0.1}+0.2667*(P_O/RM)^{0.5})$

Single-Phase, 2 Voltages: $1CCM=(AM/RM)*29.3*(0.5*(EL+EW)+EH)*((P_O/CE/V_I)+(P_O/V_O))$
$+AM*(5.22*(0.5*(EL+EW)+EH)+0.238*(P_O/RM)^{0.1}+0.2667*(P_O/RM)^{0.5})$

3-Phase, 1 Voltage: $3CCM=(AM/RM)*58.6*(3^{0.5}/2)*(0.5*(EL+EW)+EH)*(P_O/V_O)$
$+AM*(5.22*1.5*(0.5*(EL+EW)+EH)+1.5*0.238*(P_O/RM)^{0.1}+0.2667*(P_O/RM)^{0.5})$

3-Phase, 2 Voltages: $3CCM=(AM/RM)*29.3*(3^{0.5}/2)*(0.5*(EL+EW)+EH)*((P_O/CE/V_I)+(P_O/V_O))$
$+AM*(5.22*1.5*(0.5*(EL+EW)+EH)+1.5*0.238*(P_O/RM)^{0.1}+0.2667*(P_O/RM)^{0.5})$

Finned Heat Exchanger Box with Fiber Optic Control & Monitoring Conductors

Single-Phase, 1 Voltage: $1CCM=(AM/RM)*58.6*(0.5*(EL+EW)+EH)*(P_O/V_O)$
$+AM*(2.61*(0.5*(EL+EW)+EH)+0.238*(P_O/RM)^{0.1}+0.2667*(P_O/RM)^{0.5})$

Single-Phase, 2 Voltages: $1CCM=(AM/RM)*29.3*(0.5*(EL+EW)+EH)*((P_O/CE/V_I)+(P_O/V_O))$
$+AM*(2.61*(0.5*(EL+EW)+EH)+0.238*(P_O/RM)^{0.1}+0.2667*(P_O/RM)^{0.5})$

3-Phase, 1 Voltage: $3CCM=(AM/RM)*58.6*(3^{0.5}/2)*(0.5*(EL+EW)+EH)*(P_O/V_O)$
$+AM*(2.61*1.5*(0.5*(EL+EW)+EH)+1.5*0.238*(P_O/RM)^{0.1}+0.2667*(P_O/RM)^{0.5})$

3-Phase, 2 Voltages: $3CCM=(AM/RM)*29.3*(3^{0.5}/2)*(0.5*(EL+EW)+EH)*((P_O/CE/V_I)+(P_O/V_O))$
$+AM*(2.61*1.5*(0.5*(EL+EW)+EH)+1.5*0.238*(P_O/RM)^{0.1}+0.2667*(P_O/RM)^{0.5})$

Coldplate Box with Copper Control & Monitoring Conductors

Single-Phase, 1 Voltage: $1CCM=(AM/RM)*58.6*(0.5*(EL+EW)+0.75*EH)*(P_O/V_O)$
$+AM*(5.22*(0.5*(EL+EW)+0.75*EH)+0.238*(P_O/RM)^{0.1}+0.2667*(P_O/RM)^{0.5})$

Single-Phase, 2 Voltages: $1CCM=(AM/RM)*29.3*(0.5*(EL+EW)+0.75*EH)*((P_O/CE/V_I)+(P_O/V_O))$
$+AM*(5.22*(0.5*(EL+EW)+0.75*EH)+0.238*(P_O/RM)^{0.1}+0.2667*(P_O/RM)^{0.5})$

3-Phase, 1 Voltage: $3CCM=(AM/RM)*58.6*(3^{0.5}/2)*(0.5*(EL+EW)+0.75*EH)*(P_O/V_O)$
$+AM*(5.22*1.5*(0.5*(EL+EW)+0.75*EH)+1.5*0.238*(P_O/RM)^{0.1}+0.2667*(P_O/RM)^{0.5})$

3-Phase, 2 Voltages: $CCM=(AM/RM)*29.3*(3^{0.5}/2)*(0.5*(EL+EW)+0.75*EH)*((P_O/CE/V_I)+(P_O/V_O))$
$+AM*(5.22*1.5*(0.5*(EL+EW)+0.75*EH)+1.5*0.238*(P_O/RM)^{0.1}+0.2667*(P_O/RM)^{0.5})$

Coldplate Box with Fiber Optic Control & Monitoring Conductors

Single-Phase, 1 Voltage: $1CCM=(AM/RM)*58.6*(0.5*(EL+EW)+0.75*EH)*(P_O/V_O)$
$+AM*(2.61*(0.5*(EL+EW)+0.75*EH)+0.238*(P_O/RM)^{0.1}+0.2667*(P_O/RM)^{0.5})$

Single-Phase, 2 Voltages: $1CCM=(AM/RM)*29.3*(0.5*(EL+EW)+0.75*EH)*((P_O/CE/V_I)+(P_O/V_O))$
$+AM*(2.61*(0.5*(EL+EW)+0.75*EH)+0.238*(P_O/RM)^{0.1}+0.2667*(P_O/RM)^{0.5})$

3-Phase, 1 Voltage: $3CCM=(AM/RM)*58.6*(3^{0.5}/2)*(0.5*(EL+EW)+0.75*EH)*(P_O/V_O)$
$+AM*(2.61*1.5*(0.5*(EL+EW)+0.75*EH)+1.5*0.238*(P_O/RM)^{0.1}+0.2667*(P_O/RM)^{0.5})$

3-Phase, 2 Voltages: $CCM=(AM/RM)*29.3*(3^{0.5}/2)*(0.5*(EL+EW)+0.75*EH)*((P_O/CE/V_I)+(P_O/V_O))$
$+AM*(2.61*1.5*(0.5*(EL+EW)+0.75*EH)+1.5*0.238*(P_O/RM)^{0.1}+0.2667*(P_O/RM)^{0.5})$

Power Conductor Equation Segment

Single-Phase, 2 Voltages: $1CCM=(AM/RM)*\underline{29.3*(0.5*(EL+EW)+EH)*((P_O/CE/V_I)+(P_O/V_O))}$
$+AM*(5.22*(0.5*(EL+EW)+EH)+0.238*(P_O/RM)^{0.1}+0.2667*(P_O/RM)^{0.5})$

3-Phase, 2 Voltages: $3CCM=(AM/RM)*\underline{29.3*(3^{0.5}/2)*(0.5*(EL+EW)+EH)*((P_O/CE/V_I)+(P_O/V_O))}$
$+AM*(5.22*1.5*(0.5*(EL+EW)+EH)+1.5*0.238*(P_O/RM)^{0.1}+0.2667*(P_O/RM)^{0.5})$

Power conductors are primarily sized on the basis of current; therefore, the conductor mass is a function of the maximum steady state current levels within a component. If a voltage transformation occurs in the component, it is necessary to include separate factors for the input and output current levels. The length of the power conductors was estimated to be proportional to half the length plus width plus the full height of the box in the case of the finned heat exchanger (FH) box. The power cables and control and monitoring harnesses are typically run near the top of the box, above the circuit boards and devices, and are brought out by connectors located in the top half of the box. This cable routing design is indicative of a coldplate (CP) style box. However, in the case of the FH box the cables exit the main box through a cutout and are routed down the side of it, within an electrical box add-on, to connectors located on a plate approximately half way down the side of the box. This design feature is present to allow robotic replacement of the component, but it adds to the length and mass of the cables. For this reason the CP box power cable segment equation reduces this to 75% of the full height. The coefficient "29.3" was determined to yield a power conductor mass consistent with the ISS DDCU conductor mass. With the exception of the Sequential Shunt Unit (SSU), a value of "58.6" is used for the boxes that operate at a single voltage level and the factor input power divided by efficiency divided by the input voltage is removed. A value of "51.3" is used for the SSU because approximately one-third of its internal power conductors are aluminum instead of copper. For an equivalent transmission efficiency, aluminum reduces the mass of the conductors 52.5%, but at the expense of increased conductor size. The factor "$3^{0.5}/2$" was included for the 3-phase component conductor mass because 3-phase power distribution is more efficient for transmitting power than single phase [Power System Analysis textbook]. Further information is provided on the design and modeling differences between the FH and CP box in section 3.1.10.3.

Control and Monitoring Cable Harness Equation Segment

Single-Phase, 2 Voltages: $1CCM=(AM/RM)*29.3*(0.5*(EL+EW)+EH)*((P_O/CE/V_I)+(P_O/V_O))$

$+AM*(\underline{5.22*(0.5*(EL+EW)+EH)}+0.238*(P_O/RM)^{0.1}+0.2667*(P_O/RM)^{0.5})$

3-Phase, 2 Voltages: $3CCM=(AM/RM)*29.3*(3^{0.5}/2)*(0.5*(L+W)+H)*((P_O/CE/V_I)+(P_O/V_O))$

$+AM*(\underline{5.22*1.5*(0.5*(L+W)+H)}+1.5*0.238*(P_O/RM)^{0.1}+0.2667*(P_O/RM)^{0.5})$

From SSF component mass breakdowns, the average mass of a control and monitoring wiring harness for a 5 to 10 kWe rated component was estimated to be 3.6 kg. Based on discussions with component designers, this mass was estimated to drop about 50% with the use of fiber optics [Ref. 23], although the sensitivity of fiber optic cables to radiation may preclude their use in some environments. For this reason, and possible technology maturity reasons, copper or fiber optic conductors are offered as a choice in defining the control and monitoring harness mass. Replacing most of the copper wiring with fiber optic cables reduces the mass of the control and monitoring wiring to 1.8 kg. The length of the control and monitoring harness was again estimated to be proportional to half the length plus width plus height of the box in the case of the finned heat exchanger (FH) box. As before the height is removed from this equation for the CP box. The value "5.22" was chosen to provide a control and monitoring harness mass that matched the mass of the DDCU harness. This value is reduced to "2.61" for a fiber optic harness. Because the SSU has more sensors, its control and monitoring harness copper and fiber optic masses are "7.8" and "3.9", respectively.

The delta mass of the control and monitoring harness in a 3 phase component was estimated by dividing the harness into command and data/sensor cable portions and assessing how these portions would change with a move from a single-phase to 3-phase component. Lacking a breakdown, it was assumed half the harness was dedicated to commands and half for data/sensors. It was assumed the command cable mass would be the same, regardless of whether the component was single- or 3-phase. The effect on the data/sensor half was estimated by counting the number of sensors in the DDCU, 7, and dividing them into two categories, voltage and current sensors, 4, and other sensors, 3. A single phase ac to ac converter would probably still have a voltage and current sensor on the input and a set on the output, so these sensor quantities wouldn't change. However, a 3 phase component would likely have a voltage and current sensor per phase, or six on the input and six on the output. This would bring the total to 15 sensors. A 3 phase dc to ac inverter or ac to dc rectifier would probably have four less sensors, or 11 total. A rough average of these two values, 14, or twice the number in a single phase component, was used as an estimate of the sensor quantity in a 3 phase component. So based on this assessment, the data/sensor harness mass was assumed to be twice as

heavy in a 3-phase component. Since the data/sensor harness mass was previously assumed to be half the mass of the total control and monitoring harness, and it doubles with a change from single-phase to 3-phase, the result is the total control and monitoring wiring mass is 50% heavier in a 3 phase component.

Power and Control and Monitoring Connector Equation Segments

Single-Phase, 2 Voltages: $1CCM=(AM/RM)*29.3*(0.5*(EL+EW)+EH)*((P_O/CE/V_I)+(P_O/V_O))$

$+AM*(5.22*(0.5*(EL+EW)+EH)+\underline{0.238*(P_O/RM)^{0.1}+0.2667*(P_O/RM)^{0.5}})$

3-Phase, 2 Voltages: $3CCM=(AM/RM)*29.3*(3^{0.5}/2)*(0.5*(EL+EW)+EH)*((P_O/CE/V_I)+(P_O/V_O))$

$+AM*(5.22*1.5*(0.5*(EL+EW)+EH)+\underline{1.5*0.238*(P_O/RM)^{0.1}+0.2667*(P_O/RM)^{0.5}})$

Based on a survey of ISS components, DDCU, DCSU, Battery Charge/Discharge Unit (BCDU), and SSU, and an evaluation of their connector masses [Ref. 55], it was concluded about 70% of the connector mass is dedicated to the input/output power cables and the remaining 30% is used for the control and monitoring cables. The factors "0.238" and "0.2667" generate the correct connector masses for the DDCU at its 6.25 kWe full power rating. The power connector mass was estimated to increase at an exponential rate of 0.5, causing the connector mass to increase about 41% if the power level is doubled. The mass of the connectors used for the control and monitoring cables was assumed to increase at an exponential rate of 0.1 because a few more sensors, to monitor temperature for example, may be used in a higher power component because of its larger size. But, the mass increase was assumed to be very slight with an increase in power. The factor, "1.5" is added for a 3-phase component because it was previously assumed 50% more signals would be required with a 3-phase component, and the connector mass would increase correspondingly. For 3-phase components that accept 3-phase power and provide it, a factor of "1.5" will also be included in the power connector equation segment. The AC to AC frequency changer is an example of this type of component. However, if the component uses 3-phase power distribution internally, but accepts and provides dc power externally, its power connector mass was assumed to be the same as for a single-phase component. The DDCU is the best example of this type of component.

3.11.2 Control and Monitoring Subsystem Mass and Parasitic Power Equations

Each of the power conditioning components will have some type of control and monitoring subsystem. This subsystem was assumed to consist of a controller card, a data interface module, various voltage, current, and temperature sensors, and a housekeeping power supply. A component controller card responds to higher level commands and controls the minute steps necessary to implement these commands. The monitoring system queries the internal sensors and provides data on the component operating status to the internal controller or higher level computers. A data interface module, containing numerous analog to digital conversion circuits, is required to convert the sensor signals into the proper form for data bus transmission. The power supply provides the low voltage power outputs, usually +/-15 and 5 Vdc, required by these units.

SSF component documentation was utilized to formulate the control and monitoring mass equations [Ref. 14, 16, 17, 50]. Table 22 defines the variables used in these equations. Because a 3-phase system was assumed to have nearly twice as much monitoring data to collect and process, separate equations are provided for single- and 3-phase systems. The equations are broken into three parts, the controller card and data interface module, the sensors, and the housekeeping power supply.

Table 22: Control and Monitoring Equation Variable Definitions

1CMM	Single-Phase Control and Monitoring Mass
3CMM	3-Phase Control and Monitoring Mass
1CMP	Single-Phase Control and Monitoring Power
3CMP	3-Phase Control and Monitoring Power
AM	Available Modules
RM	Required Modules
P_O	Power Output (kWe)

Single-Phase Mass: $1CMM = AM*(1.2+0.158*(P_O/RM)^{0.5})+70*0.75*1.1*1CMP$

3-Phase Mass: $3CMM = AM*(1.6+0.316*(P_O/RM)^{0.5})+70*0.75*1.1*3CMP$

Single-Phase Power: $1CMP = AM*43.3*(P_O/RM)^{0.1}$

3-Phase Power: $3CMP = AM*57.4*(P_O/RM)^{0.1}$

The estimated mass of a SSF controller card and data interface module for a converter or switchgear unit was 2.8 kg. During ISS design and development, control and data processing advancements allowed the mass of the controller and data interface cards to decline to an estimated 1.8 kg. With continuing progress according to Moore's Law (computing power doubles every 2 years for the same size processor), it was felt this value would decrease a third to a mass of 1.2 kg after 2005. A value of 1.6 kg was assumed for a 3-phase component due to the additional data handling requirements. In support of this estimate, Texas Instruments already manufactures a Processor Interface Controller and Communication Module that has a MIL-STD-1750A processor, 256-K of EEPROM memory, and a MIL-STD-1553 data bus interface on a single card that weighs 0.6 kg. The ISS SSU control and data processing is considerably heavier because 88 array strings must be monitored, and a ramp generator and multiple comparator circuits are required to generate the signals that are used to control individual shunting of the array strings. Based on combined SSF and ISS SSU mass estimates, this assembly was estimated to weigh about 6.4 kg. It was assumed with advances it would be possible to reduce its mass to 5.4 kg. The BCDU controller and data module weighs 5.0 kg. The battery monitor weighs an estimated 5.4 kg. With advancements it was assumed these masses would decline to 4.0 kg and 4.9 kg respectively. A combined mass savings of 1.5 kg, approximately 15%.

Again using SSF component mass breakdowns, except for the SSU, a value of 0.6 kg was estimated for the mass of the monitoring sensors in a typical 10 kWe component. Anticipating technology improvements by the year 2005, the 0.6 value was reduced to 0.5 kg. Per the previous explanation in section 3.1.10.1, a 3-phase system was estimated to have about twice as many sensors, so a value of 1.0 kg was used for it. The mass of the sensors will increase as the component power level rises. A potential transformer used to measure high voltages will weigh considerably more than one that measures low voltages. It was estimated the mass of a potential transformer would nearly double if the voltage it was measuring was doubled. A similar estimate was made for a current transformer. To obtain this level of sensor mass gain as the power level is increased, an exponent of 0.5 was included in the sensor mass factor. The sensor mass factors were calibrated to yield 0.5 and 1.0 kg respectively for single- and 3-phase 10 kWe components. The SSU sensor mass was estimated to be 2.6 kg because of the need to monitor the individual array strings.

Power must be obtained from the component input to operate the control and monitoring subsystem, the semiconductor switch gate drive circuitry and control logic, data signal converters, relay coils, etc. The sum of these power demands represents the component's parasitic power requirement. The 6.25 kWe DDCU standby power demand is 85 watts [Ref. 56]. This value reflects the converter on, ready to deliver power. Its power supply is 65% efficient, leaving 55 watts for the actual control and monitoring elements. Most of this control and monitoring power is consumed in the processor, the gate drives, and data input/output signal conditioning cards. It was assumed their power demand would decline about 30% by

2005 with the introduction of lower voltage digital chips (5 volt to 3 volt), enabling lower power consuming processors and input/output cards. This lowered the control and monitoring power to 39 watts. Dividing this by the power supply efficiency, assumed to improve from 65% to 75%, a final value of 52 watts is obtained for a 6.25 kWe, single phase component. 3-phase components have more gate drive circuits and data input/output channels to account for the additional sensors, but the processor would probably be the same as in a single phase component. The power demand of its control and monitoring elements was estimated to be 33% higher, or 52 watts. Dividing this by power supply efficiency, a value of 69 watts is obtained for the control and monitoring power consumption of a 6.25 kWe, 3 phase component. It is expected that parasitic power demands will rise slowly as component power levels increase, because certain control and monitoring devices will need more power to perform their functions. The exponent 0.1 was included in the factor to account for these gradual power increases. The control and monitoring power demand equation coefficients were calculated to yield control and monitoring power consumption values of 52 watts for a single phase, 6.25 kWe component, and 69 watts for a 3 phase component.

The SSU, BCDU and switchgear parasitic power demands are different than those for a converter. The ISS SSU parasitic power requirements are more because of the need to individually control and monitor the array strings and power the ramp generator and comparator circuits. Currently, the SSU parasitic power demand is 91.5 watts [Ref. 56]. Of this, 24 watts are consumed in the power supply resulting in an efficiency of 73.8%. It was assumed the remaining 67.5 watts could be reduced to 57.8 watts. Dividing this by 0.75, the efficiency of the power supply is assumed to improve, results in an estimated parasitic power demand of 76.8 watts. The BCDU parasitic power demand is 94 watts [Ref. 56]. It was assumed its parasitic power demand could be reduced 20% through the use of lower power consuming chips and an improved power supply efficiency, resulting in a new value of 75 watts. The parasitic power demand of the switchgear units includes the power demanded by the switchgear control assembly (SCA) and the power required to hold in the RBI relay coils. The SCA requires 15 watts and each of the RBIs also needs 15 watts for their hold-in coil.

The control and monitoring system normally receives its power from a dedicated housekeeping power supply. The mass of this power supply was assumed directly proportional to its output power level, and its mass was computed using the previously derived control and monitoring subsystem power consumption values. The DDCU power supply is rated for 65 watts and weighs 4.8 kg. Its specific power was expected to improve 5% to about 70 kg/kWe with improved power supply topologies, switches, and higher packaging densities. The 6.25 kWe control and monitoring power demand values for the single and 3 phase units, 52 and 69 watts, were multiplied by the assumed power supply efficiency of 75%, a 1.1 factor reflecting a 10% power rating margin, and 70 kg/kWe, yielding 3.0 kg and 4.0 kg respectively. A higher power supply margin, 1.6, was incorporated into the switchgear control and monitoring algorithm to account for the high, but short term relay coil pickup power demand. Because this power demand is transitory its not included in the algorithm that estimates the switchgear units steady state parasitic power level. This value is used in the switchgear unit's efficiency calculations. The SSU mass breakdowns indicate it's power supply has a higher power density and a value of 65 kg/kWe was used for it. Although the BCDU parasitics included the power required for battery monitoring, the SSF BCDU mass breakdown did not include the two power supplies added to feed power to the cell monitor multiplexors housed in the batteries. However, using a power supply specific power of 70 kg/kWe, consistent with the DDCU, increased the SSF estimated BCDU power supply mass 2 kg, sufficient to cover the mass of the omitted battery multiplexor power supplies. The net effect of these adjustments was the stated SSF BCDU control and monitoring mass was increased 0.5 kg.

3.11.3 Component Volume, Dimension, and Enclosure Equations

Regardless of the power level, the density of the packaged electronics in power conditioning components operating under similar conditions will normally be similar. To determine appropriate component electronics densities for two types of enclosure/baseplate designs, the packaged electronics densities of five SSF components were computed using their projected weights and compared with the as-built ISS component densities. The packaged electronics density values were assumed to include all the electronics devices and hardware, plus everything they require for operation and support, cabling, circuit boards, card cages, and structural panels. This information is presented in Table 23.

Table 23: Comparison of SSF and ISS Power Conditioning Component Densities

Component	Projected SSF Packaged Electronics Density (grams/cubic cm)		As-Built ISS Packaged Electronics Density (grams/cubic cm)	
	CP	**FH**	**CP**	**FH**
DC/DC Converter Unit-Internal	0.404[1]	N/A	0.382[1]	N/A
DC/DC Converter Unit-External	N/A	0.250	N/A	0.197
Battery Charge/Discharge Unit	N/A	0.283	0.449[2]	0.250
DC Switching Unit	N/A	0.333	0.364[2]	0.203
Main Bus Switching Unit	N/A	0.339	0.428[2]	0.239
Average	0.404	0.301	0.249	0.222

(1): The DDCU-I box design is consistent with a coldplate box design but it is mounted in an internal location. Because an external box requires a more robust enclosure to withstand the external environment, the coldplate box design employed in this report is based on the DDCU-I box dimensions but with external box wall thicknesses.

(2): The coldplate electronics densities were estimated for the BCDU, DCSU, and MBSU by comparing the differences in dimensions between the DDCU-I and DDCU-E boxes, and subtracting equal amounts from the BCDU, DCSU, and MBSU Type I box dimensions.

A component requires an enclosure and baseplate to provide protection from the environment, and as a means of providing structural attachment and thermal management. Enclosure and baseplate types vary depending on the application. Two baseplate/enclosure types, finned heat exchanger (FH) and coldplate (CP), and two material options, aluminum (Al) and carbon-carbon (CC), are discussed here and offered as enclosure/baseplate design and material choices in the models.

The FH enclosure/baseplate design uses a finned heat exchanger to transfer heat from the component to a similarly finned coldplate. This concept is relatively heavy and has a higher temperature drop than other approaches, but it was selected for the ISS to allow replacement of the power conditioning units. Its electrical connectors are mounted on an external plate, pins pointing downward, to allow them to be mated to installed cable box connectors by means of robotically manipulated ACME screws that draw the component down and hold it in place. Pressure pads are present to maintain the correct tension on the ACME screws, both on-orbit and more importantly during launch. Because the FH box has an electrical connector box on its end to route the power and control cables down to the connectors and the ACME screw hardware protrudes through the box, its packaged electronics density relative to the size of its enclosure is much lower.

The coldplate enclosure/baseplate design doesn't allow on-orbit replacement, because the component's baseplate is tightly bolted to the coldplate. It also doesn't have an electrical connector box, ACME screws, or pressure pads. These items are all present to support the orbital replacement unit (ORU) removal and replacement requirements of the ISS FH design, and aren't required with the CP design. The result is a smaller, lighter box, but one that can't be replaced on-orbit. The CP design is fairly representative of a typical satellite box, while the FH design is presently unique to ISS.

The DDCU packaged electronics density values were used for all converter, inverter, rectifier and transformer type component models. The BCDU values were used for the BCDU model. The MBSU values were used for the switchgear models. It was assumed a 5% improvement in packaging densities would be realized by the year 2005 for all component types and both box types, FH and CP. Using these densities, the component volume can be calculated for either the FH or CP box using the following formula:

$$CV = CEM/(PED*1000)$$

where: CV = Component Volume in cubic meters
CEM = Component Electronics Mass in kilograms
PED = Packaged Electronics Density for Selected Box Type in g/cm^3

Knowing the component volume, it is possible to generate dimensions for the component. Using ISS box dimensions as a guide, per unit aspect ratios were defined for the FH and CP style boxes for the component types. These aspect ratios are shown in Table 24. Using these aspect ratios and computing the cube root of the volume, the component height, width, and length can be calculated for the two types of boxes. An example of the equations is shown below for the DDCU / converter box designs.

Table 24: Finned Heat Exchanger Box Aspect Ratios

Component	Length Aspect Ratio	Width Aspect Ratio	Height Aspect Ratio
FH Box (BCDU, MBSU)	1.626	1.150	0.535
FH Box (DDCU-E)	1.351	1.148	0.646
CP Box (Est. BCDU, MBSU)	1.916	1.084	0.482
CP Box (DDCU-I)	1.610	1.043	0.596

$$\text{CP Length} = 1.610 * CV^{0.3333} \quad \text{or} \quad \text{FH Length} = 1.351 * CV^{0.3333}$$

$$\text{CP Width} = 1.043 * CV^{0.3333} \quad \text{or} \quad \text{FH Width} = 1.148 * CV^{0.3333}$$

$$\text{CP Height} = 0.596 * CV^{0.3333} \quad \text{or} \quad \text{FH Height} = 0.646 * CV^{0.3333}$$

The equations that were developed to define component enclosure masses are based on the masses of two space station ORU box styles, Type I and Type IV. Both box styles are constructed from aluminum and use the FH design. The ORU box mass breakdowns shown in Table 24 were generated from a combination of SSF documentation [Ref. 14] and enclosure and baseplate delivery inspection and receiving records.

Table 25: Finned Heat Exchanger Box Mass Breakdown

Box Subassembly	Type I BCDU	Type I MBSU	Type IV DDCU
Enclosure	14.1	14.1	10.9
Connector Structure	0.6	0.6	0.6
Mounting hardware	5.3	5.3	5.3
Radiant Fin Baseplate	19.7	24.0	19.5
Total	39.7	44.0	36.3

Type I ORU Box dimensions: 104.1 cm length, 73.7 cm width, and 34.3 cm height
Type IV ORU Box dimensions: 71.8 cm length, 61.0 cm width, and 34.3 cm height

Knowing the sizes of the two box types the mass per surface area of the enclosure and baseplate can be calculated. These values are required to calculate the masses of different sized FH boxes and it is provided in Table 26. These values were also used to generate enclosure and baseplate masses for the smaller size CP style boxes.

Table 26: Finned Heat Exchanger Box Mass per Surface Area

Box Subassembly	Type I BCDU	Type I MBSU	Type IV DDCU
Enclosure Mass per Surface Area (kg/m2)	7.1	7.1	8.1
Radiant Fin Baseplate Mass per Surface Area (kg/m2)	25.7	31.3	44.6

The mass of the radiant fins is about 25% of the radiant fin baseplate mass. The remaining portion provides structural support for the attachment of the fins and the internal mounting of the component hardware and devices. The mounting plate portion of the radiant fin baseplate is the part that would serve as the coldplate if the component was enclosed by a CP type box. The electronics would be mounted directly on this coldplate and a coolant would be pumped through the heat exchanger piping contained in it to remove excess heat. The baseplate for a CP style box then has exactly one-half the mass per unit area as the FH style boxes. The FH design has hardware to allow robotic removal and replacement of the ORUs, but this hardware isn't required with the CP design and it was removed from the mass summary for it. Using the previously calculated per unit masses for the FH enclosure and the CP baseplate and applying them to an equivalently sized CP box the values shown in Table 27 are obtained. Comparing these with the value in Table 25, one can see that a CP style box is significantly lighter. Furthermore, because the packaged electronics density in a CP box is much higher, its size can be reduced lowering these masses even further.

Table 27: Coldplate Box Mass Breakdown

Box Subassembly	BCDU	MBSU	DDCU
Enclosure	14.1	14.1	10.9
Connector Structure	0.6	0.6	0.6
Baseplate	14.8	18.0	14.6
Total	29.5	32.7	26.1

Two material options offered in the models, aluminum and carbon-carbon. Aluminum's main advantage is its much less expensive than carbon-carbon. Carbon-carbon is fairly new, and it has only recently become widely available. Carbon-carbon has several advantages over aluminum: (1) its lighter 1.65 g/cm^3 versus 2.7 g/cm^3 for aluminum, (2) it provides better shielding effectiveness against radiated electromagnetic interference (EMI) at lower frequencies (< 100 MHz) and is comparable at higher frequencies (> 100 MHz), (3) its more resistant to atomic oxygen degradation, and (4) it doesn't exhibit RF pitting (corrosion), a phenomena in which radio frequency power erodes the surface of a material. Finally, carbon-carbon's shielding effectiveness against ionizing radiation is comparable to aluminum.

Because of its advantages, its expected carbon-carbon will replace much of the aluminum in future boxes. The density of aluminum is 2.7 g/cm^3, carbon-carbon is 1.65 g/cm^3. A mass reduction of about 39%. It will probably be impractical to replace the connector structure and mounting hardware materials with carbon-carbon, but it should be fine for the enclosure and baseplate. Tables 28 and 29 list projected mass breakdowns for the FH and CP box designs after the aluminum in the enclosure and baseplate has been replaced with carbon-carbon. These masses and the associated mass per unit area values were used to calculate the masses of varying sizes of carbon-carbon FH and CP style boxes.

Table 28: Carbon-Carbon Finned Heat Exchanger Box Mass Breakdowns

Box Subassembly	Type I BCDU	Type I MBSU	Type IV DDCU
Enclosure	8.6	8.6	6.7
Connector Structure	0.6	0.6	0.6
Mounting hardware	5.3	5.3	5.3
Radiant Fin Baseplate	12.0	14.7	11.9
Total	26.5	29.2	24.5

Table 29: Carbon-Carbon Coldplate Box Mass Breakdowns

Box Subassembly	BCDU	MBSU	DDCU
Enclosure	8.6	8.6	6.7
Connector Structure	0.6	0.6	0.6
Baseplate	9.0	11.0	8.9
Total	18.2	20.2	16.2

Using these mass per unit area values, its now fairly easy to develop generalized equations to calculate the masses of different sized aluminum and carbon-carbon FH and CP style box masses. The equations for the DDCU type components are shown below. The BCDU and switchgear style equations are the same, except they use different mass per unit area values for the coefficients. The connector and mounting hardware mass was assumed to double with a factor of 10 power increase, the reason for the 0.3 exponent, and was calibrated to yield 5.9 kg and 0.6 kg at 6.25 kWe for the FH and CP boxes respectively.

$$ALFHBM = 3.4*(P_O/RM)^{0.3} + 8.1*((L*W) + 2*(L*H) + 2*(W*H)) + 44.6*(L*W)$$

$$ALCPBM = 0.35*(P_O/RM)^{0.3} + 8.1*((L*W) + 2*(L*H) + 2*(W*H)) + 33.45*(L*W)$$

$$CCFHBM = 3.4*(P_O/RM)^{0.3} + 5.0*((L*W) + 2*(L*H) + 2*(W*H)) + 27.3*(L*W)$$

$$CCCPBM = 0.35*(P_O/RM)^{0.3} + 5.0*((L*W) + 2*(L*H) + 2*(W*H)) + 20.44*(L*W)$$

where: ALFHBM = Aluminum Finned Heat Exchanger Box Mass in kilograms
ALCPBM = Aluminum Coldplate Based Box Mass in kilograms
CCFHBM = Carbon-Carbon Finned Heat Exchanger Box Mass in kilograms
CCCPBM = Carbon-Carbon Coldplate Based Box Mass in kilograms
CV = Component Volume in cubic meters
L = Length in meters
W = Width in meters
H = Height in meters
P_O = Power Output (kWe)
RM = Required Modules

A generalized reference cable run length and internal packaging box mass estimate were developed from an estimate of the DDCU's elemental electronics density and its weight. For this estimate of electronics density the mass of the cabling and structural boxes was removed. The DDCU's electronics weighs about 23 kg, and its density was estimated to be 0.45 g/cm^3. These values were used to estimate the volume of the electronics using the following formula:

$$EV = 1.25 * EM / (ED * 1000)$$

where: EV is the volume of the elemental electronics

EM is the mass of the electronics

ED is the density of the electronics

The factor "1.25" was added to account for the volume occupied by structural hardware supporting the electronics such as card cages and circuit boards, and to provide routing areas for board to board wiring. With this definition of the electronics volume, a rough estimate of the length, width, and height of the electronics was made using the previously derived FH and CP box aspect ratios. These electronics length, width, height values were used to compute reference cable run lengths for the FH and CP boxes and to scale the mass of the internal packaging boxes.

The mass of the internal packaging or support boxes wasn't included in the previous version of models because of the difficulty in defining and estimating this hardware. Looking at a picture of the DDCU, its clear it occupies a significant portion of the DDCU's mass. The DDCU has four internal boxes to hold the input and output filters, direct current element (Weinberg converter chopper, transformer, and rectifier), and the control and monitoring card cage and circuit boards. There is also the hardware that holds the boards, inductors, transformers, capacitors in place, and mounting hardware such as and screws, bolts and nuts. Lacking mass information on this hardware, its mass was crudely estimated by adding all the masses of all the identified elements, and subtracting this subtotal from the total mass of the component. After identified component advancements were considered, an estimated mass of 5.35 kg was computed for the DDCU. Since most of this mass is concentrated in the four internal support boxes, its mass was referenced to and will scale with the computed end and side areas of the electronics volume. A similar approach and the same mass coefficients (13.12 and 8.02) were used for the other components except the array shunt regulator model. The values computed for this model were 11.1 and 6.78.

3.11.4 Radiator Area and Mass Equations

A radiator is needed to dissipate the waste heat a power conditioning component generates. The DDCU heat pipe (HP) radiator design was used to develop the radiator equations in these models. The models allow the selection of either a single or two sided radiator, both of which are developed from the single sided DDCU radiator design. The DDCU HP radiator is required to dissipate at least 290 watts at EOL, and it is 172.7 cm long, 59.0 cm wide, and 2.0 cm thick. It has two parts, a coldplate section on which the DDCU mounts, and a radiator section. The coldplate part is 59.1 cm by 59.0 cm, and weighs 7.8 kg. The radiator section is 113.7 cm by 59.0 cm, and weighs 14.9 kg. The total mass of the HP radiator is 22.7 kg.

The thermal analysis of the DDCU-HP was consulted to obtain sink and baseplate temperatures, and to determine an appropriate temperature drop from the baseplate to the radiator for the CP box design [Ref. 57]. The radiator equations were developed to size the component coldplate and radiator for the conditions experienced by the DDCU-HP in its worst case hot environment. Consistent with this analysis, the sink temperature default was set at 294 K and the maximum baseplate temperature was set at 63 °C. The 4° C temperature delta present between the electronics baseplate and the radiator surface [Ref. 57] was used for the CP box design and based on a discussion with an ISS thermal analyst an 11° C temperature delta was set as the default for the FH box design. The radiator area was computed using a standard radiator thermal dissipation formula, and the coefficient (1.0823E+10) was calibrated to calculate a radiator area of 0.3354 m^2 (half of the DDCU HP radiator area for the two-sided radiator case) at a heat dissipation level of 290 watts using the previously defined worst case conditions. The coefficient, 22.26, in the radiator mass equation generates masses for the coldplate and radiator equivalent to the DDCU HP's aluminum coldplate and radiator mass. These coefficients were multiplied by (1.65 g/cm^2 / 2.7 g/cm^2) to obtain the mass of a carbon-carbon radiator and its coldplate under the same conditions.

$$RA=(1.0823E+10/RS*Q)/((CPT+273-TD)^4-T_S^4)$$

$$ALRM= 22.26*(L*W)+22.26*RA$$

$$CCRM= 13.6*(L*W)+13.6*RA$$

where: RA = Radiator Area in square meters
RS = Number of Radiator Sides (1 or 2)
ALRM = Aluminum Radiator Mass in kilograms
CCRM = Carbon-Carbon Radiator Mass in kilograms
Q = Heat to be Dissipated in kWt
CPT = Coldplate Temperature in °C
TD = Temperature Delta from Coldplate to Radiator Surface in °C
T_S = Radiator Sink Temperature in Kelvin (294 K is recommended default)

4.0 POWER CONDITIONING COMPONENT MODELS

A complete power conditioning component model is created by linking individual stages and combining these with ancillary component hardware. The equations must undergo a few changes to integrate them into a component model. The power and voltage levels for each stage must be computed within their respective equations to obtain the most accurate mass estimates. These values are calculated by inserting the efficiencies of the subsequent stages and including the voltage coefficients associated with inversion and rectification. The equations that define the voltage relationships for single- and 3-phase rectification are shown below. These equations are simply reversed to obtain the corresponding relationships for inversion.

$$\text{Single-Phase: } Vdc=0.9*Vrms$$

$$\text{3-Phase: } Vdc=1.35*Vrms$$

where: Vdc = the output dc voltage from a rectifier or the input dc voltage to a chopper
Vrms = the line-to-line ac voltage from a chopper or the input line-to-line ac voltage fed to a rectifier

The component mass equations include these voltage factors and the efficiencies of the interconnected stages. They also include factors to calculate the mass impacts incurred in the devices that process the component's parasitic power.

The component models are designed to cover a range of applications, from PMAD systems that use high frequency inverters and converters to lower frequency rotary or linear alternator based power systems. To evaluate these systems they can be configured to model combinations of dc and single and 3-phase ac components. Other input options are available to allow the user to select design features and assess potential improvements such as higher frequency operation or the use of carbon-carbon for the enclosure and baseplate. The models are designed to be user friendly, but the user is responsible for inputting valid values. To assist the user in defining the models to match their application, key inputs such as frequency, filtering, and material options will be considered further. Although the models are best suited to high power applications with voltage levels above 120 volts, they can be used to assess low voltage systems if the default efficiency and ripple factor values are changed. This will also be addressed further.

4.1 FREQUENCY CONSIDERATIONS

The operating frequency of a rectifier or transformer or the switching frequency chosen for an inverter or converter is a strong determinant of component mass. Increasing the frequency generally reduces the masses of magnetic components such as inductors or transformers, and the sizes of filter elements, such as the input or output capacitor in a dc filter. The model algorithms calculate a reduction in component mass as a function of frequency, but they aren't able to reflect the increasing losses that will occur in switches, magnetic cores, capacitors, even conductors as frequency rises. The rationale built into the models is as technology advances in switches, magnetic materials, etc., it will be possible to move to higher frequencies and obtain the mass benefits without incurring higher losses. This means there is a time element to the use of higher switching frequencies. The power level also has an impact. It becomes increasingly difficult to control reactive power losses and extract internally generated heat as devices increase in size. To assist the user in selecting an appropriate switching frequency to match their application and time frame, Tables 30, 31, and 32 are offered as guides. These values are estimates intended to reflect projected switching capabilities, but there are many technical challenges to solve before these higher frequencies can be utilized in future component designs. The user is again cautioned to keep in mind that these models are only designed to generate ballpark component mass estimates.

Table 30: Suggested Converter / Inverter Switching Frequency Maximums

Inverter or Converter Power Level	2002 to 2004 Frequency (kHz)	2005 to 2007 Frequency (kHz)	2007 to 2010 Frequency (kHz)
500 Watts to 1 kWe	70	85	100
1 to 5 kWe	60	70	80
5 to 20 kWe	40	48	55
20 to 40 kWe	35	42	50
40 to 80 kWe	30	35	40
80 to 150 kWe	25	30	35
Greater than 150 kWe	20	25	30

The ISS BCDU is able to use a higher switching frequency, 80 kHz, because it can use a bi-directional buck / boost regulator topology that isn't required to provide isolation between the input and output. This design is expected to be typical of future BCDU designs. The following table is offered as guide in selecting switching frequencies for these units.

Table 31: Suggested BCDU Switching Frequency Maximums

BCDU Power Level	2002 to 2004 Frequency (kHz)	2005 to 2007 Frequency (kHz)	2007 to 2010 Frequency (kHz)
500 Watts to 1 kWe	100	110	120
1 to 5 kWe	90	100	110
5 to 10 kWe	80	90	100
10 to 20 kWe	60	70	80

The ISS SSU uses a pulse width modulation frequency (PWM) of 20 kHz to provide fine voltage control between the voltage steps resulting from switching on or off an array string. The model indicates a higher PWM frequency would save mass in the array string EMI filters. The following is offered as a guide for this unit, but the user should evaluate these suggested inputs further.

Table 32: Suggested Array Shunt Regulator Switching Frequency Maximums

Shunt Regulator Power Level	2002 to 2004 Frequency (kHz)	2005 to 2007 Frequency (kHz)	2007 to 2010 Frequency (kHz)
500 Watts to 1 kWe	50	60	70
1 to 5 kWe	40	50	60
5 to 20 kWe	30	40	50
20 to 100 kWe	20	25	30

A few applications will require a large transformation in the voltage level. Its desirable to use high frequency transformers, either stand alone or within a converter, for this function. However, because parasitic effects become more troublesome at higher frequencies, there are limits on how large of a step ratio a transformer can achieve. A more detailed discussion of the effects and guidelines for selecting an appropriate voltage step ratio as a function of frequency are discussed in section 3.1.2.1, Inverter Transformer Stage Model, under the heading Voltage Level Factors and are provided in Table 10, Transformer Step Ratio Guidelines.

Other frequency effects are addressed under Filter Frequency and Ripple Factor Considerations.

4.2 LOW VOLTAGE DESIGN ADJUSTMENTS

The models are primary designed to assess future power systems that are expected to provide more power and use higher voltage levels to meet their requirements. However, they can be used to assess lower power, low voltage designs if some of the default efficiencies are changed. As component designs decline in voltage, the current levels in conductors, switches, diodes, and numerous other devices increases, causing I^2R losses to increase. It becomes more difficult to obtain high operating efficiencies, and the normal trade is to accept some reduction in efficiency to avoid a heavy mass penalty. The default efficiencies in the models for the chopper and rectifier stages should be changed to reflect this decline as the voltage level is decreased, and the following table is offered as a guide in making these adjustments.

Table 33: Model Efficiency Values for Low Voltage Component Designs

Voltage Level (volts)	Chopper Efficiency (%)	Rectifier Efficiency (%)
120	97.60	98.70
110	97.60	98.70
100	95.57	98.68
90	97.53	98.66
80	97.47	98.62
70	97.36	98.56
60	97.23	98.50
50	97.00	98.38
40	96.67	98.20
30	96.00	97.95
20	93.60	96.70

4.3 ENCLOSURE/BASEPLATE TYPE SELECTION CONSIDERATIONS

The component models allow either a Finned Heat Exchanger (FH) or Coldplate (CP) box type to be selected. The FH enclosure/baseplate design uses a finned heat exchanger to transfer heat from the component to a similarly finned coldplate. The main advantage of this design is it allows on-orbit, in space replacement of the power conditioning units. Its finned heat exchanger is fairly heavy and exhibits a higher temperature drop from baseplate to coldplate than direct contact thermal transfer designs. The electrical connectors are mounted on an external plate, pins pointing downward, to allow them to be mated to installed cable box connectors by means of robotically manipulated ACME screws that draw the component down and hold it in place. Pressure pads are present to maintain the correct tension on the ACME screws, both on-orbit and more importantly during launch. Because the FH box has an electrical connector box on its end to route the power and control cables down to the connectors and the ACME screw hardware protrudes through the box, its packaged electronics density relative to the size of its enclosure is much lower. Presently, this box design is only used on the ISS.

The CP enclosure/baseplate design is more typical of satellite component boxes. It doesn't permit on-orbit replacement because the component's baseplate is bolted directly to a coldplate. The baseplate fins are eliminated, reducing its mass. The electrical connector box, ACME screws, and pressure pads aren't required either and they're also eliminated. These items are all present to support the removal and replacement requirements of the ISS orbital replacement units (ORUs). Eliminating the ACME screws also makes available the interior volume that had been lost with their protrusions through the box. This allows much higher packaging densities with the CP box. The result is a smaller, lighter box.

4.4 ENCLOSURE / BASEPLATE AND COLDPLATE / RADIATOR MATERIAL OPTIONS

The component models give the user the option of selecting aluminum or carbon-carbon enclosures, baseplates, and internal structural members such as panels, braces, and card cages. Aluminum's main

advantage is its much less expensive than carbon-carbon. Carbon-carbon is fairly new, and it has only recently become widely available. As a box material, carbon-carbon has several advantages over aluminum: (1) its lighter 1.65 g/cm^3 versus 2.7 g/cm^3 for aluminum, (2) it provides better shielding effectiveness against radiated electromagnetic interference (EMI) at lower frequencies (< 100 MHz) and is comparable at higher frequencies (> 100 MHz), (3) its more resistant to atomic oxygen degradation, and (4) it doesn't exhibit RF pitting (corrosion), a phenomena in which radio frequency power erodes the surface of a material. Finally, carbon-carbon's shielding effectiveness against ionizing radiation is comparable to aluminum.

4.5 CONTROL AND MONITORING HARNESS MATERIAL CONSIDERATIONS

The models estimate the use of fiber optic lines instead of copper wires will reduce the mass of the control and monitoring harness 50%. The main concern with this substitution is the sensitivity of the fiber optic lines and optical couplers to radiation. The effects of ionizing radiation on optical fiber, both from Gamma sources and the space environment, has been studied extensively. Optical fiber will darken when exposed to ionizing radiation creating centers of absorption where unwanted elements and other optical defects were present. A fiber's performance in a radiation environment depends on the materials used to make the glass, the processes used, coatings used, dose type and rate and total dose. Manufacturers supplying the space flight market are aware of these dependencies and have developed manufacturing processes to produce products capable of withstanding tens to hundreds of kRads(Si) total dose with less than one dB increase in loss per kilometer of fiber. If the planned mission will experience total integrated dose levels of radiation in excess of hundreds of kRads(Si), the user should evaluate the impact of this on fiber optic lines and devices before selecting this option in the models. Further information on this subject is available on-line [Ref. 58, 59].

4.6 FILTER FREQUENCY AND RIPPLE FACTOR CONSIDERATIONS

The mass of the component filters strongly depends on the source or switching frequency and the voltage level. The mass of a dc filter following a rectifier stage increases rapidly at lower frequencies because its filter capacitor must store more energy to bridge the span between rectifier pulses. Filter mass also rises at lower voltages because the amount of energy the filtering capacitors can store declines with voltage and the size of the capacitor must be increased to compensate. A component designer is usually free to choose the switching frequency, and its one of the main reasons inverters and converters are moving to higher frequency operation. However, the designer is often required to accept the characteristics of the power source. Low frequency power sources pose special challenges for the development of lightweight PMAD systems. Linear alternator waveforms are particularly difficult to process because their output is single phase, low frequency ac, less than 80 Hz, and its limited to voltage levels under 500 Vrms. One approach is to rectify the output and distribute the power as dc or alternately follow the rectifier with an inverter to step-up the voltage level. The ac to ac frequency converter model combines the rectifier and inverter stages. The output from a rotary alternator is less difficult to process because its typically higher in frequency, several hundred hertz to a few kilohertz, and can be provided over a wider voltage range. But, its main advantage in this context is its 3-phase output triples the number of rectifier pulses, reducing the filter mass to one-third of the value required with a single-phase machine.

The component model filter equations reflect these effects and they will calculate much higher masses for low frequency, low voltage filters. To lower this mass, the first step is for the designer to determine if an alternate power source is available or if the source can provide a higher frequency and/or higher voltage output. If this isn't possible there are a couple of other steps the user can take to reduce these masses. One is to reduce the ripple factor. Its not practical to provide the same level of filtering in a low frequency application as in a high frequency one because the filter mass penalties become prohibitive. System designers must be willing to accept a poorer power quality, which translates into a higher ripple factor. The dc to dc converter operates at 40 kHz and its filters are required to limit the ripple content to less than 0.4%. Conversely, the ripple content provided by a filter following a 70 Hz linear alternator probably can't be any lower than 5%, and may need to go as high as 20%, to obtain a reasonable mass. The efficiency of this filter will probably also have to be reduced to lower its mass. The nominal efficiency of a high frequency filter is estimated to be 99.8%, but it may be necessary to reduce the efficiency of a low frequency filter to as low as 95% to obtain an acceptable mass.

4.7 DC/DC CONVERTER MODEL

The dc/dc converter model combines the chopper, inverter transformer, and rectifier stage equations. It is completed with the addition of input and output dc filtering and equations to calculate the control and monitoring, conductor and connector, and box and radiator masses. It is only capable of generating ball-park component mass estimates. For more accurate mass values, a circuit designer should be consulted.

Application Notes: Dc/dc converters are used to change a dc voltage to a higher or lower level. They also provide isolation between the input and output to reduce transmitted interference. The dc/dc converter models can be used to estimate the masses of converters that follow a dc power source or those located near the loads. In the two applications, the main difference is expected to be the filtering demands. The filter requirements will be determined by the particular applications, but a ripple factor as high as 5% may be acceptable for converters that follow sources and feed industrial power devices such as heaters, while a ripple factor less than 1% is recommended for converters that supply sensitive loads. The ISS dc/dc converter is limited to +/-0.5 volts ripple on its ~120 Vdc output, a ripple factor of 0.4%

Model Input Parameter Ranges: The spreadsheet is designed to cover a specific range of input parameters. Using input parameters outside of these ranges could result in inaccurate mass estimates and it is not recommended. Table 34 lists appropriate input ranges and the values recommended to yield the best results. It also identifies the sources that should be consulted for certain items. It is considered to be the users responsibility to select compatible input parameters that are suitable for the application and operating conditions.

Model Validation: The dc/dc converter model was validated against the ISS flight DDCU. The model calculates a mass of 62.0 kg (136.7 lbs) for a DDCU manufactured to conform to the ISS DDCU design specifications. The ISS flight DDCU weighs 65.8 kg (145 lbs) [Ref. 17]. The ISS mass properties group estimated the dc converter element (DCE) within the DDCU would weigh 9.2 kg (20.3 lbs) [Ref. 14]. The model predicts the DCE would weigh 8.9 kg (19.7 lbs). The lower mass is attributable to semiconductor switch and diode improvements incorporated into the model. The DCE is composed of the chopper, transformer, and rectifier stages, which are common stages in several of the other models. The mass properties group estimated the DDCU filters would weigh 7.35 kg (16.2 lbs). The model is calibrated to also calculate a filter mass of 7.35 (16.2 lbs). The model is configured to calculate a combined mass reduction of 1.4 kg (3.1 lbs) in the controller, data module and power supply due to improvements. The total mass reduction calculated by the model in the electronics is then 1.7 kg (4.0 lbs). With these incorporated electronics improvements and a higher electronics packaging density, the model calculates the box mass would decline 2.1 kg (4.6 lbs). The overall mass reduction of 3.8 kg (8.4 lbs) matches the difference in mass between the ISS flight DDCU and the model calculated mass.

Table 34: DC/DC Converter Model Input Parameter Ranges

DC/DC Converter Input Parameter	Recommended Input Range	Default Value	Comments
Output Power Level	0.5 to 250 kWe		
Input Voltage Level[1]	20 to 10,000 Vdc		See par 4.2, Low Voltage Design Adjustments, for voltages below 120 Vdc
Output Voltage Level[1]	20 to 10,000 Vdc		See par 4.2, Low Voltage Design Adjustments, for voltages below 120 Vdc
Number of Phases	1 or 3	1	
Inversion Frequency	10 to 100 kHz	40 kHz	See par 4.1, Frequency Considerations
Ripple Factor Percentage	0.1 to 5%	0.4%	See par 4.6, Filter Frequency and Ripple Factor Considerations
Available Modules	1-5	1	Must be equal to or greater than the number of Required Modules
Required Modules	1-5	1	
Enclosure/Baseplate Type	FH or CP	FH	See par 4.3, Enclosure/Baseplate Type Selection Considerations
Enclosure/Baseplate Material	Al or CC	Al	See par 4.4, Enclosure / Baseplate and Coldplate / Radiator Material Options
Control & Monitoring Harness Material	Cu or FO	Cu	See par 4.5, Control and Monitoring Harness Material Considerations
Coldplate and Radiator Material	Al or CC	Al	See par 4.4, Enclosure / Baseplate and Coldplate / Radiator Material Options
Single or Two Sided Radiator	1 or 2	2	
Maximum Radiator Sink Temperature	200 to 300 K	294 K	
Maximum Baseplate Temperature	-30 to 65° C	63° C	
Maximum Baseplate to Radiator Delta Temperature	3 to 20° C	11° C 4° C	11° C Delta T for Finned Heat Exchanger 4° C Delta T for Coldplate Baseplate
Chopper Efficiency	96.8 to 98.4%	97.6%	Reduce efficiency for low voltages, see par 4.2, Low Voltage Design Adjustments
Transformer Efficiency	98.6 to 99.6%	99.2%	
Rectifier Efficiency	98.3 to 99.1%	98.7%	Reduce efficiency for low voltages, see par 4.2, Low Voltage Design Adjustments
DC Filter Efficiency	99.7 to 99.9%	99.8%	

4.8 AC/AC FREQUENCY CONVERTER MODEL

The ac/ac frequency converter model is based on a dc link frequency converter design. The ac input is rectified and lightly filtered to obtain dc. This dc is then fed to an inverter to obtain a new ac frequency output. It contains the same stages as a dc/dc converter with the addition of an intermediate dc bus filter, but the sequence of the stages is rearranged to obtain an alternate function. With the addition of output filtering and ancillary hardware, the model is completed. This model is only able to generate ballpark component mass estimates. For more accurate mass values, a circuit designer should be consulted.

Application Notes: Ac/ac frequency converters are used to change an incoming ac frequency to a higher or lower value. The internal transformer also isolates the input and output, thus reducing transmitted interference. The frequency converter model described here is best suited for estimating the masses of converters directly following an alternator power source. In this application, the alternator's low frequency output is typically stepped up to a higher frequency for transmission. The primary purpose of this frequency conversion is to reduce the mass of subsequent distribution transformers. This frequency converter model can also be used at the load end if the input frequency is relatively low, 5 kHz or less, and the waveform has a low harmonic content. These models are not suitable for high frequency inputs. High frequency conversions are typically performed by ac receivers or pulse density modulation motor drives. They require different models.

Model Input Parameter Ranges: The results generated by this spreadsheet are only valid for a certain range of input parameters. Inaccurate mass estimates may result if input parameters outside of the ranges defined in Table 35 are used and it is not recommended. Table 35 also identifies the values that should yield the best results, and lists sources that should be consulted in certain cases. The user is responsible for selecting input parameters that do not conflict and are reasonable for the application and operating conditions.

Model Validation: Because there haven't been any ac power systems flown or even developed to a high level, its not possible to validate the ac/ac frequency converter model against a flight unit. However, the ac/ac frequency converter model does have several stages in common with the dc/dc converter, rectifier, dc filter, chopper, and transformer, and it was validated against the flight ISS DDCU. See the dc/dc converter model validation paragraph.

Table 35: AC/AC Frequency Converter Model Input Parameter Ranges

AC/AC Frequency Converter Input Parameter	Recommended Input Range	Default Value	Comments
Output Power Level	0.5 to 250 kWe		
Input Voltage Level[1]	20 to 10,000 Vdc		See par 4.2, Low Voltage Design Adjustments, for voltages below 120 Vdc
Output Voltage Level[1]	20 to 10,000 Vdc		See par 4.2, Low Voltage Design Adjustments, for voltages below 120 Vdc
Number of Input Phases	1 or 3		
Number of Output Phases	1 or 3		
Input Frequency	60 Hz to 5 kHz		See par 4.1, Frequency Considerations
Output or Inversion Frequency	10 to 100 kHz	20 kHz	See par 4.1, Frequency Considerations
DC Bus Ripple Factor Percentage	1 to 20%	5%	See par 4.6, Filter Frequency and Ripple Factor Considerations
Available Modules	1-5	1	Must be equal to or greater than the number of Required Modules
Required Modules	1-5	1	
Enclosure/Baseplate Type	FH or CP	FH	See par 4.3, Enclosure/Baseplate Type Selection Considerations
Enclosure/Baseplate Material	Al or CC	Al	See par 4.4, Enclosure / Baseplate and Coldplate / Radiator Material Options
Control & Monitoring Harness Material	Cu or FO	Cu	See par 4.5, Control and Monitoring Harness Material Considerations
Coldplate and Radiator Material	Al or CC	Al	See par 4.4, Enclosure / Baseplate and Coldplate / Radiator Material Options
Single or Two Sided Radiator	1 or 2	2	
Maximum Radiator Sink Temperature	200 to 300 K	294 K	
Maximum Baseplate Temperature	-30 to 65° C	63° C	
Maximum Baseplate to Radiator Delta Temperature	3 to 20° C	11° C 4° C	11° C Delta T for Finned Heat Exchanger 4° C Delta T for Coldplate Baseplate
Chopper Efficiency	96.8 to 98.4%	97.6%	Reduce efficiency for low voltages, see par 4.2, Low Voltage Design Adjustments
Transformer Efficiency	98.6 to 99.6%	99.2%	
Rectifier Efficiency	98.3 to 99.1%	98.7%	Reduce efficiency for low voltages, see par 4.2, Low Voltage Design Adjustments
DC Bus Filter Efficiency	95 to 99.8%	95%	
Output Filter Efficiency	99.7 to 99.9%	99.8%	

4.9 AC/DC STATIC RECTIFIER UNIT MODEL

The static rectifier unit model is created by adding filtering after the rectifier stage and including ancillary hardware such as control and monitoring and an enclosure/baseplate.

Application Notes: Static rectifier units are used to convert an incoming ac waveform to a dc output. This rectifier unit model is best for applications following an alternator, but it can also be used for feeding a load or distribution network. The main difference in the two applications is loads are more likely to require an actively regulated, low ripple content power feed. The characteristics of a particular application will determine its filter specifications, but a ripple factor of 1% or better is suggested for rectifier units that supply power to sensitive user loads. Conversely, a ripple factor as high as 5% may be suitable for units that follow an alternator or feed a heater. This model is mainly suited for low frequency applications, 5 kHz or less, but it will accept high frequency inputs. Dc receivers are often used for high frequency ac to dc conversions because the loads they are supplying frequently require an actively regulated feed. A static rectifier isn't capable of actively regulating its power output. A dc receiver requires a different model.

Model Input Parameter Ranges: The results generated by this spreadsheet are only valid for a certain range of input parameters. Inaccurate mass estimates may result if input parameters outside of the ranges defined in Table 36 are used and it is not recommended. Table 36 also identifies the values that should yield the best results, and lists sources that should be consulted for certain input parameters. The user is responsible for selecting input parameters that do not conflict and are reasonable for the application and operating conditions.

Model Validation: Because there haven't been any ac power systems flown or even developed to a high level, its not possible to validate the ac/dc rectifier model against a flight unit. However, its rectifier and dc filter stages are contained in the dc/dc converter, and it was validated against the flight ISS DDCU. See the dc/dc converter model validation paragraph.

Table 36: AC/DC Static Rectifier Model Input Parameter Ranges

AC/DC Static Rectifier Input Parameter	Recommended Input Range	Default Value	Comments
Output Power Level	0.5 to 250 kWe		
Output Voltage Level[1]	20 to 10,000 Vdc		See par 4.2, Low Voltage Design Adjustments, for voltages below 120 Vdc
Number of Phases	1 or 3		
Input Frequency	60 Hz to 5 kHz		See par 4.1, Frequency Considerations
Ripple Factor Percentage	1 to 20%	2%	See par 4.6, Filter Frequency and Ripple Factor Considerations
Available Modules	1-5	1	Must be equal to or greater than the number of Required Modules
Required Modules	1-5	1	
Enclosure/Baseplate Type	FH or CP	FH	See par 4.3, Enclosure/Baseplate Type Selection Considerations
Enclosure/Baseplate Material	Al or CC	Al	See par 4.4, Enclosure / Baseplate and Coldplate / Radiator Material Options
Control & Monitoring Harness Material	Cu or FO	Cu	See par 4.5, Control and Monitoring Harness Material Considerations
Coldplate and Radiator Material	Al or CC	Al	See par 4.4, Enclosure / Baseplate and Coldplate / Radiator Material Options
Single or Two Sided Radiator	1 or 2	2	
Maximum Radiator Sink Temperature	200 to 300 K	294 K	
Maximum Baseplate Temperature	-30 to 65° C	63° C	
Maximum Baseplate to Radiator Delta Temperature	3 to 20° C	11° C 4° C	11° C Delta T for Finned Heat Exchanger 4° C Delta T for Coldplate Baseplate
Rectifier Efficiency	98.3 to 99.1%	98.7%	Reduce efficiency for low voltages, see par 4.2, Low Voltage Design Adjustments
Output Filter Efficiency	99.7 to 99.9%	99.8%	

4.10 TRANSFORMER UNIT MODEL

The transformer unit model is the easiest to create. It simply incorporates the standard transformer stage with its associated ancillary hardware.

Application Notes: The transformer unit is used to change the input ac voltage to a different level. The transformer stage also isolates the input and output, which reduces the level of transmitted interference. The transformer unit can be used anywhere in an ac power system where a change in voltage is required. In applications near a load the high transmission voltage is normally stepped down to the level desired by the load or selected for distribution. It can also be used after an alternator power source, but normally an alternator is capable of providing the desired voltage directly. Since the transformer unit does not use filtering, there are no filter considerations. This model is designed to accept any frequency input from 60 Hz to 100 kHz, but the waveform should exhibit a fairly low harmonic content consistent with external sinusoidal power transmission.

Model Input Parameter Ranges: The results generated by this spreadsheet are only valid for a certain range of input parameters. Inaccurate mass estimates may result if input parameters outside of the ranges defined in Table 37 are used and it is not recommended. Table 37 also identifies the values that should yield the best results, and lists sources that should be consulted for certain input parameters. The user is responsible for selecting input parameters that do not conflict and are reasonable for the application and operating conditions.

Model Validation: There haven't been any ac power systems flown or even developed to a high level, so its not possible to validate the ac/ac transformer model against a flight unit. However, its transformer stage is common to other components, and it was checked against two designs. TRW estimated the mass of a 5 kWe inverter power stage in a dc/ac resonant inverter would be 6.1 kg. The transformer within this stage is estimated to weigh 1.5 kg, consistent with what the transformer model predicts after the mass it calculates is increased 10% to reflect an inverter transformer design. The model calculates the mass of a standard transformer, where as the TRW inverter naturally contains an inverter transformer. The transformer stage is also contained in the dc/dc converter, and it was validated against the flight ISS DDCU. See the dc/dc converter model validation paragraph.

Table 37: AC/AC Transformer Unit Model Input Parameter Ranges

AC/AC Transformer Unit Input Parameter	Recommended Input Range	Default Value	Comments
Output Power Level	0.5 to 250 kWe		
Input Voltage Level[1]	20 to 10,000 Vdc		
Output Voltage Level[1]	20 to 10,000 Vdc		
Number of Phases	1 or 3	1	
Operating Frequency	60 Hz to 100 kHz	20 kHz	See par 4.1, Frequency Considerations
Transformer Efficiency	98.6 to 99.6%	99.2%	
Available Modules	1-5	1	Must be equal to or greater than the number of Required Modules
Required Modules	1-5	1	
Enclosure/Baseplate Type	FH or CP	FH	See par 4.3, Enclosure/Baseplate Type Selection Considerations
Enclosure/Baseplate Material	Al or CC	Al	See par 4.4, Enclosure / Baseplate and Coldplate / Radiator Material Options
Control & Monitoring Harness Material	Cu or FO	Cu	See par 4.5, Control and Monitoring Harness Material Considerations
Coldplate and Radiator Material	Al or CC	Al	See par 4.4, Enclosure / Baseplate and Coldplate / Radiator Material Options
Single or Two Sided Radiator	1 or 2	2	
Maximum Radiator Sink Temperature	200 to 300 K	294 K	
Maximum Baseplate Temperature	-30 to 65° C	63° C	
Maximum Baseplate to Radiator Delta Temperature	3 to 20° C	11° C 4° C	11° C Delta T for Finned Heat Exchanger 4° C Delta T for Coldplate Baseplate

4.11 DC RBI SWITCHGEAR MODEL

The dc RBI switchgear model integrates several dc RBIs into a single unit. The RBIs are interconnected by a main bus. To complete the model control and monitoring, enclosure, and radiator equations are incorporated.

Application Notes: The dc switchgear unit interconnects the system power sources and load distribution networks. The RBIs contained in the switchgear unit allow the sources and load distribution networks to be disconnected from the power system during maintenance periods, and provide fault protection for these components when they are operating. In a large power system, one dc switchgear unit is typically located by the power sources, while another unit is near the loads. The unit close to the power sources makes it possible to bring individual sources on line separately, and remove a source from the system if it is malfunctioning or requires maintenance. Switchgear units located near the loads typically feed local power distribution networks. The dc RBI switchgear model is intended to be very flexible. The designer is able to specify one to eight input RBIs, and one to eight output RBI power feeds.

Model Input Parameter Ranges: The results generated by this spreadsheet are only valid for a certain range of input parameters. Inaccurate mass estimates may result if input parameters outside of the ranges defined in Table 38 are used and it is not recommended. Table 38 also identifies the values that should yield the best results, and lists sources that should be consulted for some input parameters. The user is responsible for selecting input parameters that do not conflict and are reasonable for the application and operating conditions.

Model Validation: The dc RBI switchgear model was validated against the ISS DCSU. For comparison purposes the model was temporarily modified to include RPCMs and a larger power supply to support the external photovoltaic control unit (PVCU). A standard dc switchgear unit isn't expected to house RPCMs or supply an external computer, and these items weren't included in the model. The ISS DCSU weighs 98.6 kg (217.5 lbs), including the internal RPCMs and enlarged power supply [Ref. 17]. Removing the RPCMs eliminates 13.5 kg (29.7 lbs) based on a mass properties estimate [Ref. 14]. Reducing the size of the power supply to only what is required to supply the housekeeping power demand of the DCSU lowers the power supply's mass to 8.8 kg (19.4 lbs) and saves 0.4 kg (0.9 lbs). The modeled RBI design doesn't include snubbers or EMI filters, because the assumed RBI design has a semiconductor switch in parallel with the relay to mitigate the turn-on, turn-off voltage spikes and eliminate the need for EMI filtering. Semiconductor switches capable of interrupting the ISS fault currents weren't available when the ISS RBIs were manufactured, but they are expected to be available within the timeframe of these models. This lowers the DCSU's mass 4.7 kg (10.4 lbs). Adding up the subassembly mass reductions results in a DCSU savings of 18.6 kg (41 lbs). These mass savings combined with a higher electronics packaging density allows the modeled DCSU box mass to be reduced 8.6 kg (19.0 lbs). The total electronics and box mass savings is 27.2 kg (60.0 lbs). The dc RBI switchgear model currently predicts a mass of 70.4 kg (155.3 lbs). Adding on the previously mentioned ISS DCSU items yields 97.6 kg (215.3 lbs). The difference between the flight DCSU mass and the model predicted mass with the add-on is 1 kg (2.2 lbs). This mass reduction is due to improvements in the RBI design and control and monitoring hardware.

Table 38: DC RBI Switchgear Unit Model Input Parameter Ranges

DC RBI Switchgear Unit Input Parameter	Recommended Input Range	Default Value	Comments
Number of Input RBI Units	1 to 8		
Number of Output RBI Units	1 to 8		
RBI Unit Output Power Level	5 to 250 kWe		
RBI Unit Output Voltage Level	100 to 10,000 Vdc		
RBI Efficiency	99.8 to 99.9%	99.85%	
Available Modules	1-5	1	Must be equal to or greater than the number of Required Modules
Required Modules	1-5	1	
Enclosure/Baseplate Type	FH or CP	FH	See par 4.3, Enclosure/Baseplate Type Selection Considerations
Enclosure/Baseplate Material	Al or CC	Al	See par 4.4, Enclosure / Baseplate and Coldplate / Radiator Material Options
Control & Monitoring Harness Material	Cu or FO	Cu	See par 4.5, Control and Monitoring Harness Material Considerations
Coldplate and Radiator Material	Al or CC	Al	See par 4.4, Enclosure / Baseplate and Coldplate / Radiator Material Options
Single or Two Sided Radiator	1 or 2	2	
Maximum Radiator Sink Temperature	200 to 300 K	294 K	
Maximum Baseplate Temperature	-30 to 65° C	63° C	
Maximum Baseplate to Radiator Delta Temperature	3 to 20° C	11° C 4° C	11° C Delta T for Finned Heat Exchanger 4° C Delta T for Coldplate Baseplate

4.12 AC RBI SWITCHGEAR MODEL

The ac RBI switchgear model integrates several ac RBIs into a single unit by interconnecting them with a main bus. The model is completed by adding control and monitoring, an enclosure, and a radiator.

Application Notes: The ac switchgear unit interconnects the system power sources and load distribution networks. The RBIs contained in the switchgear unit allow the sources and load distribution networks to be disconnected from the power system during maintenance periods, and provide fault protection for these components during operation. In a large power system, one ac switchgear unit will probably be close to the power sources, while another unit is near the loads. The unit near the power sources makes it possible to bring individual sources on line separately, and remove a source from the system if it fails or requires maintenance. Switchgear units located close to the loads typically feed local power distribution networks. The ac RBI switchgear model is designed to be quite flexible and it allows the designer to specify one to eight input RBIs, and one to eight RBI power feeds.

Model Input Parameter Ranges: The results generated by this spreadsheet are only valid for a certain range of input parameters. Inaccurate mass estimates may result if input parameters outside of the ranges defined in Table 39 are used and it is not recommended. Table 39 also identifies the values that should yield the best results, and lists sources that should be consulted for some input parameters. The user is responsible for selecting input parameters that do not conflict and are reasonable for the application and operating conditions.

Model Validation: There haven't been any ac power systems flown or even developed to a high level, so its not possible to validate the ac RBI switchgear model against a flight unit. An ac RBI switchgear unit is expected to be very similar in mass to a dc RBI switchgear unit. Modest mass savings are expected in the RBIs because ac RBIs can interrupt fault currents at the zero current crossing. These mass savings will allow slight reductions in the internal support structure and box mass. The ac RBI switchgear is 0.6 kg (1.3 lbs) lighter than the dc RBI switchgear unit. The minor mass savings are attributable to a lighter ac RBI, because it can interrupt fault currents at the zero current crossing, and a slightly smaller volume resulting in a reduction in the box mass.

Table 39: AC RBI Switchgear Unit Model Input Parameter Ranges

AC RBI Switchgear Unit Input Parameter	Recommended Input Range	Default Value	Comments
Number of Input RBI Units	1 to 8		
Number of Output RBI Units	1 to 8		
RBI Unit Output Power Level	5 to 250 kWe		
RBI Unit Output Voltage Level	100 to 10,000 Vdc		
RBI Efficiency	99.8 to 99.9%	99.85%	
Number of Phases	1 or 3	1	
Available Modules	1-5	1	Must be equal to or greater than the number of Required Modules
Required Modules	1-5	1	
Enclosure/Baseplate Type	FH or CP	FH	See par 4.3, Enclosure/Baseplate Type Selection Considerations
Enclosure/Baseplate Material	Al or CC	Al	See par 4.4, Enclosure / Baseplate and Coldplate / Radiator Material Options
Control & Monitoring Harness Material	Cu or FO	Cu	See par 4.5, Control and Monitoring Harness Material Considerations
Coldplate and Radiator Material	Al or CC	Al	See par 4.4, Enclosure / Baseplate and Coldplate / Radiator Material Options
Single or Two Sided Radiator	1 or 2	2	
Maximum Radiator Sink Temperature	200 to 300 K	294 K	
Maximum Baseplate Temperature	-30 to 65° C	63° C	
Maximum Baseplate to Radiator Delta Temperature	3 to 20° C	11° C 4° C	11° C Delta T for Finned Heat Exchanger 4° C Delta T for Coldplate Baseplate

4.13 DC RPCM RACK MODEL

The dc Remote Power Control Module (RPCM) rack model integrates several dc RPCMs into a single unit. The RPCMs themselves contain multiple individual RPC channels. Each RPC channel is a separate power feed. The RPCMs are connected to a main bus. The dc RPCM rack model is completed with the addition of a coldplate and a radiator.

Application Notes: Dc RPCM racks are normally located in the secondary distribution network. The RPC units contained in these racks provide power to individual loads. The design of an RPC allows its power feed to be turned on and off frequently. When the RPC is supplying power, it is capable of monitoring load power demand and providing fault protection. It is assumed the RPCs in future racks will be programmable so that the current interrupt value can be changed to correspond to different load requirements.

This dc RPCM rack model is designed for external environments. The user is able to specify from one to four RPCMs, and within a module up to twenty RPC channels. To obtain the best results, it is recommended the user define RPC channel configurations that will result in RPCM power levels between 10 and 20 kWe. For example, ten 1 kWe RPCs (10 kWe), four 3 kWe RPCs (12 kWe), and one 16 kWe RPC.

Model Input Parameter Ranges: The results generated by this spreadsheet are only valid for a certain range of input parameters. Inaccurate mass estimates may result if input parameters outside of the ranges defined in Table 40 are used and it is not recommended. Table 40 also identifies the values that should yield the best results, and lists sources that should be consulted for some input parameters. The user is responsible for selecting input parameters that do not conflict and are reasonable for the application and operating conditions.

Model Validation: The dc RPCM rack model was validated against an ISS remote power distribution assembly (RPDA). An ISS RPCM weighs 4.36 kg (9.62 lbs). Depending on the RPCM configuration and power level the RPCM model predicts RPCM masses ranging from 2.9 to 5.5 kg (6.4 to 12.1 lbs). The variation in mass is due to power scaling factors incorporated into the models. This is justified by the fact that a single channel, 65 amp, RPCM doesn't use all the connector pins and coldplate capacity. It could be lighter, but commonality with the other RPCM designs increases its mass. If this design was optimized to reduce connector, enclosure, and coldplate mass, its reasonable to expect its mass to be reduced to 2.9 kg (6.4 lbs). An eight space RPCM rack, including cable harnesses and cable connector mates, weighs 15.9 kg (35 lbs). The model calculates a four space aluminum RPCM rack, with cabling, will weigh 8.0 kg (17.6 lbs). Basically, half the mass of an eight space RPCM.

Table 40: DC Remote Power Control Module Rack Model Input Parameter Ranges

DC RPCM Rack Input Parameter	Recommended Input Range	Default Value	Comments
Number of RPC Modules	1 to 4		
RPCM Rack Input Power Level	10 to 80 kWe		
RPC Channel Output Power Level	600 watts to 20 kWe		
Number of RPC Channels in RPCM	1 to 20		
RPC Output Voltage Level	20 to 500 Vdc		
RPC Efficiency	99.65 to 99.75%	99.7%	
Available RPCM Racks	1-5	1	Must be equal to or greater than the number of Required Modules
Required RPCM Racks	1-5	1	
RPCM Enclosure Material	Al or CC	Al	See par 4.4, Enclosure / Baseplate and Coldplate / Radiator Material Options
Control & Monitoring Harness Material	Cu or FO	Cu	See par 4.5, Control and Monitoring Harness Material Considerations
Coldplate and Radiator Material	Al or CC	Al	See par 4.4, Enclosure / Baseplate and Coldplate / Radiator Material Options
Single or Two Sided Radiator	1 or 2	2	
Maximum Radiator Sink Temperature	200 to 300 K	294 K	
Maximum Baseplate Temperature	-30 to 65° C	63° C	
Maximum Baseplate to Radiator Delta Temperature	3 to 20° C	11° C 4° C	11° C Delta T for Finned Heat Exchanger 4° C Delta T for Coldplate Baseplate

4.14 AC RPCM RACK MODEL

The ac RPCM rack model integrates several ac RPCMs into a single unit. The RPCMs contain multiple individual RPC channels. Each RPC channel is a separate power feed. The RPCMs are connected to a main bus. The ac RPCM rack model is completed with the addition of a coldplate and radiator.

Application Notes: Ac RPCM racks will probably be located in a secondary distribution network. The RPC units contained in these racks provide power to individual loads. The design of an RPC allows its power feed to be turned on and off frequently. When the RPC is supplying power, it is capable of monitoring load power demand and providing fault protection. It is assumed the RPCs in future racks will be programmable so that the current interrupt value can be changed to correspond to different load requirements.

This ac RPCM rack model is designed for external environments. The user is able to specify from one to four RPCM, and within a module up to twenty RPC channels. The user can also specify the number of phases that are incorporated into each RPCM. If all the RPCMs are single-phase, a single-phase, two-wire bus is automatically selected. If only 3-phase RPCMs are specified, a 3-phase, 3-wire bus is selected by the model. If the rack contains a mixture of single- and 3-phase RPCMs, the model selects a 3-phase, 4-wire bus. To obtain the best results, it is recommended the user define RPC channel configurations that will generate RPCM power levels between 10 and 20 kWe. For example, ten 1 kWe RPCs (10 kWe), four 3 kWe RPCs (12 kWe), and one 16 kWe RPC.

Model Input Parameter Ranges: The results generated by this spreadsheet are only valid for a certain range of input parameters. Inaccurate mass estimates may result if input parameters outside of the ranges defined in Table 41 are used and it is not recommended. Table 41 also identifies the values that should yield the best results, and lists sources that should be consulted for some input parameters. The user is responsible for selecting input parameters that do not conflict and are reasonable for the application and operating conditions.

Model Validation: There haven't been any ac power systems flown or even developed to a high level, so its not possible to validate the ac RPCM rack model against a flight unit. An ac RPCM rack is expected to be very similar in mass to a dc RPCM rack. A slight increase in the switch mass is expected due to the need to have parallel, back to back semiconductor switches to conduct ac. This, along with a slight increase in the rack mass, caused an equivalently configured ac RPCM rack to weigh 1 kg (2.2 lbs) more than a dc RPCM rack.

Table 41: AC Remote Power Control Module Rack Model Input Parameter Ranges

AC RPCM Rack Input Parameter	Recommended Input Range	Default Value	Comments
Number of RPC Modules	1 to 4		
RPCM Rack Input Power Level	10 to 80 kWe		
RPC Channel Output Power Level	600 watts to 20 kWe		
Number of RPC Channels in RPCM	1 to 20		
Number of Phases in RPCM	1 or 3	1	
RPC Output Voltage Level	20 to 500 Vdc		
RPC Efficiency	99.65 to 99.75%	99.7%	
Available RPCM Racks	1-5	1	Must be equal to or greater than the number of Required Modules
Required RPCM Racks	1-5	1	
RPCM Enclosure Material	Al or CC	Al	See par 4.4, Enclosure / Baseplate and Coldplate / Radiator Material Options
Control & Monitoring Harness Material	Cu or FO	Cu	See par 4.5, Control and Monitoring Harness Material Considerations
Coldplate and Radiator Material	Al or CC	Al	See par 4.4, Enclosure / Baseplate and Coldplate / Radiator Material Options
Single or Two Sided Radiator	1 or 2	2	
Maximum Radiator Sink Temperature	200 to 300 K	294 K	
Maximum Baseplate Temperature	-30 to 65° C	63° C	
Maximum Baseplate to Radiator Delta Temperature	3 to 20° C	11° C 4° C	11° C Delta T for Finned Heat Exchanger 4° C Delta T for Coldplate Baseplate

4.15 SOLAR ARRAY SHUNT REGULATOR MODEL

The solar array shunt regulator matches the power delivered by the array with the power demanded by the load. It uses numerous discreet shunt elements to short out individual array strings and control the amount of power supplied to the load. The shunt switch control signal is generated by a voltage comparitor. The bus voltage is measured and the corresponding voltage signal and a reference voltage signal are fed into a comparitor that generates a voltage error signal. This error signal is utilized by the switch gate control logic to control the number of shunt elements that are activated. Because the switches are capable of rapid switching speeds, the shunt regulator can respond to load changes in milliseconds. Coarse voltage regulation is provided by turning on and off individual shunt elements, thereby shunting power in steps. To achieve fine voltage regulation, the final shunt element is pulse width modulated (PWM). This allows the shunted power to be precisely controlled and results in accurate voltage regulation. The shunt regulator model is completed by incorporating algorithms for the control and monitoring hardware, enclosure, and thermal management subsystem.

Application Notes: An array shunt regulator would be located immediately after the solar array to regulate the bus voltage level. It controls the bus voltage level by shunting excess array current. In effect it maintains a balance between the array power being supplied and the load power being consumed.

Model Input Parameter Ranges: The dc shunt regulator model is designed to cover a wide range of input parameters; however, using parameters outside of these ranges may result in inaccurate mass estimates and it is discouraged. Table 42 lists the acceptable input ranges and provides default values that should yield good results under most conditions. The user is responsible for selecting input parameters that do not conflict and are reasonable for the application and operating conditions.

Model Validation: The solar array shunt regulator model was validated against the ISS SSU. The ISS SSU weighs 89.6 kg (197.6 lbs). The shunt regulator model predicts a mass of 85.0 kg (187.4 lbs). Shunt switch, diode, control element, data monitor unit and ramp generator improvements are projected to save 2.5 kg (5.6 lbs). With these incorporated electronics improvements and an assumed higher electronics packaging density, the model calculates the integral box-radiator mass will drop 2.1 kg (4.7 lbs). The total mass reduction the model calculates is then 4.6 kg (10.2 lbs). This value equals the difference between the ISS flight SSU mass of 89.6 kg (197.6 lbs) and the model calculated mass of 85.0 kg (187.4 lbs).

Table 42: Solar Array Shunt Regulator Model Input Parameter Ranges

Solar Array Shunt Regulator Input Parameter	Recommended Input Range	Default Value	Comments
Array Output Power Level	2 to 100 kWe		
Array Output Voltage	28 to 200 Vdc		
Number of Array Strings	10-200		Equal to the number of array strings
Pulse Width Modulation Frequency	15 to 70 kHz	20 kHz	
Available Shunt Regulator Modules	1-5	1	Must be equal to or greater than the number of Required Modules
Required Shunt Regulator Modules	1-5	1	
Enclosure/Radiator Material	Al or CC	Al	See par 4.4, Enclosure / Baseplate and Coldplate / Radiator Material Options
Control & Monitoring Harness Material	Cu or FO	Cu	See par 4.5, Control and Monitoring Harness Material Considerations
Array String Filter Efficiency	99.9 to 99.98%	99.94%	
Bus Conductor Efficiency	99.57 to 99.77%	99.67%	
Shunt Switch Efficiency	98.6 to 99.6%	99.10%	
Diode Efficiency	99.23 to 99.43%	99.33%	
Load Bus Capacitor Efficiency	99.96 to 99.98%	99.97%	
Array String Ripple Factor	1 to 5%	1.65%	
Maximum Radiator Sink Temperature	200 to 300 K	294 K	
Maximum Baseplate Temperature	-30 to 65° C	63° C	
Maximum Baseplate to Radiator Delta Temperature	3 to 8° C	4° C	4° C Delta T assumed for integral enclosure/radiator design

4.16 BATTERY CHARGE DISCHARGE UNIT MODEL

A battery charge discharge unit (BCDU) controls the charge power supplied to the battery during insolation, and draws power from the battery during eclipse to regulate the primary bus voltage level. It utilizes a buck regulator to reduce the bus voltage to the level required by the battery during charging. By controlling the battery supply voltage it controls its charging rate. During the eclipse period, it draws power from the battery and raises it to the primary bus voltage level using a boost regulator. By controlling the battery discharge rate, it regulates the bus voltage level. Its possible to merge the buck and boost regulators into a common converter, a bilateral converter. With this design approach, some of the circuit elements are shared to reduce the mass of the converter assembly. The BCDU is completed by including algorithms for the control and monitoring hardware, enclosure, and thermal management subsystem.

Application Notes: A BCDU is located between the primary dc bus and the battery. During the insolation period it controls the battery charge rate to bring it up to a full state of charge. During the eclipse period it regulates the primary dc bus voltage level by controlling the discharge rate of the battery. It also includes circuitry to monitor the performance of the battery and provide this information to higher level controllers.

Model Input Parameter Ranges: The BCDU model is designed to cover a wide range of input parameters. However, using parameters outside of these ranges may result in inaccurate mass estimates and it is not recommended. Table 43 lists the acceptable input ranges and provides default values that should yield good results under most conditions. The user is responsible for selecting input parameters that do not conflict and are reasonable for the application and operating conditions.

Model Validation: The BCDU was validated against the ISS BCDU. The ISS BCDU weighs 105.9 kg (233.5 lbs). The BCDU model predicts a mass of 90.8 kg (200.2 lbs). The model does not include the dc control bus RBI or the low voltage battery charger. These items were considered unique to the ISS BCDU design. This reduces the mass of the BCDU electronics an estimated 8.1 kg (17.9 lbs). The buck and boost regulator switch and diode masses, and the control and monitoring controller, data processor, and battery monitor masses were reduced a combined 1.8 kg based on projected improvements. With the elimination of these items, the assumed electronics improvements, and an overall higher electronics packaging density, the box mass declined 5.2 kg (11.4 lbs). The sum of these adjustments is 15.1 kg (33.3 lbs). When this is added to the model estimate of 90.8 kg (200.2 lbs), the current BCDU flight mass of 105.9 kg (233.5 lbs) is obtained.

Table 43: Battery Charge Discharge Unit Model Input Parameter Ranges

Battery Charge Discharge Unit Input Parameter	Recommended Input Range	Default Value	Comments
Max Discharge Power to Primary Bus	500 watts to 20 kWe		
Max Charge Power to Battery	500 watts to 20 kWe		
Max Primary Bus Output Voltage	28 to 200 Vdc		
Maximum Battery Charge Voltage	20 to 190 Vdc		
Battery Capacity Rating	5 to 150 AH		
Buck & Boost Switching Frequency	50 to 120 kHz	80 kHz	
Available Modules	1-5	1	Must be equal to or greater than the number of Required Modules
Required Modules	1-5	1	
Enclosure/Baseplate Type	FH or CP	FH	See par 4.3, Enclosure/Baseplate Type Selection Considerations
Enclosure/Baseplate Material	Al or CC	Al	See par 4.4, Enclosure / Baseplate and Coldplate / Radiator Material Options
Control & Monitoring Harness Material	Cu or FO	Cu	See par 4.5, Control and Monitoring Harness Material Considerations
Coldplate and Radiator Material	Al or CC	Al	See par 4.4, Enclosure / Baseplate and Coldplate / Radiator Material Options
Single or Two Sided Radiator	1 or 2	2	
Maximum Radiator Sink Temperature	200 to 300 K	294 K	
Maximum Baseplate Temperature	-30 to 65° C	63° C	
Maximum Baseplate to Radiator Delta Temperature	3 to 20° C	11° C 4° C	11° C Delta T for Finned Heat Exchanger 4° C Delta T for Coldplate Baseplate

(Table 43 continued on next page)

Table 43 (cont): Battery Charge Discharge Unit Model Input Parameter Ranges

Battery Charge Discharge Unit Input Parameter	Recommended Input Range	Default Value	Comments
Primary and Battery Bus Filter Efficiency	99.7 to 99.9%	99.8%	
Primary Bus Capacitor Efficiency	99.96 to 99.98%	99.97%	
Buck Regulator Switch Efficiency	97.0 to 98.0%	97.50%	
Boost Regulator Switch Efficiency	97.3 to 98.3%	97.8%	
Buck Inductor Efficiency	99.3 to 99.7%	99.5%	
Boost Inductor Efficiency	98.6 to 99.2%	98.9%	
Buck Regulator Diode Efficiency	99.4 to 99.8%	99.6%	
Boost Regulator Diode Efficiency	98.4 to 99.0%	98.7%	
Battery Fault Isolator Efficiency	99.8 to 99.9%	99.85%	
Primary Bus Filter Ripple Factor	0.1 to 5%	0.5%	
Battery Bus Filter Ripple Factor	0.1 to 5%	0.9%	

4.17 DC INSULATED TRANSMISSION LINE MODEL

Note, this model uses iterative calculations and its necessary to change the default EXCEL calculation settings to run it. The following steps are required. After opening this spreadsheet with EXCEL, click on "Tools", go down to "Options" and click on it. Select "Calculation" and in this window check the "Iteration" box. The iteration defaults should be: Maximum Iterations = 100 and Maximum Change = 0.001. In the calculation area select "Automatic" and it will automatically recalculate every time a number is changed or select "Manual" and then after making the input changes hit "F9" and it will recalculate.

Application Notes: The dc transmission line model is used to determine the mass of transmission lines connecting dc power conditioning components.

Model Input Parameter Ranges: The dc transmission line model is capable of accepting a wide range of power, voltage and frequency inputs. The suggested parameter input ranges are shown in Table 44. In most cases these parameters have simply been restricted to typical values and the user can go outside of this range and still obtain acceptable results. The dc transmission line model is very robust and it will accept almost any combination of values and calculate a result. If the user elects to use values outside of the ranges shown below they are responsible for selecting suitable, reasonable values.

Table 44: DC Insulated Transmission Line Model Input Parameter Ranges

Single & 3-Phase AC Transmission Line Input Parameter	Recommended Input Range	Default Value	Comments
Output Power Level	100 watts to 10 MWe		
Output Voltage Level	20 to 10,000 Vrms		
Available Transmission Line Circuits	1-5	1	Must be equal to or greater than the number of Required Circuits
Required Transmission Line Circuits	1-5	1	
Conductor Material	Copper (Cu) or Aluminum (Al)	Cu	
Transmission Line Efficiency	80% to 99.999%		
Transmission Line Distance	0.1 to 10,000 m		
Transmission Line Sink Temperature	200 to 350 K	294 K	

4.18 SINGLE AND 3-PHASE AC INSULATED TRANSMISSION LINE

Note, this model uses iterative calculations and its necessary to change the default EXCEL calculation settings to run it. The following steps are required. After opening this spreadsheet with EXCEL, click on "Tools", go down to "Options" and click on it. Select "Calculation" and in this window check the "Iteration" box. The iteration defaults should be: Maximum Iterations = 100 and Maximum Change = 0.001. In the calculation area select "Automatic" and it will automatically recalculate every time a number is changed or select "Manual" and then after making the input changes hit "F9" and it will recalculate.

Application Notes: The single- and 3-phase ac transmission line model is used to determine the mass of transmission lines connecting ac power conditioning components. It is best suited for moderate to low frequency applications. For high frequency applications, a transmission line construction specifically designed too minimize the skin effect, such as a litz wire construction, is recommended. The dc transmission line model is recommended for dc power system applications.

The skin effect is a phenomenon that occurs in ac transmission due to a rapidly changing current intensity. It arises from the fact that the inductance encountered by the current is higher at the center of the wire than at the periphery. This causes an uneven current density over the conductor cross section; the current density is a minimum at the wire center and a maximum at the periphery. The net result is an increase in the effective resistance of the conductor and higher losses. This effect becomes more pronounced as the conductor size and frequency increase. The litz wire transmission line construction was specifically developed to reduce skin effect losses and line inductance. Litz wire conductors contain numerous, individually insulated wire strands. Because each strand is insulated, the conductor behaves like many small wires run in parallel. This dramatically reduces skin effect losses because the useful conductor cross section of several individual strands is much larger than that of a single large conductor.

Another issue in ac transmission line design is line inductance. The energy stored in a transmission line is proportional to its inductance; consequently, a highly inductive line can make power switching and fault interruption more difficult. The stored energy must be controlled and dissipated by the switch. A large inductive reactance also results in a large reactive power demand. As a result the current levels in the system rise, causing higher I^2R losses, and necessitating larger conductors in the transmission lines and power conditioning components. This effect is further compounded as conductor size increases, because it causes the line inductance to increase. In addition to increasing the PMAD system mass, the power source must be oversized to feed the reactive power demand. From a system viewpoint, it is important to minimize line inductance and maximize the system power factor.

Model Input Parameter Ranges: The single- and 3-phase ac transmission line model is capable of accepting a wide range of power, voltage and frequency inputs. The suggested parameter input ranges are shown in Table 45. In many cases these parameters have simply been restricted to typical values and the user can go outside of this range and still obtain acceptable results. However, there are combinations of input parameters that will cause problems. Specifying power, voltage, and efficiency values that lead to a relatively large conductor size and combining this with a fairly high frequency will frequently lead to poor results. The problem in this case is the model is calculating a large ac resistance due to the skin effect and quite likely a poor power factor because of the calculated line inductance. These effects can be mitigated by reducing the size of the transmission line conductors. Three methods are suggested.

1. Increase the transmission line voltage to reduce the size of the conductors.

2. Lower the operating frequency. The skin effect and line inductance both increase as the frequency rises.

3. If neither of these is acceptable, the transmission line can be separated into multiple lines using the Available Transmission Line Circuits and Required Transmission Line Circuits values. For example, a single 300 kWe line can be broken into three 100 kWe lines by setting both of these equal to 3. This will reduce the size of the

conductors to one-third their original size, but there will be a small mass penalty in the form of additional conductor insulation and more cable jackets.

The user is cautioned to monitor the ac resistance ratio, K, and the power factor. Because of the importance of maintaining a K value close to 1 to minimize the size of the conductors, the model will automatically inform the user if K exceeds 1.1 and suggest the three approaches noted above to reduce it. If the power factor is less than 0.8, this circuit is highly inductive. The steps listed above should again be tried. Failure of the model to converge will almost always be marked by a very low power factor, 0.7 or less. In general, the user should be able to obtain good results if they limit the conductor size to the values shown below for frequencies up to 5 kHz.

Suggested Conductor Size Limits for Selected Frequencies

Operating Frequency	Conductor Gauge	Corresponding Conductor Radius
1 kHz	4 AWG	0.2946 cm
1.5 kHz	6 AWG	0.2337 cm
2 kHz	8 AWG	0.1626 cm
3 kHz	8 AWG	0.1626 cm
4 kHz	10 AWG	0.1295 cm
5 kHz	10 AWG	0.1295 cm

Table 45: Single- and 3-Phase AC Insulated Transmission Line Model Input Parameter Ranges

Single & 3-Phase AC Transmission Line Input Parameter	Recommended Input Range	Default Value	Comments
Output Power Level	100 watts to 10 MWe		
Output Voltage Level	20 to 10,000 Vrms		
Single or 3-Phase	1 or 3		
Operating Frequency	0 Hz (DC) to 5kHz	1	See Model Input Parameter Ranges and Suggested Conductor Size Limits for Selected Frequencies Table above
Available Transmission Line Circuits	1-5	1	Must be equal to or greater than the number of Required Circuits
Required Transmission Line Circuits	1-5	1	
Conductor Material	Copper (Cu) or Aluminum (Al)	Cu	
Transmission Line Efficiency	80% to 99.999%		
Transmission Line Distance	0.1 to 10,000 m		
Assumed Load Power Factor	0.5 to 1.0	0.9	A power factor requirement is normally imposed on loads. 0.9 is a nominal value.
Transmission Line Sink Temperature	200 to 350 K	294 K	

5.0 CONCLUSIONS AND RECOMMENDATIONS

The purpose of this task was to update eight models previously provided to NASA GRC and deliver four new ones. This report documents the basis of these models and the equation development, provides instructions on their use and defines their limitations. The models were revised to reflect flight component mass data from the ISS, and information on the performance and masses of component devices gleaned from properties sheets. They were also expanded to include options to select enclosure types, and enclosure, radiator, and control and monitoring harness materials. Dc and ac transmission line models were added to estimate the mass of the interconnecting cables. The following models were delivered at the completion of this task: (1) dc/dc converter, (2) ac/ac frequency converter, (3) ac/dc static rectifier, (4) ac/ac transformer, (5) dc RBI switchgear unit, (6) ac RBI switchgear unit, (7) dc RPCM rack, (8) ac RPCM rack, (9) solar array shunt regulator, (10) battery charge discharge unit, (11) dc transmission line, and (12) single- and 3-phase ac transmission line.

These models will continue to evolve as more data becomes available. The best way to improve them is to compare their output with data from completed component designs and revise them as necessary. The present power conditioning component data base is relatively small and confined to lower power and voltage levels. Because of this shortage, it was necessary to extrapolate a considerable distance to generate component models that will be consistent with future power and voltage levels. To obtain the information used to create these models many different sources were consulted, but the resulting models were generated by one person and must be reviewed to ensure they are reasonably accurate and can be properly applied. Further validation of the models is recommended as data becomes available.

The power conditioning models were created by generating equations for each of the stages and elements in a component. This process was particularly difficult for low frequency filters. A low frequency filter will be much heavier than a high frequency one, or the power system must be willing to accept poorer power quality. However, because there hasn't been a low frequency ac system designed for space, its difficult to estimate the ripple and efficiency requirements the filter will be expected to meet and from this derive its mass. Using a suggested ripple factor of 10% and a filter efficiency of 95% results in a fairly heavy filter but one that appears reasonable given the challenges of low frequency filtering. But because of these requirements uncertainties and the lack of design information, this part of the models is probably the least accurate and it should be checked against other sources as they become available.

The models included in this report are oriented toward low earth orbit applications, but they are designed to be flexible and can be employed in a wide variety of applications. To properly define the component and transmission line model inputs and interconnect them to form a PMAD system model, the user should have preliminary design requirements and be able to form a conceptual design. The power system architecture should be defined, and requirements such as component maintainability and system filtering should be considered. An estimate of the vehicle sink temperature should also be developed for input into the models to determine the component radiator masses and the cable conductor temperatures. This process is illustrated for a Nuclear Electric Propulsion vehicle application.

An NEP system will probably use a modular architecture to enhance reliability. This can be modeled using the available and required modules inputs. The power conditioning components in an NEP PMAD system will likely be mounted directly on coldplates for cooling. Failed components won't be replaced. These features support the use of a coldplate box. A CP box is also lighter than a finned heat exchanger box. Based on the timeframe the user can choose carbon-carbon boxes and radiators. Next the power, voltage, and frequency values that should be input into the models must be considered. Most of the models can accept power levels up to 250 kWe. This should be adequate for the near term NEP vehicles proposed for outer planetary explorations. However, the power levels envisioned for Mars NEP vehicles are much higher and may be beyond the scope of these particular models. The voltage capabilities incorporated into the models, up to 10,000 volts, seem to be adequate for all NEP applications. Finally, the system filtering requirements should by considered. Discussions with electric propulsion thruster designers indicate a ripple factor of 5-percent is acceptable. This information should be enough to allow the designer to generate a PMAD mass estimate.

REFERENCES

1) Metcalf, Kenneth. "Lunar PMAD Technology Assessment." Rockwell International, Rocketdyne Division. NASA Contractor Report CR-189225. NASA Contract NAS3-25808. February 1992.

2) Metcalf, Kenneth; Harty, Richard; and James Robin. "Issues Concerning Centralized vs. Decentralized Power Deployment." Rockwell International, Rocketdyne Division. NASA Contractor Report CR-187121. NASA Contract NAS3-25808. March 1991.

3) Julian, Duane, and Kenneth Metcalf. "Power Conditioning Component Technology Study." Rockwell International, Rocketdyne Division. IR&D Technical Report, September 1991.

4) Harris Semiconductor. "Power MOSFETs", A data book on power MOSFETs prepared by Harris Semiconductor, 1989.

5) Boylestad, Robert, and Louis Nashelsky. Electronic Devices and Circuit Theory. Englewood Cliffs, New Jersey: Prentice-Hall, 1978.

6) Kozik, Robert. "High Power MOSFETs for Multi-Megawatt Inverters", In-house Rocketdyne Survey, IL No. 119-88-RK-087, September 1988.

7) Yates, Warren. "MOSFET Availability and Performance Continues on the Upswing." Electronic Products, Vol. 33, No. 6, (November 1990), pp. 67-69.

8) Anderson, Paul, and Rene Thibodeaux. " Power Distribution Study for 10-100 kW Baseload Space Power Systems." IECEC '90, August 1990, Vol. I, pp. 428-433.

9) IXYS Corporation. Power Discretes/N-channel Power MOSFETs/MOSFETs. URL: http://www.ixys.com/pdmfet01.html

10) Powerex Power Semiconductors. Press Releases. May 2000. URL: http://www.pwrx.com/pages/newsflash/press_release.asp?file=270%2Ehtm

11) IXYS Corporation. Power Discretes/Very High Voltage IGBTs and BIMOSFETs. URL: http://www.ixys.com/pdigbt04.html

12) Silicon Power. Power Semi-Conductor Components. MOS Controlled Thyristor Specification Sheets. URL: http://www.siliconpower.com/syspqcomponents.asp

13) Powerex Power Semiconductors. Press Releases. February 1999. URL: http://www.pwrx.com/pages/newsflash/press_release.asp?file=60.htm

14) Hui, Shimooi. "Space Station WP-04 Mass Properties", An internal Rocketdyne report generated by the Space Station Freedom mass properties group.

15) TRW. "Bidirectional Power Driver/Receiver", Final technical review report prepared under contract NAS3-24653. Engineering and Test Division, TRW Space & Technology Group, 1988.

16) Ford Aerospace & Communications Corporation. "Space Station Electric Power System Phase C/D Option I", Volume I - Technical, June 1987.

17) E-Mail: "RE: ORU Weights", from Daniel T. Rowley to Kenneth J. Metcalf, February 20, 2002.

18) STMicroelectronics, Power MOSFETs, Fdmesh MOSFETs, Datasheets.
URL: http://us.st.com/stonline/prodpres/discrete/powmosft/powmosft.htm
URL: http://us.st.com/stonline/prodpres/discrete/powmosft/fdmesh.htm

19) Harris Semiconductor. "Power MOSFETs", A data book on power MOSFETs prepared by Harris Semiconductor, 1992.

20) Anderson, Paul, and Rene Thibodeaux. " Power Distribution Study for 10-100 kW Baseload Space Power Systems." IECEC '90, August 1990, Vol. I, pp. 428-433.

21) Levy, Stephen, John Carter, and John Creedon. "Comparison of Solid State with Gaseous Switches for Space Based Megawatt Inverter Applications." IECEC '87, August 1987, Vol. IV, pp. 2034-2039.

22) Borger, William, and Lowell Massie. "Space System Requirements and Issues: The Next Decade." IECEC '90, August 1990, Vol. I, pp. 1-5.

23) Informal Meeting Record. "Power Conditioning Component Mass and Efficiency Modeling", Attendees: Irv Hansen, John Biess, Ron Cull, Ken Metcalf. June 4, 1991.

24) Conversation with Jim Mildice of General Dynamics. "Mass and Volume Estimates for 70 kWe Motor Driver". June 5, 1991.

25) Mildice, J. W. "Performance of Resonant Power Processors in Direct Load PMAD Systems", High Frequency Power Distribution and Control Technology Conference, June 1991.

26) Koerner, G., and E. Siddiqui. Permanent Magnet Variable Speed Constant Frequency Power Generation System. General Electric Company, Binghamton, New York. Technical Report AFWAL-TR-85-2112, November 1984.

27) Kraus, Robert, Ira Meyers, and Eric Baumann. "Light Weight, High Power, High Voltage DC/DC Converter Technologies." IECEC '90, August 1990, Vol. I, pp. 380-385.

28) Hall, James. "Notes on Telecon with Ira Myer NASA LeRC", Documented telecon between Ira Myer of NASA LeRC and Jim Hall of Rocketdyne on the status of the NASA 1 MWe power inverter program. (Copies can be provided on request).

29) Magnetics. "Power Transformer and Inductor Design", Design notes and procedures prepared by the Magnetics Division of Spang and Company.

30) Ferroxcube. "Linear Ferrite Magnetic Design Manual", Design notes and procedures prepared by the Ferroxcube Division of Amperex Electronic Corporation.

31) Ferroxcube. "Linear Ferrite Materials and Components", A characterization of Ferrite materials prepared by the Ferroxcube Division of Amperex Electronic Corporation.

32) McLyman, Colonel Willian T. "Transformer and Inductor Design Handbook". New York, N.Y.: Marcel Dekker, 1978.

33) Honeywell Metglas overview and Metglas High Frequency C-Cores Technical Bulletin.
URL: http://www.elnaferrite.com/metglas/powerlite.htm
URL: http://www.elnaferrite.com/literature/metglas/POWERLITE4.pdf

34) Fink, Donald and H. Wayne Beaty. "Standard Handbook for Electrical Engineers", Eleventh Edition. New York, N.Y.: McGraw-Hill Book Company, 1978.

35)   Westinghouse Electric Corporation. "Westinghouse Quick Selector", Catalog 25-000, 1988.

36)   Kuhlmann, John H. "Design of Electrical Apparatus". New York, N.Y.: John Wiley & Sons, 1957.

37)   Wong, See-pok. "Power Conditioning System Technology Status." Facsimile Transmission from Space Power Incorporated for inclusion in Multimegawatt Space Nuclear Power Supply technical proposal, September 1987.

38)   IXYS Corporation. "Discreet Rectifier Diodes" and "High Voltage Rectifiers".
      URL: http://www.ixys.com/Appasp/pddiod01.asp
      URL: http://www.ixys.com/uge.pdf

39)   Unitrode Corporation. "Unitrode Applications Handbook", Application Note U-108, "Schottky Rectifiers for Low-Voltage Outputs", pp 290-297, 1988.

40)   Metcalf, Kenneth. "Power Conditioning Model Documentation." Rockwell International, Rocketdyne Division. IR&D Technical Report, IR&D Task No. 2, August 1992.

41)   Sprague Electric Company. Sprague Engineering Bulletin 3760C. "Tantalum-Case Tantalum Capacitors with Glass-to-Tantalum Hermetic Seal". 1991.

42)   Vishay Intertechnology Inc. "Type ET DC Filter Capacitors", "Type ET DC Filter Capacitors" and "Ceramic High Voltage Disc Capacitors, Class 1".
      URL: http://www.vishay.com/document/13013/13013.pdf
      URL http://www.vishay.com/document/13014/13014.pdf
      URL: http://www.vishay.com/document/22114/22114.pdf

43)   AVX Corporation. "SMPS Capacitors (SM Style)" and Sprague Engineering Bulletin 3760C.
      URL: http://www.AVX.com/docs/Catalogs/sm9.pdf

44)   Boeing Canoga Park Capacitor Procurement Specifications: RM2486, "Capacitors, SM Series, NPO, Ceramic". RM2497, "Capacitor, SM Series, N1500 Ceramic, 50 Amp". RM2566, "Capacitor, High Voltage, NPO, Ceramic". RM2638, "Capacitor, Ceramic, High Voltage, X7R Dielectric". RM2676, "Capacitor, Module, Ceramic".

45)   Gilmour, A. "High Power Study - Power Conditioning." Department of Electrical Engineering, State University of New York at Buffalo. Technical Report AFAPL-TR-76-101, January 1976.

46)   Moriarty, J. "Power Conditioning Subsystem Design." Raytheon Company, Missile Systems Division, Bedford Laboratories. Technical Report AFWAL-TR-82-2108, November 1982.

47)   Yu, Yuan, Max Bachmann, and Fred Lee. "Formulation of a Methodology for Power Circuit Design Optimization." 1976 Power Electronics Specialists Conference Record, pp. 35-44.

48)   Rockwell International, Rocketdyne Division. "SP-100 Reactor-Stirling Power System GES Baseline System Definition and Characterization Study", JPL Contract No. 956935, 1985.

49)   Biess, John J. "Power Management and Distribution (PMAD) Technology Overview", High Frequency Power Distribution and Control Technology Conference, June 1991.

50)   Ford Aerospace & Communications Corporation. "PWR Splinter Meeting Power Electronics." A tabulated mass and power loss breakdown for the sequential shunt unit (SSU), battery charge/discharge unit (BCDU), and direct current switching unit (DCSU). November, 1989.

51)   Dupass, W. "Parasitics - Based on the Standard ORU DC Architecture", Rockwell International, Rocketdyne Division, EID-00344. November, 1989.

52)   Han, Augustina. EID-00668 Rev AA1, "Electric Power System On-Orbit Performance (EPSOP) Modeling Data", April 2001.

53)   Telephone conversation with Dave Fox of Westinghouse. "Design Details and Mass Estimates for AC RBIs and RPCs". September 9, 1991.

54)   SSP 30263:002 Rev. N, "Remote Power Controller Module (RPCM) Standard Interface Control Document". December 4, 1998.

55)   SSQ 22680 Rev. E, "Connectors, Rectangular, (ORU), Space Quality, General Specification For". January 15, 2000

56)   RI/RD94-616-A-S, SDRL No. RD074F, SDS No. SS-VE-046J, "Power Status Report Part A". January 10, 2002

57)   Rovang, R. D., EID-02094, "Thermal Analysis of Z1 DDCU-HP". July 30, 1996.

58)   "Radiation Effects".   URL: http://epims.gsfc.nasa.gov/tva/meldoc/cabass/rad.htm

59)   LaBel, K.A. et al. "A Compendium of Recent Optocoupler Radiation Test Data". URL: http://radhome.gsfc.nasa.gov/radhome/papers/nsrec00_W22.pdf

1. REPORT DATE *(DD-MM-YYYY)* 01-11-2011	2. REPORT TYPE Final Contractor Report	3. DATES COVERED *(From - To)*

4. TITLE AND SUBTITLE Power Management and Distribution (PMAD) Model Development Final Report	5a. CONTRACT NUMBER NAS3-01140
	5b. GRANT NUMBER
	5c. PROGRAM ELEMENT NUMBER

6. AUTHOR(S) Metcalf, Kenneth, J.	5d. PROJECT NUMBER
	5e. TASK NUMBER
	5f. WORK UNIT NUMBER WBS 432938.08

7. PERFORMING ORGANIZATION NAME(S) AND ADDRESS(ES) Boeing Corporation	8. PERFORMING ORGANIZATION REPORT NUMBER E-18023

9. SPONSORING/MONITORING AGENCY NAME(S) AND ADDRESS(ES) National Aeronautics and Space Administration Washington, DC 20546-0001	10. SPONSORING/MONITOR'S ACRONYM(S) NASA
	11. SPONSORING/MONITORING REPORT NUMBER NASA/CR-2011-217268

12. DISTRIBUTION/AVAILABILITY STATEMENT
Unclassified-Unlimited
Subject Categories: 20 and 44
Available electronically at http://www.sti.nasa.gov
This publication is available from the NASA Center for AeroSpace Information, 443-757-5802

13. SUPPLEMENTARY NOTES

14. ABSTRACT
Power management and distribution (PMAD) models were developed in the early 1990's to model candidate architectures for various Space Exploration Initiative (SEI) missions. They were used to generate "ballpark" component mass estimates to support conceptual PMAD system design studies. The initial set of models was provided to NASA Lewis Research Center (since renamed Glenn Research Center) in 1992. They were developed to estimate the characteristics of power conditioning components predicted to be available in the 2005 timeframe. Early 90's component and device designs and material technologies were projected forward to the 2005 timeframe, and algorithms reflecting those design and material improvements were incorporated into the models to generate mass, volume, and efficiency estimates for circa 2005 components. The models are about ten years old now and NASA GRC requested a review of them to determine if they should be updated to bring them into agreement with current performance projections or to incorporate unforeseen design or technology advances. This report documents the results of this review and the updated power conditioning models and new transmission line models generated to estimate post 2005 PMAD system masses and sizes. This effort continues the expansion and enhancement of a library of PMAD models developed to allow system designers to assess future power system architectures and distribution techniques quickly and consistently.

15. SUBJECT TERMS
Transformers; Switches; Circuits; Inverters; Estimates; Voltage converters (DC to DC); Power conditioning; High voltages; Transmission lines; Harnesses; High frequencies; Regulators; Frequency converters; AC generators; Inverted converters (DC to AC)

16. SECURITY CLASSIFICATION OF:			17. LIMITATION OF ABSTRACT	18. NUMBER OF PAGES	19a. NAME OF RESPONSIBLE PERSON STI Help Desk (email:help@sti.nasa.gov)
a. REPORT U	b. ABSTRACT U	c. THIS PAGE U	UU	118	19b. TELEPHONE NUMBER *(include area code)* 443-757-5802